"Design and implementation of a nonlinear controller for a robotic arm with flexible joints and rigid links"

Juan José Padilla Mora

Supervisor: **Dr. Mauricio Muñoz-Arias**

Academic Area of Mechatronics Engineering
Tecnológico de Costa Rica

This dissertation is submitted for the degree of
Licentiate in Mechatronics Engineering

August 2017

Instituto Tecnológico de Costa Rica
Área Académica de Ingeniería en Mecatrónica
Proyecto de Graduación
Tribunal Evaluador

Proyecto de graduación defendido ante el presente Tribunal Evaluador como requisito para optar por el título de Ingeniero en Mecatrónica con el grado académico de Licenciatura del Instituto Tecnológico de Costa Rica.

Miembros del Tribunal

MSc. Arys Carrasquilla Batista
Profesora Lectora

Dr. Juan Crespo Mariño
Profesor Lector

Dr. Mauricio Muñoz Arias
Profesor Asesor

Los miembros de este Tribunal dan fe de que el presente trabajo de graduación ha sido aprobado y cumple con las normas establecidas por el Área Académica de Ingeniería en Mecatrónica

Cartago, 24 de agosto de 2017

I would like to dedicate this work to my mother, the first teacher I ever had, whose caring hands always held me since my first steps until now. She taught me the importance of an academic education as well as a discipline for life, with the values and principles that govern my life. This is for you.

I would like to dedicate this work to my father, whose hard work ensured that our plates were never empty and taught me the importance of hard work and loyalty. He has been my role model, the kind of man I want to become, always ready to lend a helping hand to whoever is in need. This is for you.

I would like to dedicate this work to my girlfriend, the moon of my life, my inspiration, whose presence warmed my soul even from the other side of the world. You are my muse, my inspiration, the one who changed my world and makes me improve everyday to become the man you deserve. This, my love, is for you.

Declaration

I hereby declare that except where specific reference is made to the work of others, the contents of this dissertation are original and have not been submitted in whole or in part for consideration for any other degree or qualification in this, or any other university. This dissertation is my own work and contains nothing which is the outcome of work done in collaboration with others, except as specified in the text and Acknowledgements.

Juan José Padilla Mora
August 2017

Acknowledgements

I would like to express my sincere gratitude to every person who in one way or another helped me to get here:

To my assessment committee: Mauricio Muñoz, Juan Crespo and Arys Carrasquilla.

To my professor Mauricio Muñoz, for the opportunity to work alongside him in The Netherlands.

To Hildeberto Jardón and Rodolfo Reyes for the design of the mathematical control law and for all their help and guidance.

To all my teachers in my 18 years of study, because they are builders of a better tomorrow.

To Arlette van Berkel for all her help with the preparations for my stay in Groningen.

To the people of Fundación Ciudadelas de Libertad for their friendship trough all my studies and specially for all their help during the last six months.

To the people of the Engineering and Technology Institute Groningen, because they all were partners, teachers and friends.

To my family, for all their support and love.

Abstract

The robotic systems are becoming more and more complex and the traditional control law theories lose robustness, increasing the difficulty with which the robot can be controlled to interact with the environment around it. The objective of this research work is the study of complex nonlinear systems with the particularity of having flexible joints and rigid links. Such flexibility causes an interesting behavior in the robotic systems because duplicates the number of variables involved in the control task.

Several studies have been carried out in the research of flexible robots, however most of them use the classical Euler-Lagrange framework to describe the mechanical systems. This work has been focused on the implementation of nonlinear controllers within the port-Hamiltonian framework, and the singular perturbation multi-scale systems theory.

In this sense, the mathematical description of two different control laws proposed by Jardón-Kojakhmetov et al. (2017) and Reyes-Báez et al. (2016) are presented and adapted to the physical plant of the two degrees of freedom Quanser robotic arm. Moreover, the equations of the proposed port-Hamiltonian controllers have been implemented into a simulation to test the validity of the control laws for the rigid and the flexible configuration of the robot. Finally, the controllers have been implemented into the physical plant of the robotic arm to validate experimentally the proposed mathematical control theory.

The experimental implementation of the proposed port-Hamiltonian controllers showed an improvement in the control of the position error for the rigid and the flexible configuration in comparison with a benchmark controller proposed by the manufacturer of the robotic arm, with an error rate for the RMS value of the signal lower than 1.2% of the RMS value of the desired trajectory. Further studies and experimental tests should be aimed to the implementation of port-Hamiltonian controllers to achieve an even lower error rate.

Keywords: mechanical system, nonlinear control, port-Hamiltonian systems, robotics, singular perturbation, slow-fast systems.

Contents

List of Figures **xv**

List of Tables **xxi**

1 Introduction. **1**
- 1.1 Context. 1
- 1.2 Definition of the problem. 2
  - 1.2.1 Overview. 2
  - 1.2.2 Problem synthesis. 2
- 1.3 Solution Approach. 3
- 1.4 Objectives. 3
  - 1.4.1 General Objective. 3
  - 1.4.2 Specific Objectives. 3
- 1.5 Synopsis. 4

2 Theoretical framework. **5**
- 2.1 Nonlinear systems behavior. 5
- 2.2 Description of a mechanical system. 6
  - 2.2.1 Euler-Lagrange equations. 7
  - 2.2.2 Legendre Transform. 8
  - 2.2.3 Hamiltonian equations. 9
- 2.3 Stability of nonlinear systems. 11
  - 2.3.1 Lyapunov stability. 11
  - 2.3.2 Asymptotic stability and exponential stability. 12
  - 2.3.3 Lyapunov's direct method. 13
- 2.4 Singular Perturbation Methods. 14
  - 2.4.1 Slow-fast systems. 15
- 2.5 Chapter 2 concluding remarks. 16

3 Mathematical design. **17**
3.1 Experimental setup. 17
3.2 Mathematical description of the model. 18
3.2.1 Port-Hamiltonian rigid model. 19
3.2.2 Port-Hamiltonian flexible model. 20
3.3 Control design. 22
3.3.1 LQR controller. 22
3.3.2 Reyes-Báez et al. multi-scale controller. 25
3.3.3 Jardón-Kojakhmetov et al. multi-scale controller. 27
3.4 Chapter 3 concluding remarks. 29

4 Simulations. **31**
4.1 Explicit description of the controllers. 31
4.1.1 Rigid model explicit description. 31
4.1.2 Flexible model explicit description. 33
4.1.3 Reyes-Báez et al. multi-scale controller explicit description. 34
4.1.4 Jardón-Kojakhmetov et al. multi-scale controller explicit description. 35
4.2 Rigid model simulations. 37
4.2.1 Reyes-Báez et al. controller. 37
4.2.2 Dirksz and Scherpen controller. 39
4.3 Flexible model simulations. 41
4.3.1 Reyes-Báez et al. multi-scale controller. 41
4.3.2 Jardón-Kojakhmetov et al. multi-scale controller. 43
4.4 Chapter 4 concluding remarks. 47

5 Experimental results. **49**
5.1 Rigid model. 49
5.1.1 Set-point experiment. 50
5.1.2 Trajectory tracking experiment. 54
5.2 Flexible model. 58
5.2.1 Set-point experiment. 58
5.2.2 Trajectory tracking experiment. 64
5.3 Chapter 5 concluding remarks. 70

6 Discussion. **71**
6.1 Rigid configuration analysis. 71

6.2 Flexible configuration analysis. 74
6.3 Chapter 6 concluding remarks. 76

7 Conclusion and recommendations. 79
7.1 Conclusions. 79
7.2 Recommendations. 80

Bibliography 81

Appendix A Robot Specifications. 83

Appendix B Simulink diagrams. 85

Appendix C Matlab code. 89
C.1 Reyes-Báez et al. controller for the rigid model. 89
C.2 Dirksz and Scherpen controller for the rigid model. 92
C.3 Reyes-Báez et al. multi-scale controller for the flexible model. 95
C.4 Jardón-Kojakhmetov et al. multi-scale controller for the flexible model. 99

Appendix D Spring coupling mechanical design. 105
D.1 Proposal 1. 106
D.2 Proposal 2. 108
D.3 Discussion. 109

List of Figures

2.1 Concepts of Stability: (1) asymptotically stable, (2) marginally stable and (3) unstable 12
2.2 Nonlinear mass-damper-spring system 13

3.1 2DoF Quanser manipulator schematic 18
3.2 2DoF Quanser manipulator physical plant 18

4.1 Trajectory tracking simulation, rigid configuration, Reyes-Báez et al. controller: (a) Position for J_1. (b) Position for J_2. 38
4.2 Position error, trajectory tracking simulation, rigid configuration, Reyes-Báez et al. controller: (a) Position error for J_1. (b) Position error for J_2. 38
4.3 Control signal, trajectory tracking simulation, rigid configuration, Reyes-Báez et al. controller: (a) Control signal for J_1. (b) Control Signal for J_2. 38
4.4 Trajectory tracking simulation, rigid configuration, Dirksz and Scherpen controller: (a) Position for J_1. (b) Position for J_2. 40
4.5 Position error, trajectory tracking simulation, rigid configuration, Dirksz and Scherpen controller: (a) Position error for J_1. (b) Position error for J_2. 40
4.6 Control signal, trajectory tracking simulation, rigid configuration, Dirksz and Scherpen controller: (a) Control signal for J_1. (b) Control Signal for J_2. 40
4.7 Trajectory tracking simulation, flexible configuration, Reyes-Báez et al. multi-scale controller: (a) Position for J_1. (b) Position for J_2. 42
4.8 Position error, trajectory tracking simulation, flexible configuration, Reyes-Báez et al. multi-scale controller: (a) Position error for J_1. (b) Position error for J_2. 42

4.9 Flexible error, trajectory tracking simulation, flexible configuration, Reyes-Báez et al. multi-scale controller: (a) Position error for J_1. (b) Position error for J_2. 43
4.10 Control signal, trajectory tracking simulation, flexible configuration, Reyes-Báez et al. slow controller: (a) Control signal for J_1. (b) Control signal for J_2. 43
4.11 Control signal, trajectory tracking simulation, flexible configuration, Spong fast controller: (a) Control signal J_1. (b) Control signal J_2. . . . 44
4.12 Trajectory tracking simulation, flexible configuration, Jardón-Kojakhmetov et al. multi-scale controller: (a) Position for J_1. (b) Position for J_2. . . . 45
4.13 Position error, trajectory tracking simulation, flexible configuration, Jardón-Kojakhmetov et al. multi-scale controller: (a) Position error for J_1. (b) Position error for J_2. 45
4.14 Flexible error, trajectory tracking simulation, flexible configuration, Jardón-Kojakhmetov et al. controller: (a) J_1 Position error. (b) J_2 Position error for. 46
4.15 Control signal, trajectory tracking simulation, flexible configuration, Dirksz and Scherpen slow controller: (a) J_1 Control signal for. (b) J_2 Control signal for. 46
4.16 Control signal, trajectory tracking simulation, flexible configuration, Jardón-Kojakhmetov et al. fast controller: (a) Control signal J_1. (b) Control signal J_2. 46

5.1 Set-point experiment, rigid configuration: (a) Position trajectory for J_1. (b) Position trajectory for J_2 50
5.2 Position error comparison for J_1, set-point experiment, rigid configuration: LQR (blue), Reyes-Báez et al. (orange) and Dirksz and Scherpen (yellow). 51
5.3 Position error for J_1, set-point experiment, rigid configuration: (a) LQR. (b) Reyes-Báez et al.. (c) Dirksz and Scherpen. 51
5.4 Position error comparison for J_2, set-point experiment, rigid configuration: LQR (blue), Reyes-Báez et al. (orange) and Dirksz and Scherpen (yellow). 52
5.5 Position error for J_2, set-point experiment, rigid configuration: (a) LQR. (b) Reyes-Báez et al.. (c) Dirksz and Scherpen. 52

5.6 Control signal, set-point experiment, rigid configuration: (a) Reyes-Báez et al. controller for J_1. (b) Dirksz and Scherpen controller for J_1. (c) Reyes-Báez et al. controller for J_2. (d) Dirksz and Scherpen controller for J_2 53
5.7 Trajectory tracking experiment, rigid configuration: (a) Position trajectory for J_1. (b) Position trajectory for J_2 54
5.8 Position error comparison for J_1, trajectory tracking experiment, rigid configuration: LQR (blue), Reyes-Báez et al. (orange) and Dirksz and Scherpen (yellow). 55
5.9 Position error for J_1, trajectory tracking experiment, rigid configuration: (a) LQR. (b) Reyes-Báez et al.. (c) Dirksz and Scherpen. 55
5.10 Position error comparison for J_2, trajectory tracking experiment, rigid configuration: LQR (blue), Reyes-Báez et al. (orange) and Dirksz and Scherpen (yellow). 56
5.11 Position error for J_2, trajectory tracking experiment, rigid configuration: (a) LQR. (b) Reyes-Báez et al.. (c) Dirksz and Scherpen. 56
5.12 Control signal, trajectory tracking experiment, rigid configuration: (a) Reyes-Báez et al. controller for J_1. (b) Dirksz and Scherpen controller for J_1. (c) Reyes-Báez et al. controller for J_2. (d) Dirksz and Scherpen controller for J_2 57
5.13 Set-point experiment, flexible configuration: (a) Position trajectory for J_1. (b) Position trajectory for J_2 58
5.14 Position error comparison for J_1, set-point experiment, flexible configuration: Partial-state feedback LQR (blue), Full state feedback LQR (orange) Reyes-Báez et al. slow controller (yellow) and Jardón-Kojakhmetov et al. slow controller (purple). 59
5.15 Position error for J_1, set-point experiment, flexible configuration: (a) Partial-state feedback LQR. (b) Full-state feedback LQR. (c) Reyes-Báez et al. slow controller. (d) Jardón-Kojakhmetov et al. slow controller 59
5.16 Position error comparison for J_2, set-point experiment, flexible configuration: Partial-state feedback LQR (blue), Full-state feedback LQR (orange) Reyes-Báez et al. slow controller (yellow) and Jardón-Kojakhmetov et al. slow controller (purple). 60
5.17 Position error for J_2, set-point experiment, flexible configuration: (a) Partial-state feedback LQR. (b) Full-state feedback LQR. (c) Reyes-Báez et al. slow controller. (d) Jardón-Kojakhmetov et al. slow controller. 60

5.18 Flexible error comparison for J_1, set-point experiment, flexible configuration: Partial-state feedback LQR (blue), Full-state feedback LQR (orange) Spong fast controller (yellow) and Jardón-Kojakhmetov et al. fast controller (purple). 61
5.19 Flexible error for J_1, set-point experiment, flexible configuration: (a) Partial-state feedback LQR. (b) Full-state feedback LQR. (c) Spong fast controller. (d) Jardón-Kojakhmetov et al. fast controller 61
5.20 Flexible error comparison for J_2, set-point experiment, flexible configuration: Partial-state feedback LQR (blue), Full-state feedback LQR (orange) Spong fast controller (yellow) and Jardón-Kojakhmetov et al. fast controller (purple). 62
5.21 Flexible error for J_2, set-point experiment, flexible configuration: (a) Partial-state feedback LQR. (b) Full-state feedback LQR. (c) Spong fast controller. (d) Jardón-Kojakhmetov et al. fast controller 62
5.22 Control signal, set-point experiment, flexible configuration: (a) Reyes-Báez et al. multi-scale controller for J_1. (b) Jardón-Kojakhmetov et al. multi-scale controller for J_1. (c) Reyes-Báez et al. multi-scale controller for J_2. (d) Jardón-Kojakhmetov et al. multi-scale controller for J_2 . . . 63
5.23 trajectory tracking experiment experiment, flexible configuration: (a) Position trajectory for J_1. (b) Position trajectory for J_2 64
5.24 Position error comparison for J_1, trajectory tracking experiment, flexible configuration: Partial-state feedback LQR (blue), Full-state feedback LQR (orange) Reyes-Báez et al. slow controller (yellow) and Jardón-Kojakhmetov et al. slow controller (purple). 65
5.25 Position error for J_1, trajectory tracking experiment, flexible configuration: (a) Partial-state feedback LQR. (b) Full-state feedback LQR. (c) Reyes-Báez et al. slow controller. (d) Jardón-Kojakhmetov et al. slow controller 65
5.26 Position error comparison for J_2, trajectory tracking experiment, flexible configuration: Partial-state feedback LQR (blue), Full-state feedback LQR (orange) Reyes-Báez et al. slow controller (yellow) and Jardón-Kojakhmetov et al. slow controller (purple). 66
5.27 Position error for J_2, trajectory tracking experiment, flexible configuration: (a) Partial-state feedback LQR. (b) Full-state feedback LQR. (c) Reyes-Báez et al. slow controller. (d) Jardón-Kojakhmetov et al. slow controller 66

5.28 Flexible error comparison for J_1, trajectory tracking experiment, flexible configuration: Partial-state feedback LQR (blue), Full-state feedback LQR (orange) Spong fast controller (yellow) and Jardón-Kojakhmetov et al. fast controller (purple). 67

5.29 Flexible error for J_1, trajectory tracking experiment, flexible configuration: (a) Partial-state feedback LQR. (b) Full-state feedback LQR. (c) Spong fast controller. (d) Jardón-Kojakhmetov et al. fast controller . . 67

5.30 Flexible error comparison for J_2, trajectory tracking experiment, flexible configuration: Partial-state feedback LQR (blue), Full-state feedback LQR (orange) Spong fast controller (yellow) and Jardón-Kojakhmetov et al. fast controller (purple). 68

5.31 Flexible error for J_2, trajectory tracking experiment, flexible configuration: (a) Partial-state feedback LQR. (b) Full-state feedback LQR. (c) Spong fast controller. (d) Jardón-Kojakhmetov et al. fast controller. . 68

5.32 Control signal, trajectory tracking experiment, flexible configuration: (a) Reyes-Báez et al. multi-scale controller for J_1. (b) Jardón-Kojakhmetov et al. multi-scale controller for J_1. (c) Reyes-Báez et al. multi-scale controller for J_2. (d) Jardón-Kojakhmetov et al. multi-scale controller for J_2. 69

B.1 System diagram Reyes-Báez et al. controller 86

B.2 System diagram Jardón-Kojakhmetov et al. controller 87

C.1 Matlab code for Reyes-Báez et al. controller, rigid configuration, part 1. 89

C.2 Matlab code for Reyes-Báez et al. controller, rigid configuration, part 2. 90

C.3 Matlab code for Reyes-Báez et al. controller, rigid configuration, part 3. 91

C.4 Matlab code Dirksz and Scherpen controller, rigid configuration, part 1. 92

C.5 Matlab code Dirksz and Scherpen controller, rigid configuration, part 2. 93

C.6 Matlab code Dirksz and Scherpen controller, rigid configuration, part 3. 94

C.7 Matlab code for Reyes-Báez et al. multi-scale controller, flexible configuration, part 1. 95

C.8 Matlab code for Reyes-Báez et al. multi-scale controller, flexible configuration, part 2. 96

C.9 Matlab code for Reyes-Báez et al. multi-scale controller, flexible configuration, part 3. 97

C.10 Matlab code for Reyes-Báez et al. multi-scale controller, flexible configuration, part 4. 98

C.11 Matlab code for Jardón-Kojakhmetov et al. multi-scale controller, flexible configuration, part 1. 99
C.12 Matlab code for Jardón-Kojakhmetov et al. multi-scale controller, flexible configuration, part 2. 100
C.13 Matlab code for Jardón-Kojakhmetov et al. multi-scale controller, flexible configuration, part 3. 101
C.14 Matlab code for Jardón-Kojakhmetov et al. multi-scale controller, flexible configuration, part 4. 102
C.15 Matlab code for Jardón-Kojakhmetov et al. multi-scale controller, flexible configuration, part 5. 103

D.1 Original spring attachments 105
D.2 Spring attachment components: (from left to right) upper bronze coupling, lower bronze coupling, mechanical spacer, stainless steel pin, spring. 106
D.3 Schematic of spring attachments: 1. springs, 2. designed mechanical spacers, 3. upper bronze coupling, 4. lower bronze coupling, 5. support bar, 6. stainless steel pin and 7. original mechanical spacer . 107
D.4 Schematic of spring attachments: 1. springs, 2. nut, 3. mechanical spacer, 4. upper bronze coupling, 5. lower bronze coupling and 6. support bar. 109

List of Tables

3.1 Torsional stiffness parameters 21

4.1 Parameters values for the 2DoF Quanser manipulator 32
4.2 Reyes-Báez et al. controller parameters 37
4.3 Dirksz and Scherpen controller parameters 39
4.4 Jardón-Kojakhmetov et al. multi-scale controller parameters 41
4.5 Jardón-Kojakhmetov et al. multi-scale controller parameters 44

6.1 l_2 norm for the position error, trajectory tracking for the rigid model 73
6.2 RMS analysis for the position error, trajectory tracking for the rigid model 73
6.3 l_2 norm for the position error, trajectory tracking for the rigid model 76
6.4 RMS analysis for the position error, trajectory tracking for the rigid model 76

A.1 2DoF Quanser robot parameters 83

Chapter 1

Introduction.

This chapter introduces the reader to the context of the research in which the state of the art in the study of flexible robotics have been analyzed. Furthermore, the definition of the problem have been stated, including the problem synthesis, the solution approach and the objectives of the project.

1.1 Context.

Robotics is one of the major industrial and research areas at the present day, due to its characteristic of being highly multidisciplinary. Robotic systems involve mechanical, electronic and computational aspects to meet the required needs. These needs are progressively demanding better performance and control of the robotic systems, increasing the complexity of the robot, hindering their interaction with the environment, as it is stated in Feliu (2006).

According to Canudas de Vit et al. (1996), a flexible robot is one in which some components have some range of flexibility, the ability to deform elastically upon the application of a force or torque. This flexibility can occur in both joints and links of the robot. Specifically, the flexibility of joints appears as a result of torsion in elements connecting the motors with the links and it has a rotational nature, resulting in oscillating angle variations, as stated in Feliu (2006).

There is currently a great interest within the scientific community in the research of flexible robots, mainly motivated by the need of the aerospace industry to build robots that fit in a better way to various environmental conditions. As stated in Feliu (2006), these systems have a high complexity, because they are multivariable systems, highly nonlinear, with distributed parameters and are time-dependent.

One of the complications that these conditions cause to the robot are the undesirables oscillations at the end of the robot, hardly damped, causing problems when using the end effector.

Traditionally the flexibility in robotic systems has been considered as an unwanted effect. However for robotic systems that require certain materials, very large sizes or high accuracy, Canudas de Vit et al. (1996) proposes that the flexibility not only must be taken into account as an undesirable phenomenon, but also mathematical models must be established to have better control over these features.

1.2 Definition of the problem.

1.2.1 Overview.

Most studies in the field of flexible robotics are based in the classical model of the Euler-Lagrange equation, as is shown in Canudas de Vit et al. (1996), de Luca (2014) and Spong (2014). This method presents problems because the quantities involved have no physical interpretation, increasing the difficulty in implementing controllers.

In the other hand, when being dimensioned, flexible robots present the difficulty that its models are at least twice more complex than rigid systems, complicating their study. The theory of singularly perturbed systems was developed to address the analysis of these systems, providing techniques for reducing the mathematical model of flexible robots in Kokotovic et al. (1986), Kokotovic (1984) and Kokotovic et al. (1976) . However this theory individually is not enough to establish a decisive mathematical model for a flexible system.

Given this difficulty, a new approach based on shaping the energy of the system has arisen. This new paradigm is called: port-controlled Hamiltonian systems. Van Der Schaft and Maschke (2003) mentions that it is not until recently that researchers managed to integrate singularly perturbed systems with port-controlled Hamiltonian systems. Such integration would ease greatly the analysis of mathematical models for flexible robots.

1.2.2 Problem synthesis.

Creation of better controllers for a robotic arm with a flexible joint and a rigid link.

1.3 Solution Approach.

It is intended to use the method of port-Hamiltonian systems to the study of flexible robots, specifically robots with flexible joints and rigid links. There have been a few studies with rigid robots using this method which resulted in a significant success, yet still there are no formal results for the study of flexible robots.

As already mentioned, in Van Der Schaft and Maschke (2003) analysis of port-controlled Hamiltonian systems and singularly perturbed systems is integrated. The study states that under certain assumptions and conditions the same drivers can be used for both rigid robots and flexible robots. Besides, unlike the Euler-Lagrange approach, the reduction method of port-controlled Hamiltonian systems preserves the structure of the initial mathematical model.

1.4 Objectives.

1.4.1 General Objective.

Develop nonlinear controllers for a two degrees of freedom robot with a flexible joint and rigid links, based in the port Hamiltonian-approach.

1.4.2 Specific Objectives.

- Simulation of the slow PH controllers for the rigid configuration, with a settling time of 1s.
- Simulation of the multi-scale PH controllers for the flexible configuration, with a settling time of 2s.
- Implementation of the slow PH controller in the Quanser robotic arm with the rigid configuration, with a maximum error of 0.1°.
- Implementation of the multi-scale PH controller in the Quanser robotic arm with the flexible configuration, with a maximum error of 0.5°.

1.5 Synopsis.

This document is divided into seven different chapters as well as four appendices. The sequence of the chapters, besides being quite rational, reflects the development of the work carried out to give a solution to the targeted problem.

Chapter 1 corresponds to the present chapter, the Introduction of the project detailing the context in which the research has been carried out, the state of the art, the problem we are trying to solve, the strategy used in order to give a solution, the objectives of the research and finally the present section detailing the structure of the document.

Chapter 2 sums up the basic theory necessary to understand the mathematics and the physics involved in the problem, including the nonlinear systems theory, the Lyapunov stability, the PH mathematical theory and the singular perturbation methods.

Chapter 3 covers the mathematical description for the rigid and flexible configuration of the two degrees of freedom (2DoF) Quanser manipulator robot, as well as the mathematical framework for the proposed PH controllers.

Chapter 4 addresses the implementation of the proposed controllers into the rigid and flexible mathematical model of the 2DoF Quanser manipulator robot, including the explicit equations used to achieve the simulations presented in the chapter.

Chapter 5 presents the results obtained after the implementation of the proposed controllers into the physical plant of the 2DoF Quanser manipulator robot including the rigid and the flexible configuration.

Chapter 6 focuses in the analysis of the data obtained in Chapter 4 and 5, comparing the different results obtained for the PH controllers as well as the controller proposed by the manufacturers of the 2DoF Quanser manipulator robot, having as reference the theoretical background and previous work carried out by researchers.

Finally, Chapter 7 corresponds to the final conclusions obtained after all the work realized in the research.

The Appendices included in this document are the 2DoF Quanser manipulator robot information, the Simulink diagrams implemented in the robot, the matlab code used in order to achieve the results and finally some mechanical changes proposed for the physical plant.

Chapter 2

Theoretical framework.

This chapter is an abridgment of the theoretical concepts necessary to understand the mathematical framework developed throughout this document. For this purpose, an overall description of the nonlinear system behavior is presented, as well as the Lyapunov theory necessary to the study of the stability in nonlinear systems. Furthermore, the theory for the mathematical description of mechanical systems in Euler-Lagrange (EL) variables and in Port-Hamiltonian (PH) variables is covered, with emphasis in the PH structure which has been used throughout the document. Finally, the mathematical concepts such as multi-scale systems, contraction methods and singular-perturbation methods are presented in order to ease the understanding of the proposed control laws.

2.1 Nonlinear systems behavior.

As it is stated in Slotine and Li (1991), every physical system is inherently nonlinear. In fact, linear systems are described as a special kind of nonlinear system, in which the operational range of the control system is small, or the nonlinearities can be despised because of the simplicity of the model. However, certain nonlinear system can not be analyzed due to the difference in the response to the external inputs compared to linear systems.

There are several typical behaviors of a nonlinear system as detailed in Slotine and Li (1991), such as:

- **Multiple equilibrium points:** According to the initial conditions, a nonlinear system may stabilize around different equilibrium points, understanding them as points where the system can stay without changing the current state until an external perturbation is applied.

- **Limit cycles:** Sometimes the response of a system without external perturbations are oscillations of fixed amplitude. Contrary to linear systems these oscillations are not affected by changes in the initial conditions or the parameters of the system.
- **Bifurcations:** As the parameters of the system are changed, sometimes the equilibrium point change as well. In fact, the number of equilibrium points or even the presence of a limit cycle can be determined by changes in the parameters of the system.
- **Chaos:** Nonlinear systems are highly sensitive to it's initial conditions, so the behavior of the system can't be predicted with certainty even with an exact model of the system.

The dynamics of a nonlinear system can be described by a set of nonlinear differential equations in the form of

$$\dot{x} = f(x,t), \tag{2.1}$$

with f as a $nx1$ nonlinear vector function and x as a $nx1$ state vector. The most used equations to describe the dynamics of a nonlinear system are the Euler-Lagrange equations as in Canudas de Vit et al. (1996), de Luca (2014) and Spong (2014), and the Hamiltonian equations as in Van Der Schaft and Maschke (2003).

An important consideration about nonlinear system's is the dependence on the variable time t. A nonlinear vector function f is considered autonomous if the function is independent respect to time. On the other hand, a nonlinear function with the variable t among it's parameters will be classified as non-autonomous.

2.2 Description of a mechanical system.

As it is stated in Ortega et al. (1998), a classical physical system is described by a set of quantities called coordinates. For example, the position of a single mass particle in space can be described in terms of a set of three dimensional vector of quantities relative to some reference point, usually the vector $[x,y,z]$ in a Cartesian coordinate system.

Furthermore, Ortega et al. (1998) states that "the dynamic motion of a physical holonomic system with n degrees of freedom can be completely described by a set of independent coordinates $q_1(t),...,q_n(t)$ establishing the configuration of the system as a function of time, and a set of n dynamic variables, given either as generalized *velocities* $\dot{q}_1(t),...,\dot{q}_n(t)$ or generalized *momenta* $p_1(t),...,p_n(t)$.

To summarize the above, a classical mechanical system with n degrees of freedom can be described in terms of n coordinates and n velocities/momenta. The n coordinates are called the configuration state of the system, and the space formed by the coordinates and the velocities/momenta is called the the $2n$ dimensional phase space of the system.

2.2.1 Euler-Lagrange equations.

The derivation of the Euler-Lagrange (EL) equations can be found in Shapiro (2003) as a simple change of coordinates in an unconstrained system. As stated in Canudas de Vit et al. (1996), since the joint variables q_i for a robot are a set of generalized coordinates the dynamic model can be derived by the Lagrangian equations:

$$\frac{d}{dt}\frac{\partial L(q,\dot{q})}{\partial \dot{q}_i} - \frac{\partial L(q,\dot{q})}{\partial q_i} = \tau_i(q,\dot{q}), \tag{2.2}$$

where

$$L(q,\dot{q}) = T(q,\dot{q}) - U(q,\dot{q}), \tag{2.3}$$

is the Lagrangian parameter, which is the difference between the kinetic energy an the potential energy of the system, and τ_i corresponds to the generalized force at joint i. According to the nature of the joint τ_i can be a torque or a force, if the joint is revolute or prismatic respectively.

In a classical mechanic system, there can be many origins for the potential energy, such as

$$U_{gravitational} = mgh, \tag{2.4}$$

$$U_{inv.distance} = C_1/r, \tag{2.5}$$

$$U_{spring} = \frac{1}{2}K(\Delta q)^2, \tag{2.6}$$

where m is the mass, g is the gravitational force, h is the height, r is a distance, C_1 is a constant, K is the spring coefficient and Δq is the elongation of the spring.

Furthermore, the kinetic energy of a classical mechanical system is in general described by

$$T(q,\dot{q}) = \frac{1}{2}m\dot{q_i}^2. \tag{2.7}$$

If the motion involves more than one dimension, all the component of the velocities must be taken into account.

2.2.2 Legendre Transform.

The Legendre transformation is an involutive transformation which takes a function $f(x,y)$ to a different function $g(x,y)$, as stated in Shapiro (2003) and Arnold (1989). In classical mechanics it is used to get the derivative of the Hamiltonian $H(q_i,p_i)$ from the Lagrangian $L(q_i,\dot{q}_i)$. Considering a function $f(x,y)$ with a derivative of the form

$$df = \frac{\partial f}{\partial x}dx + \frac{\partial f}{\partial y}dy, \tag{2.8}$$

another function $g(x,y) = ux - f(x,y)$ can be defined in terms of x, y and u, as in Arnold (1989). The derivative of g has the form

$$dg = udx + xdu - \frac{\partial f}{\partial x}dx - \frac{\partial f}{\partial y}dy. \tag{2.9}$$

Moreover, assuming u as a function in terms of x and y of the form

$$u(x,y) = \frac{\partial f}{\partial x}, \tag{2.10}$$

thus, (2.9) can be rewritten as

$$dg = xdu - \frac{\partial f}{\partial y}dy. \tag{2.11}$$

Now, we have a function g in terms of u and y from another equation f in terms of x and y. Then, (2.4) can be solved for x in terms of u and y, to get $x = x(u,y)$. With this expression, an explicit function $g(u,y)$ can be found from (2.11):

$$g(u,y) = ux(u,y) - f(x(u,y),y). \tag{2.12}$$

As stated in Arnold (1989), an important consideration regarding the Legendre transformation is that no information was lost. In fact, a property detailed in Arnold

(1989) states that if under the Legendre transformation f is taken to g, then the Legendre transformation of g will again be f. This property is called the Involutivity of the Legendre transformation:

$$\left.\frac{\partial g}{\partial u}\right|_y = x(u,y), \tag{2.13}$$

$$\left.\frac{\partial g}{\partial y}\right|_u = \frac{\partial f}{\partial y}. \tag{2.14}$$

The importance of such property in the context of this documents is that every classical mechanical system described in EL equations can be transformed into port-Hamiltonian (PH) equations, and every classical mechanical system described in PH equations can be transformed into EL equations.

2.2.3 Hamiltonian equations.

The Lagrangian equations described a classical mechanical system in terms of a $2n$ phase space with parameters $[q_i, \dot{q}_i]^\top$. However, Ortega et al. (1998) assures that even when the system can indeed be analyzed and described by these variables, they are not ideal to describe the phase space.

For this reason, a change of variables is then proposed in Ortega et al. (1998), describing the system in terms of a $2n$ phase space with parameters $[q_i, p_i]^\top$. Instead of using the generalized velocities, the system will be described in terms of the generalized momenta. Thus, a relation between p_i and $\dot{q}_i$ is given by definition as

$$p_i = \frac{\partial L(q,\dot{q})}{\partial \dot{q}_i}, \tag{2.15}$$

which corresponds to a term in (2.2). Solving for $\dot{p}_i$ we have

$$\dot{p}_i = \frac{\partial L(q,\dot{q})}{\partial q_i}. \tag{2.16}$$

Now, the passage from the velocities to the momenta have been described in Landau and Lifshitz (1969) as a Legendre's transformation. Landau and Lifshitz (1969) states that the total differential of the Lagrangian as a function of the coordinates and velocities is

$$dL(q,\dot{q}) = \sum_i \frac{\partial L(q,\dot{q})}{\partial q_i} dq_i + \sum_i \frac{\partial L(q,\dot{q})}{\partial \dot{q}_i} d\dot{q}_i. \tag{2.17}$$

Replacing (2.15) and (2.16) in (2.17), the equation above can be rewritten as

$$dL(q,\dot{q}) = \sum_i \dot{p}_i dq_i + \sum_i p_i d\dot{q}_i. \tag{2.18}$$

Moreover, through algebra, the second term of (2.18) can be expressed as

$$\sum_i p_i d\dot{q}_i = d(\sum_i p_i\dot{q}_i) - \sum_i \dot{q}_i dp_i. \tag{2.19}$$

Hence, (2.18) can be rewritten as

$$d(\sum_i p_i\dot{q}_i - L(q,\dot{q})) = -\sum_i \dot{p}_i dq_i + \sum_i \dot{q}_i dp_i. \tag{2.20}$$

Now, Landau and Lifshitz (1969) defines the argument of the differential in 2.20 as the energy of the system, expressed in term of the coordinates and the momenta. This energy is also called the Hamiltonian of the system, which can be described as

$$H(p,q) = \sum_i p_i\dot{q}_i - L(q,\dot{q}), \tag{2.21}$$

From 2.20 we obtain also the differential of the Hamiltonian

$$dH(p,q) = -\sum_i \dot{p}_i dq_i + \sum_i \dot{q}_i dp_i, \tag{2.22}$$

from where we have

$$\dot{q}_i = \frac{\partial H(p,q)}{\partial p_i}, \tag{2.23}$$

$$\dot{p}_i = \frac{-\partial H(p,q)}{\partial q_i}. \tag{2.24}$$

These are the Hamilton's equations of motion in terms of q_i and p_i. A classical mechanical system can be described with the Hamilton's equations as well as the Lagrangian equations. However, the $2n$ first order differential equations from the Hamiltonian approach replaces the n second order differential equations from the Lagrangian approach. As it is stated in Landau and Lifshitz (1969), for solving problems this change of variables is not particularly helpful, but conceptually is very useful.

2.3 Stability of nonlinear systems.

Intuitively, Slotine and Li (1991) defines the concept of stability as a "well-behavedness around a certain point". Even though this definition gets close to the practical meaning of stability of linear systems, the complexity of the nonlinear systems described in Section 2.1 deserves a better theoretical framework. In this section, the basic concepts regarding the Lyapunov theory have been summarized. For this purpose, the same notation as in Slotine and Li (1991) have been used.

Let B_R denote a spherical region defined as $\|x\| < R$ in state-space, and S_R the sphere itself.

2.3.1 Lyapunov stability.

In Slotine and Li (1991) the stability is formally defined by the following definition: The equilibrium state $x = 0$ is said to be stable if, for any $R > 0$ there exists $r > 0$, such that if $\|x(0)\| < r$ then $\|x(t)\| < R$ for all $t \geq 0$. Otherwise, the equilibrium point is unstable.

Mathematically, the former definition can be described as

$$\forall R > 0, \exists r > 0, \|x(0)\| < r \Rightarrow \forall t \geq 0, \|x(t)\| < R. \tag{2.25}$$

Basically, (2.25) establishes that the system trajectory can be kept inside an arbitrary ball B_R of radius R if a value $r(R)$ is found such that the initial position of the system $x(0)$ is a value within the radius of a ball B_r of radius r. See Figure 2.1. In fewer words, stability in the sense of Lyapunov can be achieved if the system is started near the desired equilibrium point.

An important consideration of stability is that in nonlinear systems there is no such thing as stability of the system, at least in the same sense as in linear systems, because as stated in Section 2.1 a nonlinear system can have multiple equilibrium points.

In the other hand, Slotine and Li (1991) states that an equilibrium point is unstable if there exists some ball B_R such that for every $r > 0$ no matter how close to the origin the system position is started, there is always a possibility that the system trajectory escapes the range of the ball B_R. See Figure 2.1 for a better understanding.

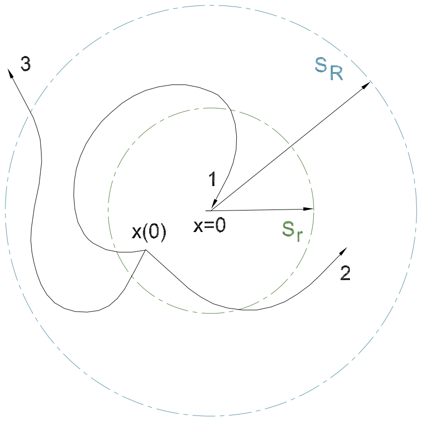

Figure 2.1 Concepts of Stability: (1) asymptotically stable, (2) marginally stable and (3) unstable

2.3.2 Asymptotic stability and exponential stability.

In Slotine and Li (1991) the asymptotic stability is formally defined by the following definition: An equilibrium point is asymptotically stable if it is stable, and there exists some $r > 0$ such that $\|x(0)\| < r$ implies that $\|x(t)\| \rightarrow 0$ as $t \rightarrow \infty$.

Under this definition, an equilibrium point which is asymptotically stable not only keeps the system trajectory within the margins of the ball B_R, but also assures that the system trajectory eventually will converge to the equilibrium point. In this case, Slotine and Li (1991) calls the ball B_R the domain of attraction of the equilibrium point. An equilibrium point which is stable but not asymptotically stable is called marginally stable. See Figure 2.1 for more details.

In Slotine and Li (1991) the exponential stability is formally defined by the following definition: An equilibrium point is exponentially stable if there exist two strictly positive numbers α and λ such that

$$\forall t > 0, \|x(t)\| \leq \alpha \|x(0)\| e^{-\lambda t}, \tag{2.26}$$

in some ball B_r around the origin. In this sense, (2.26) means that the state vector x of a system exponentially stable converges to the equilibrium point faster than an exponential function. The importance of exponentially stabilized systems lies in the need to assure the convergence of a system in a determined time, as it is exemplified in Slotine and Li (1991).

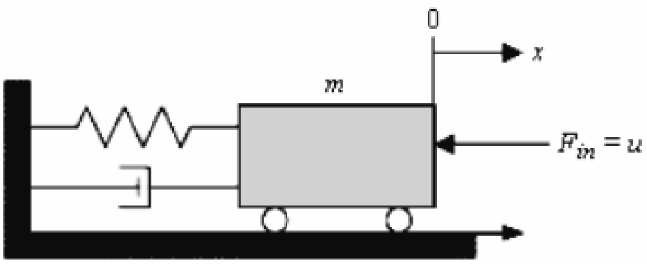

Figure 2.2 Nonlinear mass-damper-spring system

2.3.3 Lyapunov's direct method.

Lyapunov proposed this method based in the observation of the physics behavior of classical mechanical systems: as stated in Slotine and Li (1991), if the total energy of a mechanical system is continuously dissipated, then the system must eventually settle down to an equilibrium point.

To demonstrate the former statement, Slotine and Li (1991) proposes the example of the nonlinear mass-damper-spring depicted in Figure 2.2. It consists of a mass attached to a spring and a damper. If a force f_{in} is applied, the cart will move in the x axis. The dynamic equation for this system is

$$m\ddot{x} + b\dot{x}|\dot{x}| + k_0 x + k_1 x^3 = 0, \tag{2.27}$$

with $b\dot{x}|\dot{x}|$ as the nonlinear damping and $k_0 x + k_1 x^3$ as the nonlinear spring. The spring will remain in it's natural position until an external force is applied to the mass, pulling away the spring from it's natural position. The result will be the motion of the system.

Now, It is known that the total energy of the system is given by the sum of the potential and the kinetic energy of the system:

$$V(x) = \frac{1}{2}m\dot{v}^2 + \int_0^x (k_0 x + k_1 x^3)dx = \frac{1}{2}m\dot{v}^2 + \frac{1}{2}k_0\dot{x}^2 + \frac{1}{4}k_1\dot{x}^4. \tag{2.28}$$

Then, some relations are established in Slotine and Li (1991) in order to link together the concepts of stability and mechanical energy:

- Zero energy is achieved in the equilibrium point of the system, that is $(x = 0, \dot{x} = 0)$.
- For the system to achieve the asymptotic stability, the mechanical energy must be equal to zero.

- Instability will occur as the mechanical energy grows.

Thus, Slotine and Li (1991) establishes that the scalar value of the system's energy indirectly describes the current status of the state vector, and that the stability properties can be analyzed based on variations in the mechanical energy. The rate of energy variation is defined by

$$\dot{V}(x) = m\dot{x}\ddot{x} + (k_0 x + k_1 x^3)\dot{x} = \dot{x}(-b\dot{x}|\dot{x}|) = b|\dot{x}|^3, \tag{2.29}$$

by which can be determined that the mechanical energy of the system will be continuously dissipated by the damper, until the position and velocity are equal to zero, that is until the system gets to the equilibrium point, proving the initial statement of this chapter.

As described in Slotine and Li (1991), the energy function $V(x)$ has two properties: Is strictly positive unless x and $\dot{x}$ are zero (positive definite function); and the function is monotonically decreasing if the variables vary according to the dynamics of the system, that is if a function V(x) is positive definite with continuous partial derivatives, and if it's time derivative along any trajectory is negative semi-definite (Lyapunov function).

2.4 Singular Perturbation Methods.

This sections describes the basic theory involving the singular perturbation methods, as detailed in Kokotovic et al. (1986). Having a classical mechanical system described by a set of dynamic equations, in which the derivatives of some of the states are multiplied by a small positive scalar ϵ, the singular perturbation model is described by

$$\dot{x} = f(x,z,\epsilon,t), \;\; x \in \mathbb{R}^n, \tag{2.30}$$

$$\epsilon\dot{z} = g(x,z,\epsilon,t), \;\; z \in \mathbb{R}^n, \tag{2.31}$$

where f and g are functions with sufficient continuous differentiable functions with respect to the arguments x, z, ϵ and t. The small ϵ parameter is the representation of some other small parameters which are neglected in the model.

Furthermore, Kokotovic et al. (1986) assures that the model described by (2.30) and (2.31) is one of the first steps necessary to the model order reduction of a more complex system, as have been done in Jardón-Kojakhmetov et al. (2017).

2.4.1 Slow-fast systems.

As it is briefly described in Jardón-Kojakhmetov et al. (2017) and detailed in Kokotovic et al. (1986), a slow-fast system is a singular perturbation model with dynamic equations in the form of (2.30) and (2.31). The presence of the parameter ϵ means that the variable z evolves faster than the variable x. In that sense, x is called the slow variable while z is called the fast variable.

The existence of a slow and a fast variable implies that there is a different time scale for each variable. Defining t as the time for the slow variable and τ as the time for the fast variable, the relation between the variables can be expressed as in Jardón-Kojakhmetov et al. (2017) as

$$\tau = \frac{t}{\epsilon}. \tag{2.32}$$

Thus, (2.30) and (2.31) can be rewritten as

$$x' = \epsilon f(x,z,\epsilon,\tau), \;\; x \in \mathbb{R}^n, \tag{2.33}$$

$$z' = g(x,z,\epsilon,\tau), \;\; z \in \mathbb{R}^n, \tag{2.34}$$

with the x' and z' as the derivatives of each variable with respect to the re-scaled time variable τ, For the analysis of the system, an useful method to study the slow and fast subsystems separately is to analyze the system when $\epsilon \to 0$ which yields the differential algebraic equations (slow subsystem)

$$\dot{x} = f(x,z,0,t), \;\; x \in \mathbb{R}^n, \tag{2.35}$$

$$0 = g(x,z,0,t), \;\; z \in \mathbb{R}^n, \tag{2.36}$$

and the layer equation (fast subsystem)

$$0 = \epsilon f(x,z,0,\tau), \;\; x \in \mathbb{R}^n, \tag{2.37}$$

$$z' = g(x,z,0,\tau), \;\; z \in \mathbb{R}^n. \tag{2.38}$$

As a final remark, it is important to notice that while both subsystems have different time scales, the variables of each one have a different behavior. For instance, in the analysis of the slow sub-system the fast variables are neglected due to the result of the limit of $\epsilon \to 0$. In Jardón-Kojakhmetov et al. (2017), the result of such limit implies that the slow sub-system for the flexible configuration of the Quanser robot is not other but the rigid configuration of the same robot, as proposed in Dirksz (2011). Finally, for the analysis of the fast subsystem, the difference in the time scales means that the slow-variables are taken as constant values, leaving the description of the sub-system in terms of the fast variables.

2.5 Chapter 2 concluding remarks.

In this chapter the basic theory necessary to understand the mathematical framework for the compliance with the proposed objectives has been summarized. The basic equation to describe a nonlinear system can be found in (2.1) as well as the basic concepts regarding the nonlinear systems. Furthermore, the equations necessary to describe a classical mechanical system in terms of position and velocity within the Lagrangian framework are shown in (2.2) and (2.3). The mathematical methods to transform the EL equations into PH equations can be found in (2.11) and (2.12), and the proper PH equations are introduced in (2.23) and (2.24).

Moreover, the definition of stability in the sense of Lyapunov has been described by (2.25) and the different kinds of stability of nonlinear systems can be found in Figure 2.1. Finally, the singular perturbation equations are described in (2.30) and (2.31), while the slow-fast system equations have been described by (2.35), (2.36), (2.37) and (2.38).

Next, the theory introduced in this chapter is used in order to described mathematically the 2DoF Quanser robot model, as well as for the design of the proposed PH controllers.

Chapter 3

Mathematical design.

This chapter details the mathematical description of the system in terms of port-Hamiltonian variables, following closely the description of the system approached in Dirksz (2011) and designed in Dirksz and Scherpen (2013). Furthermore, it expands the description of the system for the flexible configuration, based in the theory proposed by Jardón-Kojakhmetov et al. (2017).

Here, the mathematical description of the control laws used for the research have been introduced. For the linear-quadratic regulator (LQR) controller proposed by Quanser the controller design follows the description in Quanser (2006), for the Reyes-Báez et al. controller the design follows the mathematical description in Reyes-Báez et al. (2016) and for the Dirksz and Scherpen (2013) controller the design follows the description in Jardón-Kojakhmetov et al. (2017).

3.1 Experimental setup.

The experimental setup consists of two DC motors, each driving a two bar-serial link. The primary link is coupled to the first drive by means of a flexible joint and carries at it's end the second harmonic drive, to which the second rigid link is attached. The flexible joint can be jammed in order to assure a rigid joint.

The manipulator has links with lengths l_i, angles θ_i, mass m_i, distance to the center of the mass r_i and moment of inertia I_i with $i = 1,2$. As the system works in the horizontal plane, the gravitational forces are neglected. Finally, The joints have been defined as J_1 and J_2, the position of the links as q_i and the position of the motor as q_{mi}. Figure 3.1 shows the diagram for the model and Figure 3.2 shows the physical plant.

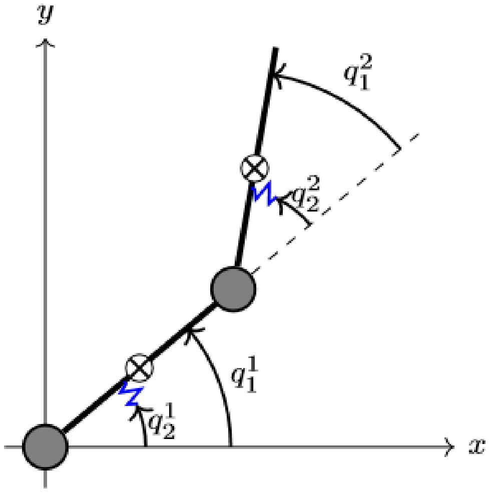

Figure 3.1 2DoF Quanser manipulator schematic

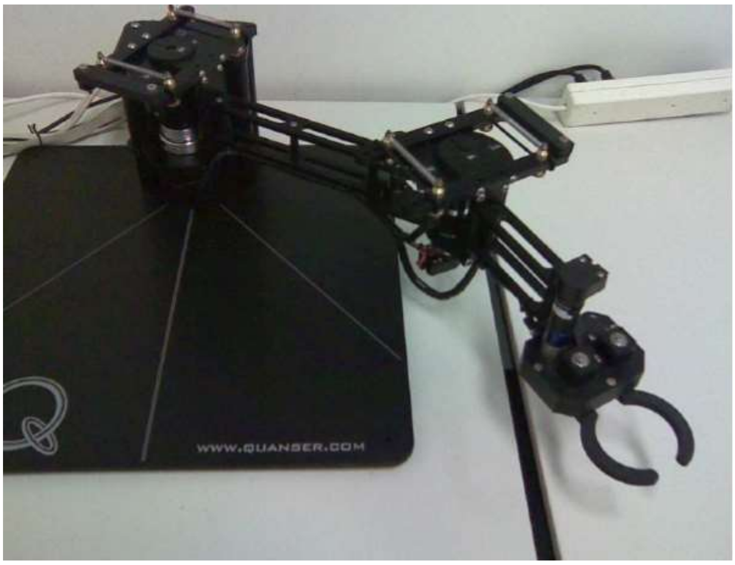

Figure 3.2 2DoF Quanser manipulator physical plant

3.2 Mathematical description of the model.

In this section the mathematical description of the 2DoF Quanser manipulator robot is presented. For the rigid configuration, the description follows closely the mathematical proposal of Dirksz (2011), while for the flexible configuration the theory of Spong (1990) and the work of Jardón-Kojakhmetov et al. (2017) have been used in order to create the model.

3.2.1 Port-Hamiltonian rigid model.

The Hamiltonian is defined according to the kinetic and potential energy as in (2.3) and (2.21). Due to the lack of springs and that the manipulator moves in the horizontal plane, as has been stated in Dirksz (2011), the Hamiltonian for the rigid configuration of the 2DoF Quanser manipulator robot can be defined only by its kinetic energy as

$$H(q,p) = \frac{1}{2}p^\top M(q)^{-1}p, \tag{3.1}$$

with $q = (q_1, q_2)^\top \epsilon \, \mathbb{R}^n$ the vector joint angles and $p = M(q)\dot{q}$ the angular momenta. For an easier interpretation of the inertia matrix $M(q)$, the inner parameters are defined as

$$a_1 = m_1 r_{21} + m_2 l_{21} + I_1, \tag{3.2}$$

$$a_2 = m_2 r_{22} + I_2, \tag{3.3}$$

$$b = m_{21} r_2, \tag{3.4}$$

thus the mass-inertia matrix is given by

$$M(q) = \begin{bmatrix} a_1 + a_2 + 2b\cos\theta_2 & a_2 + b\cos\theta_2 \\ a_2 + 2b\cos\theta_2 & a_2 \end{bmatrix}. \tag{3.5}$$

Furthermore, the system can be described in the PH structure in terms of the coordinates and the momenta. The system belongs to the classical mechanical systems as expanded in Van Der Schaft (2000), therefore it can be described as

$$\begin{bmatrix} \dot{q} \\ \dot{p} \end{bmatrix} = \begin{bmatrix} 0 & I \\ -I & -D(q,p) \end{bmatrix} \begin{bmatrix} \dfrac{\partial H(q,p)}{\partial q} \\ \dfrac{\partial H(q,p)}{\partial p} \end{bmatrix} + \begin{bmatrix} 0 \\ B(q) \end{bmatrix} u, \tag{3.6}$$

where we assume that the system is fully actuated, that being $u \, \epsilon \, \mathbb{R}^m$, $m = n$, $n \rightarrow$ order of the system. The input matrix B(q) can be taken equal to the identity matrix as

$$B(q) = B = \begin{bmatrix} 1 & 0 \\ 0 & 1 \end{bmatrix}, \tag{3.7}$$

and defining the damping matrix as

$$D(q,p) = \begin{bmatrix} d_1 & 0 \\ 0 & d_2 \end{bmatrix}, \tag{3.8}$$

with d_1, d_2 positive constants. Finally, the control input is given by $u \in \mathbb{R}^n$ with (u_1, u_2).

3.2.2 Port-Hamiltonian flexible model.

For the flexible configuration, the mathematical expression for the Hamiltonian must be expanded in order to include not only the kinetic energy of the system, but also the potential energy stored in the springs, as in Jardón-Kojakhmetov et al. (2017). The basic structure of the Hamiltonian is defined as

$$H(q,p) = \frac{1}{2} p^\top M(q)^{-1} p + V(q), \tag{3.9}$$

where $V(q)$ is the potential energy of the system defined as

$$V(q) = \rho_g(q) + \rho_s(q), \tag{3.10}$$

being $\rho_g(q)$ the potential energy due to gravity and $\rho_s(q)$ the potential energy due to the stiffness of the springs. The articulations move in the horizontal plane which means that the gravity force is neglected. The potential energy due to the stiffness is given by

$$\rho_s(q) = \frac{1}{2}(q - q_m)^\top K (q - q_m), \tag{3.11}$$

where $q_m = [q_{m1}, q_{m2}]^\top \in \mathbb{R}^n$ is the angular position of the motors and $K = diag(K_1, K_2)$ $\in \mathbb{R}^{nxn}$ is a symmetric positive definite matrix of the stiffness coefficients for J_1 and J_2. Quanser (2006) defines K_i as

$$K_i = 2 K_r r_i d_i, \tag{3.12}$$

where K_r is the stiffness constant of the springs, r_i the radius from the joint axis of rotation to the outer hole and d_i the distance from the joint centerline to the outer hole. As stated in Jardón-Kojakhmetov et al. (2017) and Spong (1990), the torsional stiffness values shall be very high in comparison with the other parameters of the system, that is when the joints are almost rigid. The parameters used in the

Table 3.1 Torsional stiffness parameters

Joint	Spring rate (N/m)	d_i (m)	r_i (m)
J_1	610	0.0976	0.08636
J_1	440	0.07366	0.08556
J_1	1000	0.07366	0.08556
J_1	1440	0.06096	0.07991
J_1	2875	0.06096	0.07991
J_2	420	0.0976	0.08636
J_2	420	0.07366	0.08556
J_2	480	0.07366	0.08556
J_2	1200	0.07366	0.08556
J_2	232	0.06096	0.07991

experimental setup are specified in Table 3.1. Experimental tests required a higher stiffness constant for J_1 than for J_2 due to the higher moment of inertia experienced by J_1 which provoked bigger oscillations in the articulation, as was proved in the experimental results.

Now, replacing (3.11) in (3.9) the Hamiltonian is given by

$$H(q,p) = \frac{1}{2}p^\top M(q)^{-1}p + \frac{1}{2}(q - q_m)^\top K(q - q_m), \tag{3.13}$$

therefore, a set of $2n$ Hamiltonian differential equations are needed in order to describe the system (with $n = 4$ due to the position variables for the links and the motors) is

$$\begin{bmatrix} \dot{q} \\ \dot{q_m} \\ \dot{p} \\ \dot{p_m} \end{bmatrix} = \begin{bmatrix} 0_{4x4} & I_{4x4} \\ -I_{4x4} & -D_{4x4}(q,p) \end{bmatrix} \begin{bmatrix} \dfrac{\partial H(q,p,q_m,p_m)}{\partial q} \\ \dfrac{\partial H(q,p,q_m,p_m)}{\partial q_m} \\ \dfrac{\partial H(q,p,q_m,p_m)}{\partial p} \\ \dfrac{\partial H(q,p,q_m,p_m)}{\partial p_m} \end{bmatrix} + \begin{bmatrix} 0 \\ 0 \\ 0 \\ B(q) \end{bmatrix} u. \tag{3.14}$$

Then, as proposed by Spong (1990) and replicated by Jardón-Kojakhmetov et al. (2017), to achieve a singular perturbation slow-fast structure with the form of (2.30) and (2.31), let us define new coordinates as $(q,\epsilon z) = (q, q - q_m)$ where ϵ is a small positive scalar which represents all the small parameters to be neglected, as is stated in Kokotovic et al. (1986). Thus the new generalized coordinates are

$$q_\epsilon = (q,z)^\top, \tag{3.15}$$

which gives place to the basic PH structure of the system

$$\begin{bmatrix} \dot{q} \\ \dot{z} \\ \dot{p} \\ \dot{\gamma} \end{bmatrix} = \begin{bmatrix} 0_{4x4} & I_{4x4} \\ -I_{4x4} & -D_{4x4}(q,p) \end{bmatrix} \begin{bmatrix} \dfrac{\partial H(q,p,q_m,p_m)}{\partial q} \\ \dfrac{\partial H(q,p,q_m,p_m)}{\partial z} \\ \dfrac{\partial H(q,p,q_m,p_m)}{\partial p} \\ \dfrac{\partial H(q,p,q_m,p_m)}{\partial \gamma} \end{bmatrix} + \begin{bmatrix} 0 \\ 0 \\ 0 \\ B(q,p) \end{bmatrix} u. \tag{3.16}$$

Hence, the expanded system has a slow-fast structure described in terms of the PH variables, therefore, the control input u shall be defined as well as a PH structure with a suitable system error.

3.3 Control design.

This section expands the mathematical description of the control laws used for the research. For the Linear Quadratic Regulator (LQR) controller proposed by Quanser the controller design follows the description in Quanser's reference manual. Furthermore, for the Reyes-Báez et al. controller the design follows the mathematical description in Reyes-Báez et al. (2016), while for the Dirksz and Scherpen controller the design follows the description in Jardón-Kojakhmetov et al. (2017).

3.3.1 LQR controller.

This controller has been proposed by Quanser, the manufacturer of the 2DoF manipulator, therefore has been used for benchmarking the results of the proposed Hamiltonian controllers. The LQR (Linear Quadratic Regulator) controller have been designed following the Lagrange's method.

Quanser defines the subsystem of the first articulation including the motor, the joint and the link as the first stage of the manipulator. The system's state vector for the first stage is defined as

$$X_1 = \begin{bmatrix} q_1(t) & q_{1m}(t) & \dot{q}_1(t) & \dot{q}_1 m(t) \end{bmatrix}^\top, \tag{3.17}$$

and the system input U_1 is the current I_{m1} applied to the first motor

$$U_1 = I_{m1}. \tag{3.18}$$

The dynamic representation of the system is then given by

$$\frac{\partial X_1}{\partial t} = A_1 X_1 + B_1 U_1, \tag{3.19}$$

where the matrices A_1 and B_1 have been defined as

$$A_1 = \begin{bmatrix} 0 & 0 & 1 & 0 \\ 0 & 0 & 0 & 1 \\ -\frac{K_{s1}}{J_{11}} & \frac{K_{s1}}{J_{11}} & -\frac{B_{11}}{J_{11}} & 0 \\ \frac{K_{s1}}{J_{12}} & -\frac{K_{s1}}{J_{12}} & 0 & -\frac{B_{12}}{J_{12}} \end{bmatrix}, \tag{3.20}$$

$$B_1 = \begin{bmatrix} 0 & 0 & \frac{K_{t1}}{J_{11}} & 0 \end{bmatrix}^\top, \tag{3.21}$$

where K_{s1} is the first flexible joint torsional stiffness constant, J_{11} is the first flexible joint actuated transition equivalent moment of inertia, J_{12} is the first flexible joint actuated transition equivalent viscous damping coefficient, B_{11} the first flexible joint actuated transition equivalent viscous damping coefficient and B_{12} is the first flexible joint load transition equivalent moment of inertia.

Besides, for the control action of the stage 1 system position, a state-feedback controller is implemented as

$$I_{m1} = -K_1 X_1 \tag{3.22}$$

where K_1 in a gain vector calculated by the LQR tuning algorithm provided by Quanser. By default, the tuning algorithm return the the parameters

$$K_1 = \begin{bmatrix} 76.57 & 81.55 & 2.86 & 23.02 \end{bmatrix}.$$

Quanser defines the subsystem of the second articulation including the motor, the joint and the link as the second stage of the manipulator. The system's state vector for the second stage is defined as

$$X_2 = \begin{bmatrix} q_2(t) & q_{2m}(t) & \dot{q}_2(t) & \dot{q}_2m(t) \end{bmatrix}^\top, \tag{3.23}$$

and the system input U_2 is the current I_{m2} applied to the second motor

$$U_2 = I_{m2}. \tag{3.24}$$

The dynamic representation of the system is given by

$$\frac{\partial X_2}{\partial t} = A_2 X_2 + B_2 U_2, \tag{3.25}$$

where the matrices A_2 and B_2 have been defined as

$$A_2 = \begin{bmatrix} 0 & 0 & 1 & 0 \\ 0 & 0 & 0 & 1 \\ -\frac{K_{s2}}{J_{21}} & \frac{K_{s2}}{J_{21}} & -\frac{B_{21}}{J_{21}} & 0 \\ \frac{K_{s2}}{J_{22}} & -\frac{K_{s2}}{J_{22}} & 0 & -\frac{B_{22}}{J_{22}} \end{bmatrix}, \tag{3.26}$$

$$B_2 = \begin{bmatrix} 0 & 0 & \frac{K_{t2}}{J_{21}} & 0 \end{bmatrix}^\top, \tag{3.27}$$

where K_{s2} is the first flexible joint torsional stiffness constant, J_{21} is the first flexible joint actuated transition equivalent moment of inertia, J_{22} is the first flexible joint actuated transition equivalent viscous damping coefficient, B_{21} the first flexible joint actuated transition equivalent viscous damping coefficient and B_{22} is the first flexible joint load transition equivalent moment of inertia.

Likewise, for the control action of the stage 2 system position, a state-feedback controller is implemented as

$$I_{m2} = -K_2 X_2, \tag{3.28}$$

where K_2 in a gain vector calculated by the LQR tuning algorithm provided by Quanser. By default, the tuning algorithm return the the parameters

$$K_2 = \begin{bmatrix} 47.95 & -7.13 & 0.67 & 2.90 \end{bmatrix}.$$

As a final remark, this controller has been proposed directly by the manufacturers of the 2DoF Quanser manipulator and while it is a simple LQR controller, it has proved to accomplish the control task for both the rigid and the flexible configuration.

3.3.2 Reyes-Báez et al. multi-scale controller.

This section follows the mathematical theory for the design of the control law for a multi-scale controller using the contraction based control method for the slow system and the controller proposed by Spong (1990) as the fast controller.

As it is stated in Reyes-Báez et al. (2016), the proposed controller preserves the structure of a Hamiltonian system combining the techniques of transient exponential stability described in Andrieu et al. (2016) and the sliding-manifold approach described in Ghorbel and Spong (2016).The idea is to create a contraction-based control law where an invariant manifold becomes attractive and another control law which ensures that on that invariant manifold, the trajectory follows the desired movement.

As in Spong (1990), new coordinates for the system are proposed as $(q_1, \epsilon z) = (q_1, q_1 - q_2)$ in order to achieve a singular perturbation slow-fast model. New generalized coordinates have been defined as $q_\epsilon = (q_1, z)$. As the system parameters are doubled, the inertia matrix also must be expanded as in Reyes-Báez et al. (2017), in the form of

$$M_\epsilon = \begin{bmatrix} M_l(q_1) & 0 \\ 0 & I \end{bmatrix}, \tag{3.29}$$

where I is the inertia associated with the motors. This means that the generalized momenta p_ϵ is then defined as $p_\epsilon = M_\epsilon(q_\epsilon)\dot{q}_\epsilon$.

Reyes-Báez et al. slow controller.

This section follows the mathematical description for the trajectory tracking control described in Reyes-Báez et al. (2016). To solve the control problem for the system it is necessary to create an error system for the port-Hamiltonian system.

Considering a twice differentiable desired trajectory $X_d(t) = [q_d(t), p_d(t)]^\top$, with $p_d(t) = M(q_d(t))\dot{q}_d(t)$ and the change of coordinates

$$\tilde{x} := \begin{bmatrix} \tilde{q} \\ \sigma \end{bmatrix} = \begin{bmatrix} q - q_d(t) \\ p - p_r(t) \end{bmatrix}, \tag{3.30}$$

and the dynamics of $\tilde{q}$ are

$$\dot{\tilde{q}} = M^{-1}(\tilde{q} + q_d)p - M^{-1}(q_d)p_d, \tag{3.31}$$

where $M^{-1}(q_d)$ is the inertia matrix evaluated in $q = q_d$. From (3.30) it is clear that $p = \sigma + p_r$ is a control input for (3.31) with σ as a new state and p_r as a stabilizing term. With the definitions

$$p_r = p_{d\sigma} - \Lambda\tilde{q}, \tag{3.32}$$

$$p_{d\sigma} = M_d\dot{q}_d, \tag{3.33}$$

and Λ as a Hurwitz matrix, and the substitution of p in (3.31), the results in the position error dynamics are given by

$$\dot{\tilde{q}} = M^{-1}(\sigma - \Lambda\tilde{q}), \tag{3.34}$$

with σ as input. When $\sigma = 0$ in (3.34), the error signal $\tilde{q} = 0$ is asymptotically stable, due to the fact that $-M^{-1}\Lambda$ is a Hurwitz matrix. The above implies that $q \to q_d$ as $t \to \infty$, and that $p_r \to p_d$ as $t \to \infty$. The dynamics for σ is $\dot{\sigma} = \dot{p} - \dot{p}_r$ according to the change of coordinates in (3.30). Thus, the error system dynamics are given by

$$\dot{\tilde{q}} = M^{-1}(\sigma - \Lambda\tilde{q}) \tag{3.35}$$

$$\dot{\sigma} = -\left[\frac{\partial H}{\partial q}(x) + D(q)\frac{\partial H}{\partial p}(x) - G(q)U_s + \dot{p}_r\right]. \tag{3.36}$$

where U_s is the slow controller for the multi-scale system, proposed by Reyes-Báez et al. (2016) with the dynamics

$$U_{s_R} = u_{eq} - u_{at}, \tag{3.37}$$

$$u_{eq} = \dot{p}_r + \frac{\partial H}{\partial q}(q, p_r) + D(q)\frac{\partial H}{\partial p}(q, p_r), \tag{3.38}$$

$$u_{at} = -K_d\frac{\partial H}{\partial p}(q, \sigma) - M^{-1}(q)\Lambda\tilde{q} + \frac{\partial}{\partial q}({p_r}^{\top}M^{-1}(q)\sigma), \tag{3.39}$$

where K_d fulfills

$$D(q) + K_d + \frac{1}{2}I_n - \frac{1}{4}(M^{-1} + M) > 0, \tag{3.40}$$

and the derivative of p_r is

$$p_r = p_{d\sigma} - \Lambda \tilde{q}, \tag{3.41}$$

$$p_r = M_d \dot{q}_d - \Lambda \tilde{q}, \tag{3.42}$$

$$\dot{p}_r = \dot{M}_d \dot{q}_d + M_d \ddot{q}_d - \Lambda(\dot{q} - \dot{q}_d). \tag{3.43}$$

Spong fast Controller.

In Spong (1990) the author proposes a very simple control law for the fast controller in the form of

$$U_{f_S} = K_v(\dot{q} - \dot{q_m}). \tag{3.44}$$

The validity of such controller is based in the proportionality of 3.54 with z, thus becoming valid for the fast feedback term. The obvious advantage of such controller is the simplicity and the easiness to implement.

3.3.3 Jardón-Kojakhmetov et al. multi-scale controller.

This section follows the mathematical description of the multi-scale trajectory tracking control described in Jardón-Kojakhmetov et al. (2017). The author uses the slow controller proposed by Dirksz and Scherpen (2013) and furthermore proposes a fast controller with the same structure, as well as the multi-scale system linking the two subsystems. To solve the control problem, the author derives a PH model using a coordinate transformation.

The idea is to establish a control law for trajectory tracking using only position measurements. For this task, and as stated in Dirksz and Scherpen (2013), a dynamic feedback and a Coriolis matrix are applied without using the reference velocities instead of the actual velocities of the system.

As in Spong (1990), new coordinates for the system are proposed as $(q_1, \epsilon z) = (q_1, q_1 - q_2)$. Likewise, new generalized coordinates have been defined as $q_\epsilon = (q_1, z)$. As the system parameters are doubled, the inertia matrix also must be expanded as in Jardón-Kojakhmetov et al. (2017) in the form of

$$M_\epsilon = \begin{bmatrix} M_l(q_1) + I & -\epsilon I \\ \epsilon I & \epsilon^2 I \end{bmatrix}, \tag{3.45}$$

which means that the generalized momenta p_ϵ is then defined as $p_\epsilon = M_\epsilon(q_\epsilon)\dot{q}_\epsilon$.

Furthermore, a canonical transformation is then carried out in order to transform the PH system with a non-constant inertia matrix to a PH system with a constant inertia matrix. The change of coordinates for the canonical transformation is given by

$$\begin{bmatrix} \bar{q}_\epsilon \\ \bar{p}_\epsilon \end{bmatrix} = \begin{bmatrix} q_\epsilon \\ \bar{T}_\epsilon(\bar{q}_\epsilon)^\top \dot{\bar{q}}_\epsilon \end{bmatrix}, \tag{3.46}$$

where the matrix $\bar{T}_\epsilon(\bar{q}_\epsilon)\epsilon\mathbb{R}^{2x2}$ is lower triangular and defined by $M_\epsilon = \bar{T}_\epsilon(\bar{q}_\epsilon)\bar{T}_\epsilon(\bar{q}_\epsilon)^\top$. Finally, the transformed structure of the PH system is expressed as

$$\begin{bmatrix} \bar{q}_\epsilon \\ \bar{p}_\epsilon \end{bmatrix} = \begin{bmatrix} 0_{nxn} & \bar{T}_\epsilon(\bar{q}_\epsilon)^{-\top} \\ -\bar{T}_\epsilon(\bar{q}_\epsilon)^{-1} & \bar{J}_\epsilon(\bar{q}_\epsilon) - \bar{D}_\epsilon(\bar{q}_\epsilon) \end{bmatrix} \begin{bmatrix} \dfrac{\partial \bar{H}(\bar{q}_\epsilon, \bar{p}_\epsilon)}{\partial \bar{q}_\epsilon} \\ \dfrac{\partial \bar{H}(\bar{q}_\epsilon, \bar{p}_\epsilon)}{\partial \bar{p}_\epsilon} \end{bmatrix} + \begin{bmatrix} 0_{nxn} \\ G(\bar{q}_\epsilon, \bar{p}_\epsilon) \end{bmatrix} \bar{u}. \tag{3.47}$$

Dirksz and Scherpen (2013) slow controller.

This section follows the mathematical description for the trajectory tracking control described in Dirksz (2011). To solve the control problem for the system it is necessary to create an error system for the port-Hamiltonian system, by the transformation

$$\bar{q} = q - q_d(t), \tag{3.48}$$

$$\bar{p} = p - M(q)\dot{q}_d(t), \tag{3.49}$$

Moreover, the controller dynamics proposed by Dirksz (2011) are

$$\dot{q}_c = K_d^{-1} K_c(\bar{q} - q_c), \tag{3.50}$$

$$v = \bar{q} - q_c, \tag{3.51}$$

in addition with the control input for the torque in the articulations

$$U_{s_D} = M(q)\ddot{q}_d + \frac{\partial(M(q)\dot{q})}{\partial q}\dot{q} - \frac{1}{2}\frac{\partial \dot{q}^\top M(q)\dot{q}}{\partial q} - K_p\bar{q} - K_c v \tag{3.52}$$

where $K_d = diag(K_{d1}, K_{d2})\ \epsilon\ \mathbb{R}^{nxn}$, $K_c = diag(K_{c1}, K_{c2})\ \epsilon\ \mathbb{R}^{nxn}$ and $K_p = diag(K_{p1}, K_{p2})$ $\epsilon\ \mathbb{R}^{nxn}$ are positive definite diagonal matrices.

Jardón-Kojakhmetov et al. fast controller.

In Jardón-Kojakhmetov et al. (2017) a controller with the same structure of a PH controller is proposed, which has the system dynamics

$$U_{f_J} = -L_p z - L_c(z - z_c), \tag{3.53}$$

with the controller dynamics

$$\dot{z}_c = L_d^{-1} L_c(z - z_c), \tag{3.54}$$

where $L_d = diag(L_{d1}, L_{d2}) \in \mathbb{R}^{nxn}$, $L_c = diag(L_{c1}, L_{c2}) \in \mathbb{R}^{nxn}$ and $L_p = diag(L_{p1}, L_{p2}) \in \mathbb{R}^{nxn}$ are positive definite diagonal matrices.

3.4 Chapter 3 concluding remarks.

This chapter described the mathematical description of the Quanser 2DoF manipulator robot for the rigid model and the flexible model. Both configurations have been described in a port-Hamiltonian structure as in (3.6) for the rigid model as well as in the (3.16) for the flexible configuration.

Furthermore, the mathematical design of the controllers for the 2DoF Quanser manipulator robot have been described. First, (3.22) and (3.28) describe the model for the LQR controller proposed by Quanser. Furthermore, (3.37), (3.38) and (3.39) describe the dynamics for the control input for the Reyes-Báez et al. controller, while (3.54) describes the dynamics for the Spong fast controller. Moreover, (3.52) describes the dynamics for the Dirksz and Scherpen slow controller and finally, (3.53) describes the dynamics for Jardón-Kojakhmetov et al. fast controller.

Next, the controllers proposed in this chapter have been simulated in order to test the performance of the control law according to the mathematical description of the 2DoF Quanser manipulator robot. The explicit description of the PH controllers proposed in this chapter and necessary to the simulations can be found in the next chapter.

Chapter 4

Simulations.

In this chapter, the two proposed PH controllers have been simulated in order to prove the validity of the control law. For this, a Matlab code have been implemented to simulate the behavior of the 2DoF Quanser manipulator robot, and the explicit equations described in the previous chapter are provided. Similar experiments have been carried out in Jardón-Kojakhmetov et al. (2017) for the Quanser manipulator and in Reyes-Báez et al. (2016) for a 3DoF Scara manipulator robot.

4.1 Explicit description of the controllers.

In this section the equations theoretically described in Chapter 3 have been developed in order to get the explicit description for each controller for the rigid and flexible configuration of the 2DoF Quanser manipulator robot. The expressions presented here have been achieved by the Matlab implementation of the system, and are provided to ease the future analysis of such controllers.

4.1.1 Rigid model explicit description.

In Dirksz (2011) a set of simulations have been carried out in order to prove the response of the manipulator implementing a controller using only position measurements, while in van Logtestijn (2010) the same controllers have been implemented in order to experimentally test the response of the system. Even tough the system parameters used in both documents are slightly different, up to the author experience the parameters used by van Logtestijn (2010) are closer to the actual parameters of the physical plant. Hence, Table 4.1 shows the system parameters as proposed by van Logtestijn (2010).

Table 4.1 Parameters values for the 2DoF Quanser manipulator

Parameter	Value	Parameter	Value
m_1	1.9585	r_1	0.2
m_2	0.1504	r_2	0.25
I_1	0.23041858	l_1	0.343
I_2	0.010724	l_2	0.275

According to the parameters in Table 4.1, the explicit description for the inertia matrix given in (3.5) is

$$M(q) = \begin{bmatrix} 0.0257936cos(q_2) + 0.346577 & 0.0128968cos(q_2) + 0.020124 \\ 0.0128968cos(q_2) + 0.020124 & 0.020124 \end{bmatrix}, \tag{4.1}$$

$$M(q) = \begin{bmatrix} M_{11} & M_{12} \\ M_{21} & M_{22} \end{bmatrix}. \tag{4.2}$$

With such explicit description of the inertia matrix, the Hamiltonian given by (3.1) for the rigid model is described in terms of

$$H(q,p) = p_1 \left(\frac{M_{11}p_1}{2} + \frac{M_{21}p_2}{2} \right) + p_2 \left(\frac{M_{12}p_1}{2} + \frac{M_{22}p_2}{2} \right), \tag{4.3}$$

and the derivatives for the Hamiltonian in (4.3) are given by

$$\frac{\partial H(q,p)}{\partial q_1} = 0, \tag{4.4}$$

$$\frac{\partial H(q,p)}{\partial q_2} = p_1 \left(\frac{p_1 \frac{\partial M_{11}}{\partial q_2}}{2} + \frac{p_2 \frac{\partial M_{21}}{\partial q_2}}{2} \right) + p_2 \left(\frac{p_1 \frac{\partial M_{12}}{\partial q_2}}{2} + \frac{p_2 \frac{\partial M_{22}}{\partial q_2}}{2} \right), \tag{4.5}$$

$$\frac{\partial H(q,p)}{\partial p_1} = p_1 M_{11} + \frac{p_2 M12}{2} + \frac{p_2 M21}{2}, \tag{4.6}$$

$$\frac{\partial H(q,p)}{\partial p_2} = p_2 M_{22} + \frac{p_1 M21}{2} + \frac{p_1 M12}{2}. \tag{4.7}$$

With the derivatives of the Hamiltonian in (4.4), (4.5), (4.6) and (4.7) and the explicit inertia matrix in (4.1) the rigid model for the 2DoF Quanser robot can be represented in terms of PH variables, according to the structure proposed in (3.6).

4.1.2 Flexible model explicit description.

For the flexible configuration several changes in the mathematical model are made in order to control the displacement between the links and the motor positions, as was stated in Chapter 3.

In Reyes-Báez et al. (2017) as well as in Jardón-Kojakhmetov et al. (2017) an expanded inertia matrix is presented, as it is proposed in (3.29) and (3.45) respectively. For the Reyes-Báez et al. multi-scale controller, the expanded inertia matrix (3.29) has been described by

$$M_{E1} = \begin{bmatrix} M_{11} & M_{12} & 0 & 0 \\ M_{21} & M_{22} & 0 & 0 \\ 0 & 0 & I_{n1} & 0 \\ 0 & 0 & 0 & I_{n2}, \end{bmatrix}, \tag{4.8}$$

with M_{11}, M_{12}, M_{21} and M_{22} the same parameters described for the inertia matrix of the rigid model in (4.1) and (4.2), and I_{n1} and I_{n2} the inertia associated to the motors. For the Jardón-Kojakhmetov et al. multi-scale controller, the expanded inertia matrix (3.45) has been described by

$$M_{\epsilon 1} = \begin{bmatrix} I_{n1} + M_{11} & M_{12} & -\epsilon I_{n1} & 0 \\ M_{21} & I_{n2} + M_{22} & 0 & -\epsilon I_{n2} \\ -\epsilon I_{n1} & 0 & \epsilon^2 I_{n1} & 0 \\ 0 & -\epsilon I_{n2} & 0 & \epsilon^2 I_{n2}, \end{bmatrix}, \tag{4.9}$$

with ϵ as the small parameter for the slow-fast structure.

The Hamiltonian changes too, in order to add not only the kinetic energy, but also the potential energy stored in the springs as it is proposed in (3.9). With this, the explicit description for the Hamiltonian is

$$H(q,p,z,p_z) = \frac{K_1 \epsilon^2 z_1^2}{2} + \frac{K_2 \epsilon^2 z_2^2}{2} + \frac{p_1^2}{2} + \frac{p_2^2}{2} + \frac{p_{z1}^2}{2} + \frac{p_{z2}^2}{2}, \tag{4.10}$$

and the derivatives of the Hamiltonian in (4.10) are given by

$$\frac{\partial H(q,p,z,p_z)}{\partial q_1} = \frac{K_1(2q_1 - 2q_{m1})}{2}, \tag{4.11}$$

$$\frac{\partial H(q,p,z,p_z)}{\partial q_2} = \frac{K_2(2q_2 - 2q_{m2})}{2}, \tag{4.12}$$

$$\frac{\partial H(q,p,z,p_z)}{\partial z_1} = E^2 K_1 z_1, \tag{4.13}$$

$$\frac{\partial H(q,p,z,p_z)}{\partial z_2} = E^2 K_2 z_2, \tag{4.14}$$

$$\frac{\partial H(q,p,z,p_z)}{\partial p_1} = p_1 + \frac{2p_1 - 2p_{m1}}{2E^2}, \tag{4.15}$$

$$\frac{\partial H(q,p,z,p_z)}{\partial p_2} = p_2 + \frac{2p_2 - 2p_{m2}}{2E^2}, \tag{4.16}$$

$$\frac{\partial H(q,p,z,p_z)}{\partial p_{z1}} = p_{z1}, \tag{4.17}$$

$$\frac{\partial H(q,p,z,p_z)}{\partial p_{z2}} = p_{z2}. \tag{4.18}$$

With the derivatives of the Hamiltonian in (4.11), (4.12), (4.13), (4.14), (4.15), (4.16), (4.17) and (4.18) and the inertia matrix given by (4.8) and (4.9), the flexible model for the 2DoF Quanser robot can be represented in term of PH variables, with the proposed structure in (3.14).

4.1.3 Reyes-Báez et al. multi-scale controller explicit description.

In this section the equations theoretically proposed in Reyes-Báez et al. (2016) and Spong (1990) and described in Chapter 3 have been developed in order to get the explicit description for the Reyes-Báez et al. multi-scale controller.

First, a suitable system error is proposed in (3.30) with the position error described by

$$\tilde{q} = \begin{bmatrix} q_1 - q_{d1} \\ q_2 - q_{d2} \end{bmatrix} = \begin{bmatrix} q_1 - 0.1667(\pi \sin(0.2t)) \\ q_2 - 0.1667(\pi \sin(0.4t)) \end{bmatrix}. \tag{4.19}$$

Moreover, for the momenta error in (3.30) the parameter p_r defined in (3.33) is described by

$$p_r = \begin{bmatrix} \dot{q}_{d1} M_{11} + \dot{q}_{d2} M_{12} - \Lambda_1 \tilde{q}_1 \\ \dot{q}_{d1} M_{21} + \dot{q}_{d2} M_{22} - \Lambda_2 \tilde{q}_2 \end{bmatrix}. \tag{4.20}$$

Now, for the description of the first component of the Reyes-Báez et al. slow controller as defined in (3.38) the last two parameters are the same derivatives of the Hamiltonian described in (4.4), (4.5), (4.6) and (4.7), while the first parameter needed is given by

$$\dot{p}_r = \begin{bmatrix} \dot{q}_{d1}\dfrac{\partial M_{11}}{\partial t} + \dot{q}_{d2}\dfrac{\partial M_{12}}{\partial t} + \ddot{q}_{d1}M_{11} + \ddot{q}_{d2}M_{12} - \Lambda_1(\dot{q}_1 - \dot{q}_{d1}) \\ \dot{q}_{d1}\dfrac{\partial M_{21}}{\partial t} + \dot{q}_{d2}\dfrac{\partial M_{22}}{\partial t} + \ddot{q}_{d1}M_{21} + \ddot{q}_{d2}M_{22} - \Lambda_2(\dot{q}_2 - \dot{q}_{d2}) \end{bmatrix}. \tag{4.21}$$

Furthermore, for the second component of the slow controller as defined in (3.39) the first term is also defined by the derivatives of the Hamiltonian in in (4.6) and (4.7). For the second term, the explicit description corresponds to

$$M^{-1}(q)\Lambda\tilde{q} = \begin{bmatrix} \dfrac{L_1\tilde{q}_1M_{22} - L_2\tilde{q}_2M_{12}}{M_{11}M_{22} - M_{12}M_{21}} \\ \dfrac{L_2\tilde{q}_2M_{11} - L_1\tilde{q}_1M_{21}}{M_{11}M_{22} - M_{12}M_{21}} \end{bmatrix}, \tag{4.22}$$

and for the final term, the explicit description is given by

$$\frac{\partial}{\partial q}({p_r}^{\top}M^{-1}(q)\sigma) = \frac{\partial}{\partial q}\left(\left(\frac{p_{r1}M_{22} - p_{r2}M_{21}}{M_{11}M_{22} - M_{12}M_{21}}\right)\sigma_1 - \left(\frac{p_{r1}M_{12} - p_{r2}M_{11}}{M_{11}M_{22} - M_{12}M_{21}}\right)\sigma_2\right). \tag{4.23}$$

Finally, the explicit description for the Spong fast controller in (3.54) is

$$U_{f_S} = \begin{bmatrix} k_{v1}(\dot{q}_1 - \dot{q}_{m1}) \\ k_{v2}(\dot{q}_2 - \dot{q}_{m2}) \end{bmatrix}. \tag{4.24}$$

The explicit description for this controller is computed using the software Matlab to achieve the results presented in this chapter.

4.1.4 Jardón-Kojakhmetov et al. multi-scale controller explicit description.

In this section the equations theoretically proposed in Dirksz and Scherpen (2013) and described in Chapter 3 have been developed in order to get the explicit description for the Dirksz and Scherpen controller. First, a suitable error system is proposed. As well as for the Reyes-Báez et al. controller, the position error is defined by (4.19).

Recalling the structure of the proposed slow controller in (3.52), the control input is formed by five different terms. The explicit description for each term is described by

$$M(q)\ddot{q}_d = \begin{bmatrix} \ddot{q}_{d1}M_{11} + \ddot{q}_{d2}M_{12} \\ \ddot{q}_{d1}M_{21} + \ddot{q}_{d2}M_{22} \end{bmatrix}, \tag{4.25}$$

$$\frac{\partial(M(q)\dot{q})}{\partial q}\dot{q} = \begin{bmatrix} \dfrac{\partial(M_{11}\dot{q}_{d1} + M_{12}\dot{q}_{d2})}{\partial q_1}\dot{q}_{d1} + \dfrac{\partial(M_{11}\dot{q}_{d1} + M_{12}\dot{q}_{d2})}{\partial q_2}\dot{q}_{d2} \\ \dfrac{\partial(M_{12}\dot{q}_{d1} + M_{22}\dot{q}_{d2})}{\partial q_1}\dot{q}_{d1} + \dfrac{\partial(M_{21}\dot{q}_{d1} + M_{22}\dot{q}_{d2})}{\partial q_2}\dot{q}_{d2} \end{bmatrix}, \tag{4.26}$$

$$\frac{\partial \dot{q}^\top M(q)\dot{q}}{\partial q} = \begin{bmatrix} \dfrac{\partial(\dot{q}_{d1}(M_{11}\dot{q}_{d1} + M_{21}\dot{q}_{d2}) + \dot{q}_{d2}(M_{12}\dot{q}_{d1} + M_{22}\dot{q}_{d2}))}{\partial q_1} \\ \dfrac{\partial(\dot{q}_{d1}(M_{11}\dot{q}_{d1} + M_{21}\dot{q}_{d2}) + \dot{q}_{d2}(M_{12}\dot{q}_{d1} + M_{22}\dot{q}_{d2}))}{\partial q_2} \end{bmatrix}, \tag{4.27}$$

$$K_p\bar{q} = \begin{bmatrix} K_{p1}(q_1 - q_{d1}) \\ K_{p2}(q_2 - q_{d2}) \end{bmatrix}, \tag{4.28}$$

$$K_c v = \begin{bmatrix} K_{c1}(q_1 - q_{d1} - q_{c1}) \\ K_{c2}(q_2 - q_{d2} - q_{c2}) \end{bmatrix}, \tag{4.29}$$

and the explicit dynamics for the slow controller in (3.51) are

$$\dot{q}_{c1} = \begin{bmatrix} \dfrac{K_{c1}(q_1 - q_{d1} - q_{c1})}{K_{d1}} \\ \dfrac{K_{c2}(q_2 - q_{d2} - q_{c2})}{K_{d2}} \end{bmatrix}. \tag{4.30}$$

Now, for the Jardón-Kojakhmetov et al. fast controller in (3.53), the explicit description is given by

$$U_{f_J} = \begin{bmatrix} L_{c1}(z_{c1} - z_1) - L_{p1}z_1 \\ L_{c2}(z_{c2} - z_2) - L_{p2}z_2 \end{bmatrix}, \tag{4.31}$$

while for the explicit dynamic for the fast controller in (3.54) is

$$\dot{z}_c = \begin{bmatrix} \dfrac{L_{c1}(z_1 - z_{c1})}{L_{d1}} \\ \dfrac{L_{c2}(z_2 - z_{c2})}{L_{d2}} \end{bmatrix}. \tag{4.32}$$

The explicit description for this controller is computed using the software Matlab to achieve the results presented in this chapter.

Table 4.2 Reyes-Báez et al. controller parameters

Parameter	Value
K_{d1}	-20
K_{d2}	-2.8
Λ_1	35
Λ_2	3.1

4.2 Rigid model simulations.

In this section the proposed PH controllers have been simulated to test the response of the system with the rigid configuration. For this, the desired position have been set to follow a sinusoidal wave (trajectory tracking simulation), and the theoretical equations of Chapter 3 have been implemented in the explicit form presented in Section 4.1 to achieve the results. Similar experiments for the rigid configuration have been carried out in Dirksz (2011) and Reyes-Báez et al. (2016). The explicit description of this controller can be found in Section 4.1.

4.2.1 Reyes-Báez et al. controller.

In this section the Reyes-Báez et al. controller has been simulated to test the validity of the proposed control law. Recalling Chapter 3 for the rigid configuration the system has a PH structure described in (3.6), while the Dirksz and Scherpen slow controller has been described in (3.37), (3.38) and (3.39). For the explicit description of the rigid model we recall the derivatives of the Hamiltonian in (4.4), (4.5), (4.6) and (4.7), while for the controller explicit description we recall (4.21) and (4.23).

While the system parameters are given by Table 4.1, there is no method to calculate the values for K_d and Λ for the controller. In Dirksz (2011) and van Logtestijn (2010) a systematic trial-and-error procedure is used in order to find the optimal values. In that sense, the proposed parameters used for this simulations are given by Table 4.2.

For the tracking control, a twice differentiable trajectory in the form of $q_d = c\sin(\omega t)$ is chosen, with parameters $c_1 = 30°$ and $w_1 = 0.2$ for J_1 and $c_2 = 30°$ and $w_1 = 0.4$ for J_2. Furthermore, all the initial parameters were set to zero, this is [q_1, q_2, p_1, p_2] = [0 0 0 0].

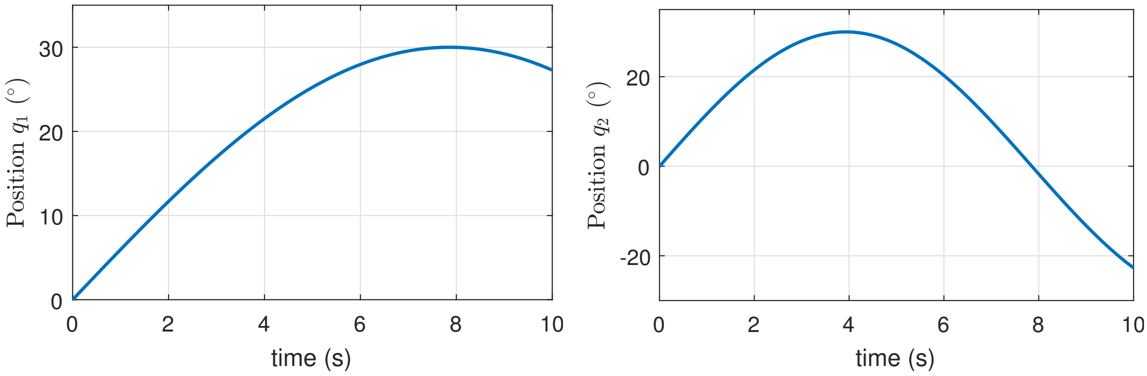

(a) (b)

Figure 4.1 Trajectory tracking simulation, rigid configuration, Reyes-Báez et al. controller: (a) Position for J_1. (b) Position for J_2.

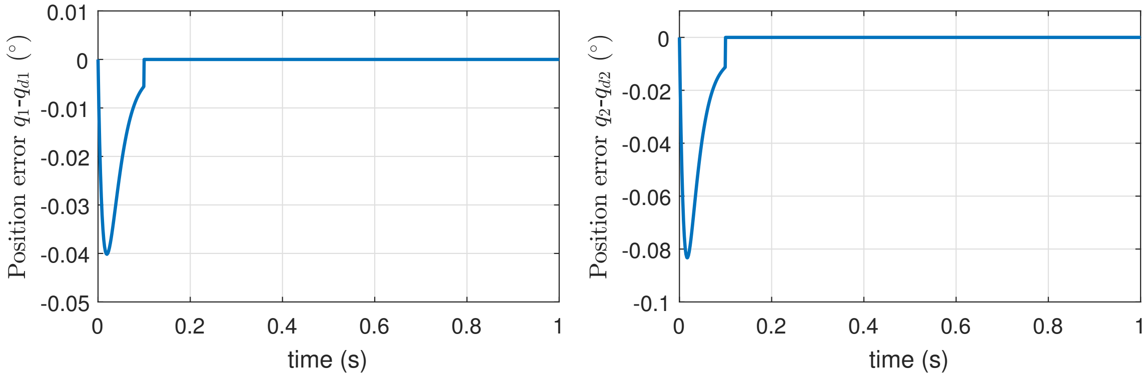

(a) (b)

Figure 4.2 Position error, trajectory tracking simulation, rigid configuration, Reyes-Báez et al. controller: (a) Position error for J_1. (b) Position error for J_2.

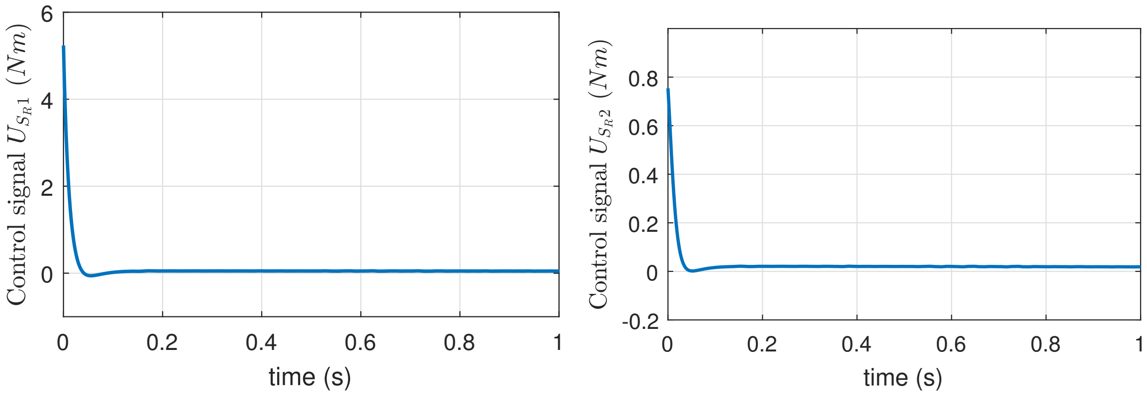

(a) (b)

Figure 4.3 Control signal, trajectory tracking simulation, rigid configuration, Reyes-Báez et al. controller: (a) Control signal for J_1. (b) Control Signal for J_2.

Table 4.3 Dirksz and Scherpen controller parameters

Parameter	Value
K_{p1}	5000
K_{p2}	600
K_{c1}	3000
K_{c2}	400
K_{d1}	3
K_{d2}	3

The results of the simulations are shown in Figures 4.1, 4.2 and 4.3. The position error of the articulations is able to converge to zero in less than $0.2s$ in both articulations, without any visible overshoot as can be seen in Figure 4.2, while the energy used by the controller to stabilize the system is very low as is shown in Figure 4.3.

4.2.2 Dirksz and Scherpen controller.

In this section the Dirksz and Scherpen controller has been simulated to test the validity of the proposed control law. Recalling Chapter 3 for the rigid configuration the system has a PH structure described in (3.6), while the Dirksz and Scherpen slow controller has been described in (3.52). For the explicit description of the rigid model we recall the derivatives of the Hamiltonian in (4.4), (4.5), (4.6) and (4.7), while for the explicit description of the controller we recall (4.25), (4.26), (4.27), (4.28) and (4.29).

Once again, a systematic trial-and-error procedure is used in order to find the optimal values for the controllers. In that sense, the proposed parameters used for this simulations are given by Table 4.3

As in the previous simulation, for the tracking control, a twice differentiable trajectory in the form of $q_d = c\sin(\omega t)$ is chosen, with parameters $c_1 = 30^\circ$ and $w_1 = 0.2$ for J_1 and $c_2 = 30^\circ$ and $w_1 = 0.4$ for J_2. Furthermore, all the initial parameters were set to zero, this is $[q_1, q_2, p_1, p_2, q_{c1}, q_{c2}] = [0\ \ 0\ \ 0\ \ 0\ \ 0\ \ 0]$.

The results of the simulations are shown in Figures 4.4, 4.5 and 4.6. This controller have a bigger settling time, and bigger oscillations in the transient state than the Reyes-Báez et al. (2016) controller. The position error of the articulations is able to converge to zero without oscillations approximately at $1s$ in both articulations as can be seen in Figure 4.5, while the energy used by the controller follows the same pattern as it is shown in Figure 4.6.

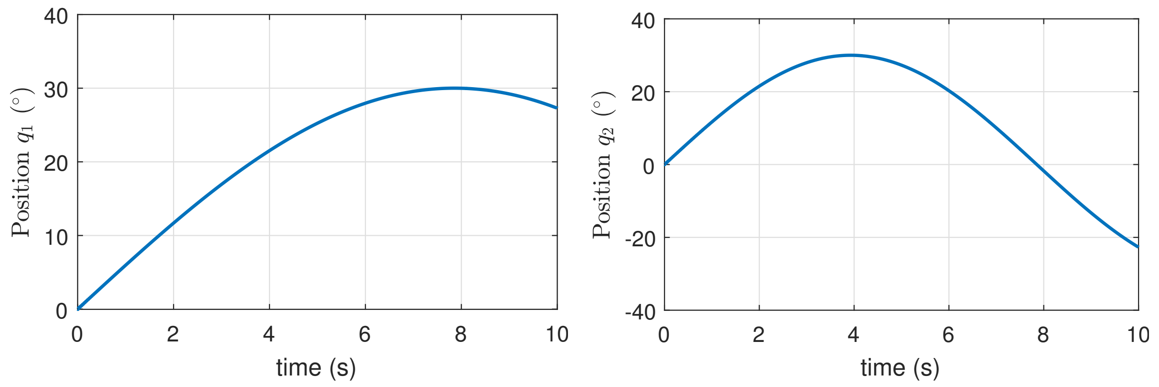

(a) (b)

Figure 4.4 Trajectory tracking simulation, rigid configuration, Dirksz and Scherpen controller: (a) Position for J_1. (b) Position for J_2.

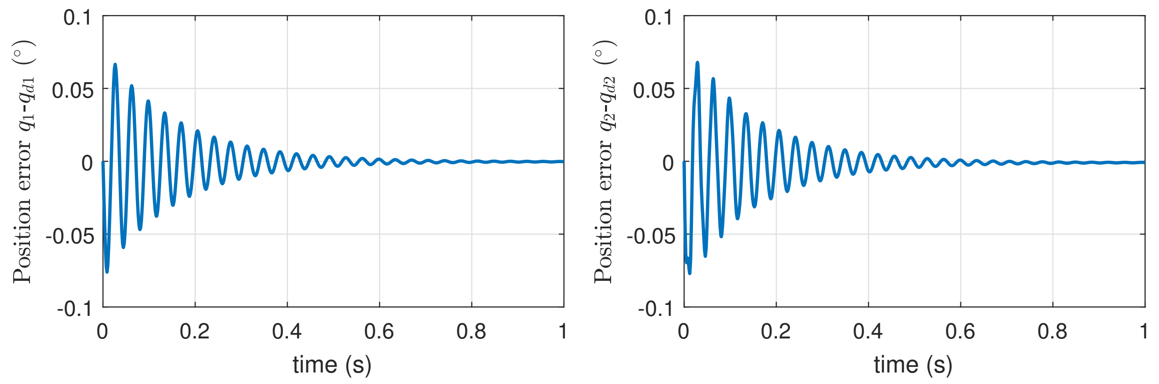

(a) (b)

Figure 4.5 Position error, trajectory tracking simulation, rigid configuration, Dirksz and Scherpen controller: (a) Position error for J_1. (b) Position error for J_2.

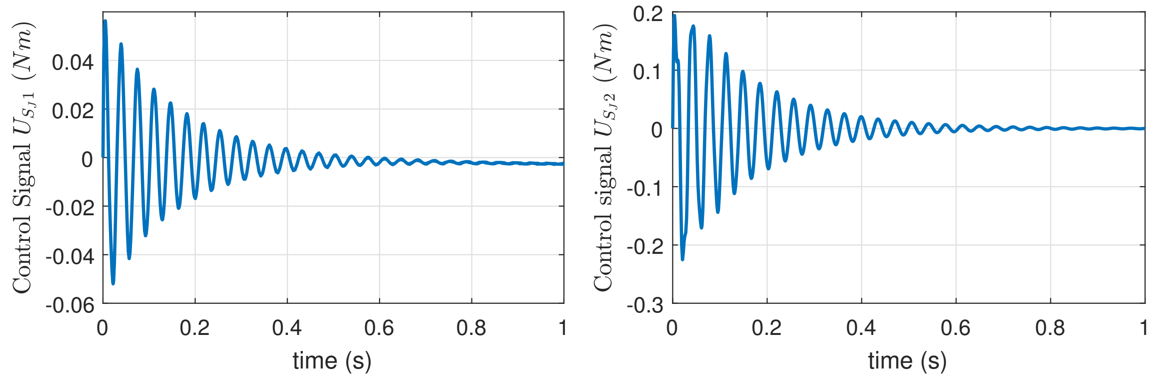

(a) (b)

Figure 4.6 Control signal, trajectory tracking simulation, rigid configuration, Dirksz and Scherpen controller: (a) Control signal for J_1. (b) Control Signal for J_2.

Table 4.4 Jardón-Kojakhmetov et al. multi-scale controller parameters

Slow parameter	Value
K_{d1}	-5.5
K_{d2}	-1
Λ_1	50
Λ_2	5
K_{v1}	-14
K_{v2}	-16

4.3 Flexible model simulations.

In this section the proposed PH controllers have been simulated to test the response of the system with the flexible configuration. For this, the desired position have been set to follow a sinusoidal wave (trajectory tracking simulation). Similar experiments for the flexible configuration have been carried out in Jardón-Kojakhmetov et al. (2017).

4.3.1 Reyes-Báez et al. multi-scale controller.

In this section the Reyes-Báez et al. controller has been simulated to test the validity of the proposed control law. Recalling Chapter 3 for the flexible configuration the system has a PH structure described in (3.16). Moreover, the Reyes-Báez et al. slow controller has been described in (3.37), (3.38) and (3.39), while the fast controller has been proposed in (3.54). For the explicit description of the rigid model we recall the derivatives of the Hamiltonian in (4.11), (4.12), (4.13), (4.15), (4.16), (4.17) and (4.18) and the expanded inertia matrix in (4.8) while for the explicit description of the controller we recall (4.21), (4.23) and (4.24).

Like for the rigid configuration there is no method to calculate the values for K_v, K_d and Λ for the controller, thus the same systematic trial-and-error procedure is used in order to find the optimal values. Then, the system parameters are given by Table 4.1 while the proposed parameters used for this controller are given by Table A.1.

For the tracking control, a twice differentiable trajectory in the form of $q_d = c\sin(\omega t)$ is chosen, with parameters $c_1 = 30°$ and $w_1 = 0.2$ for J_1 and $c_2 = 30°$ and $w_1 = 0.4$ for J_2. Furthermore, all the initial parameters were set to zero, this is [q_1, q_2, z_1, z_2, p_1, p_2, p_{z1}, p_{z2}] = [0 0 0 0 0 0 0 0].

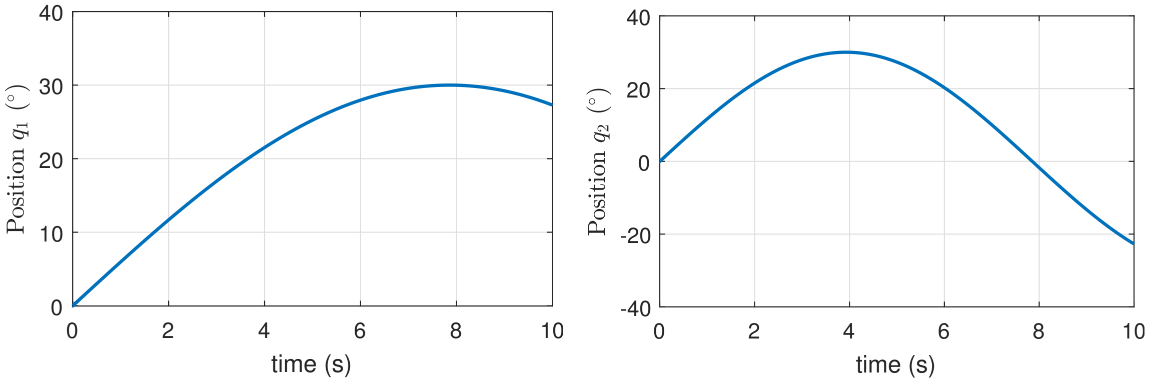

(a) (b)

Figure 4.7 Trajectory tracking simulation, flexible configuration, Reyes-Báez et al. multi-scale controller: (a) Position for J_1. (b) Position for J_2.

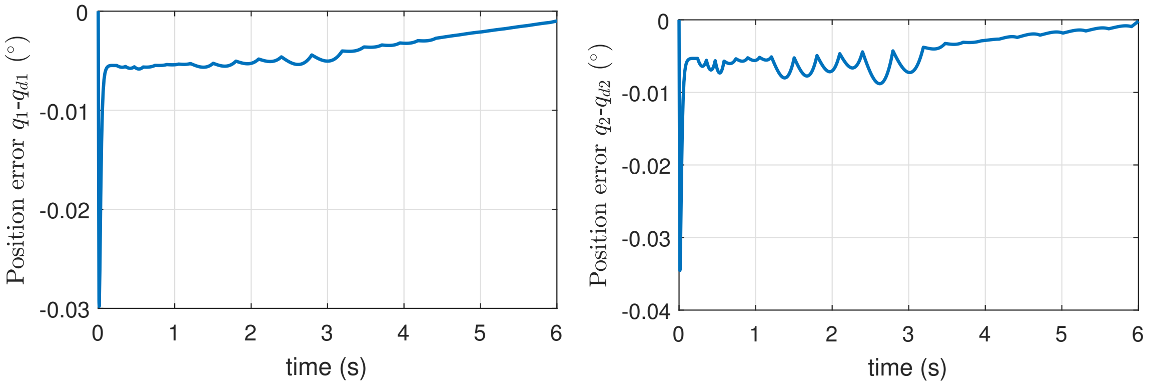

(a) (b)

Figure 4.8 Position error, trajectory tracking simulation, flexible configuration, Reyes-Báez et al. multi-scale controller: (a) Position error for J_1. (b) Position error for J_2.

As can be seen in Figure 4.8, the position error for the flexible model has roughly the same behavior with a fast settling time as in the rigid configuration. However, the position error is not able to converge completely to zero after that first fast slope and presents an important difference which is eliminated until six seconds had passed. On the other hand, Figure 4.9 shows a flexible error that can be dismissed due to the low magnitude of the signal, insignificant in comparison with the position error in Figure 4.8. Finally, Figures 4.10 and 4.11 shows the energy used by both the slow and the fast controllers. For the last, the magnitude of the energy used is a considerably lower than the energy used by the slow controller, due to the low flexible error.

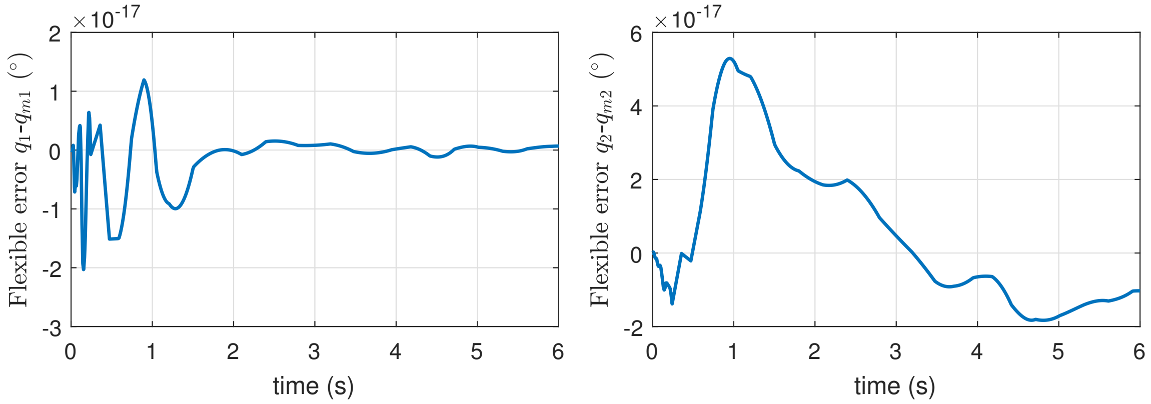

(a) (b)

Figure 4.9 Flexible error, trajectory tracking simulation, flexible configuration, Reyes-Báez et al. multi-scale controller: (a) Position error for J_1. (b) Position error for J_2.

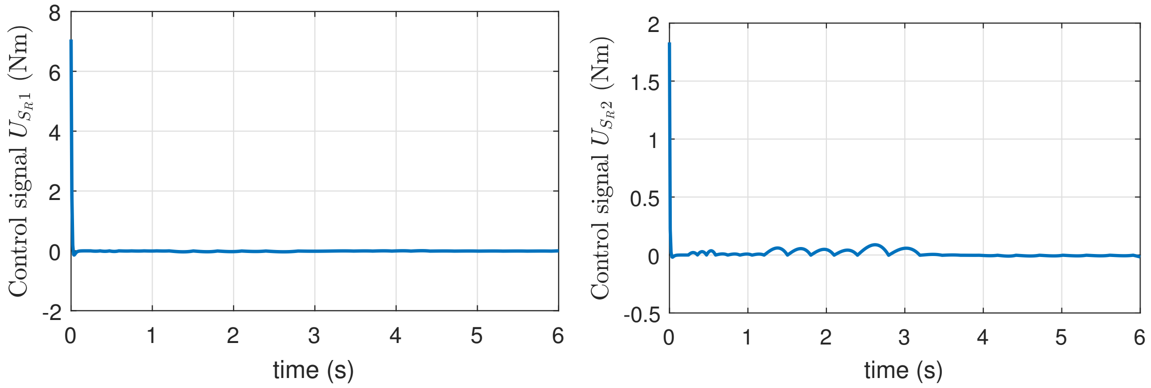

(a) (b)

Figure 4.10 Control signal, trajectory tracking simulation, flexible configuration, Reyes-Báez et al. slow controller: (a) Control signal for J_1. (b) Control signal for J_2.

4.3.2 Jardón-Kojakhmetov et al. multi-scale controller.

In this section the Jardón-Kojakhmetov et al. controller has been simulated to test the validity of the proposed control law. Recalling Chapter 3 for the flexible configuration the system has a PH structure described in (3.16). Moreover, the Dirksz and Scherpen slow controller has been presented in (3.52) while the fast controller has been described in (3.53). For the explicit description of the rigid model we recall the derivatives of the Hamiltonian in (4.11), (4.12), (4.13), (4.15), (4.16), (4.17) and (4.18) and the expanded inertia matrix in (4.9) while for the explicit description of the controller we recall (4.25), (4.26), (4.27), (4.28), (4.29) and (4.31).

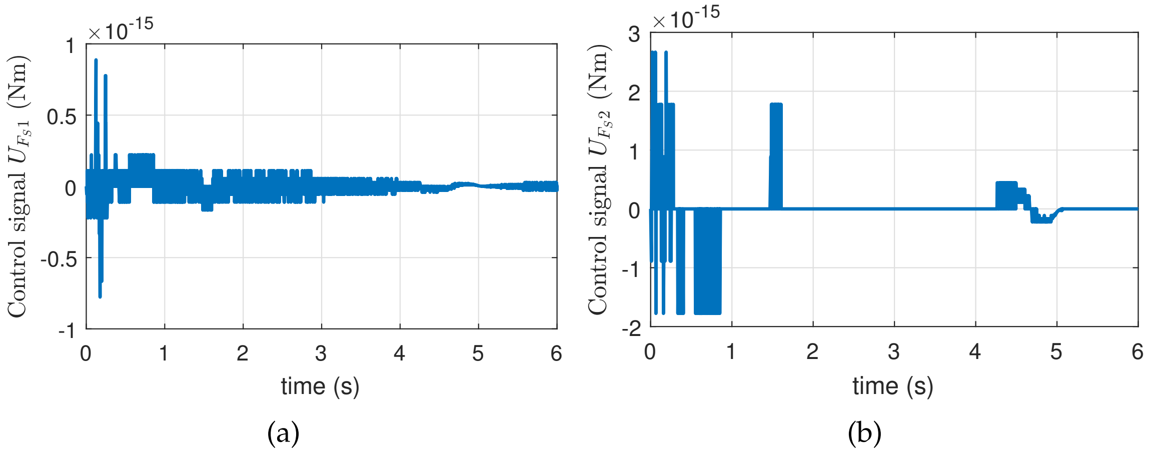

Figure 4.11 Control signal, trajectory tracking simulation, flexible configuration, Spong fast controller: (a) Control signal J_1. (b) Control signal J_2.

Like for the rigid configuration there is no method to calculate the values for K_d, K_p, K_c, L_d, L_p and L_c for the controller, thus the same systematic trial-and-error procedure is used in order to find the optimal values. Hence, the system parameters are given by Table 4.1 while the proposed parameters used for this controller are given by Table A.1.

For the tracking control, a twice differentiable trajectory in the form of $q_d = c\sin(\omega t)$ is chosen, with parameters $c_1 = 30°$ and $w_1 = 0.2$ for J_1 and $c_2 = 30°$ and $w_1 = 0.4$ for J_2. Furthermore, all the initial parameters were set to zero, this is [q_1, q_2, z_1, z_2, p_1, p_2, p_{z1}, p_{z2}, q_{c1}, q_{c2}, z_{c1}, z_{c2}] = [0 0 0 0 0 0 0 0 0 0 0 0].

As can be seen in Figure 4.13, according to the parameters used the settling time for the Dirksz and Scherpen (2013) slow controller is bigger in comparison with the simulations for the same experiment for the rigid configuration, increasing thrice it's value. Besides, it keeps the same behavior for the transient state for the position error. Furthermore, Figure 4.14 shows the flexible error of the joint, converging

Table 4.5 Jardón-Kojakhmetov et al. multi-scale controller parameters

Slow parameter	Value	Fast parameter	Value
K_{p1}	300	L_{p1}	200
K_{p2}	200	L_{p2}	100
K_{c1}	100	L_{c1}	300
K_{c2}	100	L_{c2}	300
K_{d1}	3	L_{d1}	3
K_{d2}	3	L_{d2}	3

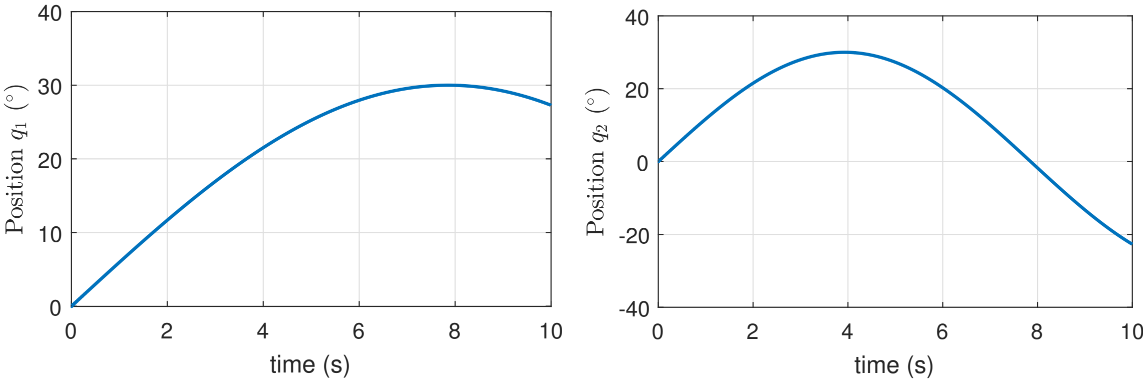

(a) (b)

Figure 4.12 Trajectory tracking simulation, flexible configuration, Jardón-Kojakhmetov et al. multi-scale controller: (a) Position for J_1. (b) Position for J_2.

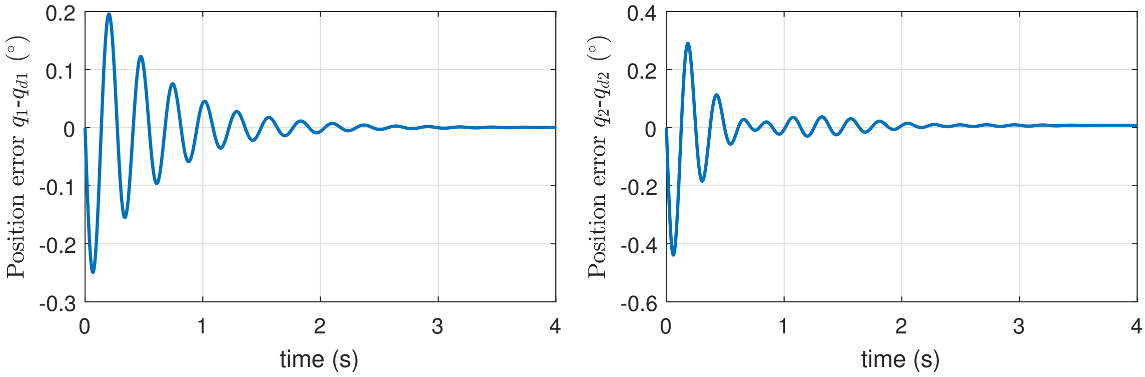

(a) (b)

Figure 4.13 Position error, trajectory tracking simulation, flexible configuration, Jardón-Kojakhmetov et al. multi-scale controller: (a) Position error for J_1. (b) Position error for J_2.

to zero after small oscillations that can be despised due to the proportionality in comparison with the position error in Figure 4.13. Finally, Figures 4.15 and 4.16 shows the energy used by both the slow and the fast controllers, which are similar in their magnitude, due to the fact that both controllers have the same passivity-based PH structure.

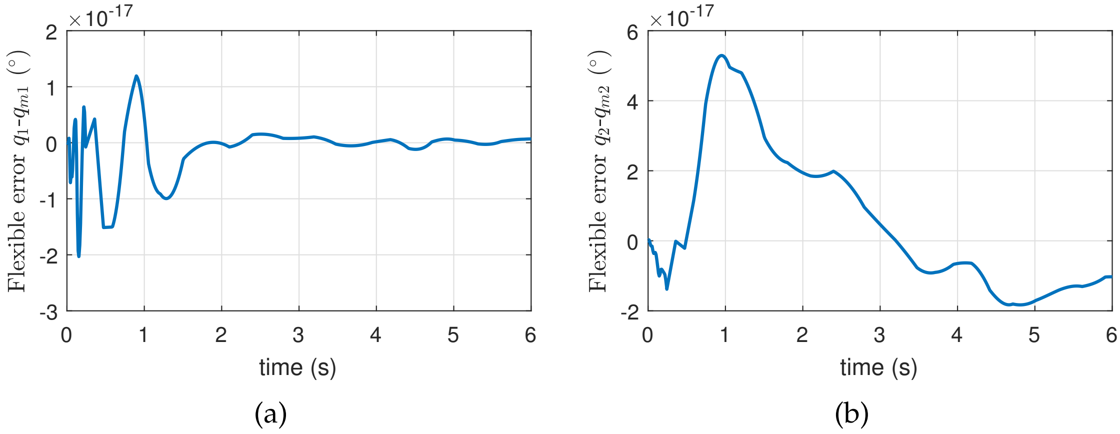

Figure 4.14 Flexible error, trajectory tracking simulation, flexible configuration, Jardón-Kojakhmetov et al. controller: (a) J_1 Position error. (b) J_2 Position error for.

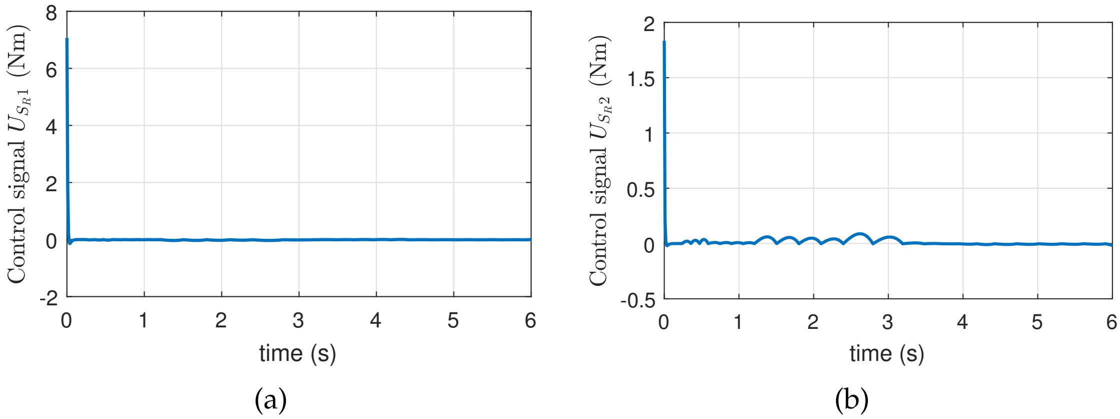

Figure 4.15 Control signal, trajectory tracking simulation, flexible configuration, Dirksz and Scherpen slow controller: (a) J_1 Control signal for. (b) J_2 Control signal for.

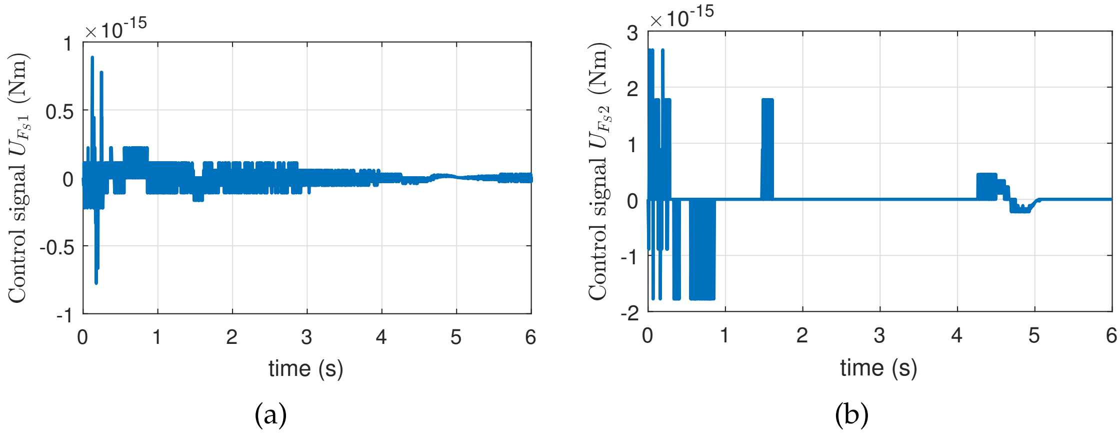

Figure 4.16 Control signal, trajectory tracking simulation, flexible configuration, Jardón-Kojakhmetov et al. fast controller: (a) Control signal J_1. (b) Control signal J_2.

4.4 Chapter 4 concluding remarks.

The theoretical equations defined in Chapter 3 have been developed and expanded in Section 4.1 in order to adjust them to the 2DoF Quanser model, using the system parameters provided by van Logtestijn (2010) and the explicit equations achieved after the implementation of the controllers in the software Matlab.

In Section 4.2, recalling the PH structure for the rigid system in (3.6) and the explicit description of the system in Section 4.1, the Reyes-Báez et al. controller in (3.37), (3.38) and (3.39) and the Dirksz and Scherpen controller in (3.52) have been simulated using the software Matlab. The results are similar to the simulations already performed in Reyes-Báez et al. (2016) for the first and in Jardón-Kojakhmetov et al. (2017) and van Logtestijn (2010) for the second PH controller, which proves that the control law should be able to stabilize the movement of the system.

In Section 4.3, recalling the PH structure for the rigid system in (3.16) and the explicit description of the system in Section 4.1, the multi-scale controller formed by the Reyes-Báez et al. slow controller in (3.37), (3.38) and (3.39) and the Spong fast controller in (3.54), and the multi-scale controller formed by Dirksz and Scherpen controller in (3.52) and the Jardón-Kojakhmetov et al. fast controller in (3.53), have been simulated using the software Matlab. For the second controller the results are similar to those presented in Jardón-Kojakhmetov et al. (2017) , which proves that the control law should be able to stabilize the movement of the system.

Next, using the explicit description of the equations presented in this chapter, the results of the implementation of the controller in th physical plant are presented.

Chapter 5

Experimental results.

This chapter shows the results obtained after the implementation of the different controllers for both, the rigid model and the flexible model. Before starting the experiment, the different controllers have to be implemented trough a a real-time control interface using Simulink. The software actuates the robot and reads the encoder's position measurements for the joints. The Simulink diagram for the proposed controllers can be seen in Appendix B. There are no sensors for the momenta, so a derivative filter is used to calculate the velocity and therefore the momenta.

There are some restrictions regarding the input given to the robot, as the maximum voltage and current for the motors. As can be seen in the robot specifications in Appendix A, the maximal electrical current for the motor #1 and motor #2 are $0.944A$ and $1.21A$ respectively. Furthermore, the current input I_R supplied to the motor obeys

$$I_R = \frac{\tau}{K_\tau G_R}, \tag{5.1}$$

where τ is the desired toque, K_τ is the torque constants and G_R is the gear ratio for the motor. The last two parameters can be found in Appendix A.

5.1 Rigid model.

In this section, the trajectory tracking controller for the 2R planar manipulator is tested in order to prove the performance of the proposed control law for a rigid robot. Two different experiments have been carried out in order to test the performance of the control law: the movement of the joints to a fixed position and the movement following a time-variant trajectory.

The joints for the manipulator were mechanically jammed in order to neglect the effects caused by the springs. However, a small difference between the position of the link and the position of the motor exists. For experimental purposes let us assume an ideal rigid model, that is $q = q_m$. Therefore, the position measured by the motor encoder will be used for the position of the links.

Recalling Chapter 3 for the rigid configuration the system has a PH structure described in (3.6) with the explicit equations for the derivatives of the Hamiltonian in (4.4), (4.5), (4.6) and (4.7). For the Reyes-Báez et al. controller described in (3.37), (3.38) and (3.39), the explicit equations can be found in (4.21) and (4.23), while for the Dirksz and Scherpen controller described in (3.52), the explicit equations can be found in (4.25), (4.26), (4.27), (4.28) and (4.29).

5.1.1 Set-point experiment.

For this test, both joints were set to a fixed position of 30° for J_1 and -30° for J_2. To avoid damages due to high peaks of current, the change of position have been set to follow a smooth trajectory using a sigmoid block function in Simulink. Now, for the Reyes-Báez et al. (2016) controller the parameters used have been set as $K_d = diag(-20, -2.6)$ and $\lambda = diag(35, 3.1)$, while for the Dirksz and Scherpen controller the parameters used have been set as $K_d = diag(3, 3)$, $K_c = diag(300, 40)$ and $K_p = diag(300, 50)$. The trajectory measured by the sensors in each articulations can be seen in Figure 5.2.

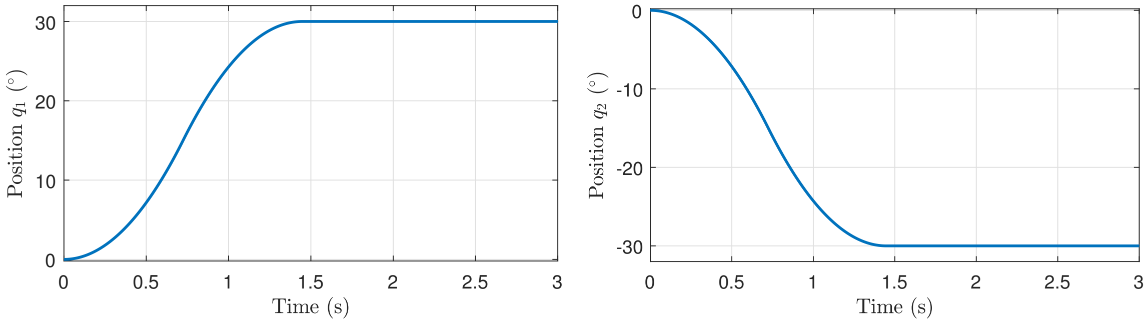

(a) (b)

Figure 5.1 Set-point experiment, rigid configuration: (a) Position trajectory for J_1. (b) Position trajectory for J_2

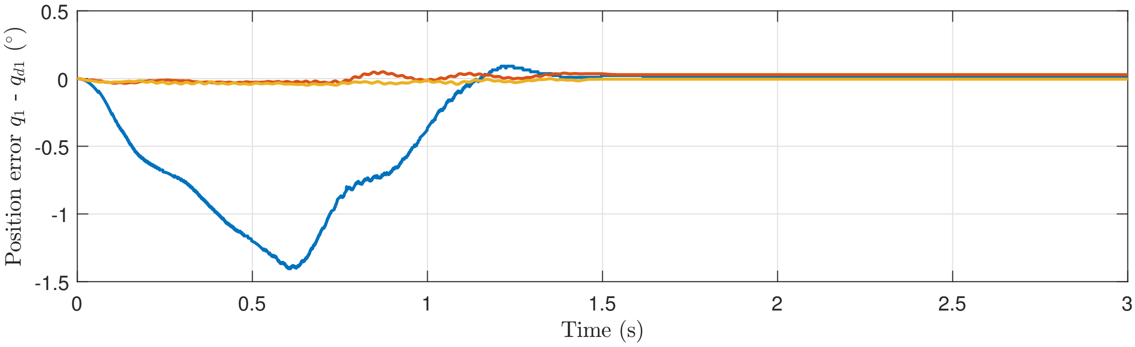

Figure 5.2 Position error comparison for J_1, set-point experiment, rigid configuration: LQR (blue), Reyes-Báez et al. (orange) and Dirksz and Scherpen (yellow).

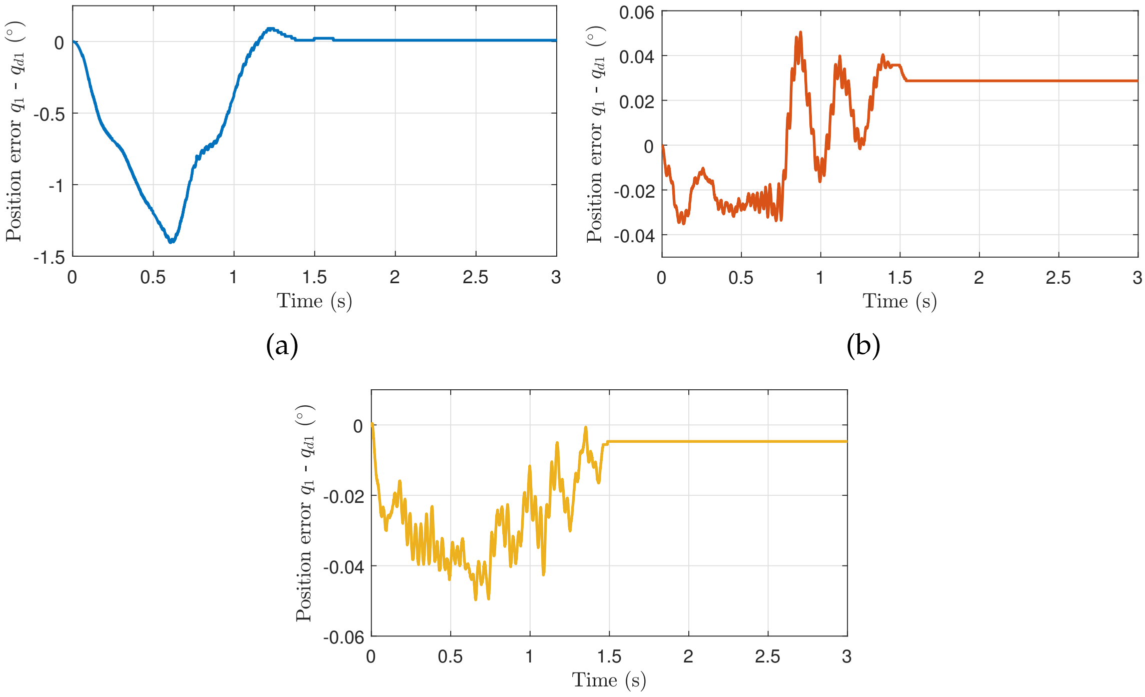

(a) (b)

(c)

Figure 5.3 Position error for J_1, set-point experiment, rigid configuration: (a) LQR. (b) Reyes-Báez et al.. (c) Dirksz and Scherpen.

Figures 5.2 and 5.3 show the position error for J_1. Both port-Hamiltonian controllers prove to have a better performance in the position error than the LQR controller proposed by Quanser. The position error for the Reyes-Báez et al. controller have a lower accuracy in comparison with Dirksz and Scherpen controller, while the transient behavior is similar in both controllers with an overshoot of 0.05°.

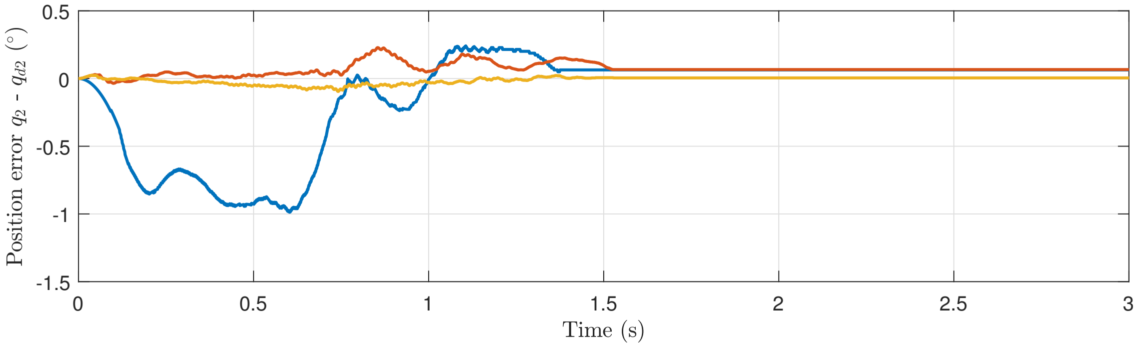

Figure 5.4 Position error comparison for J_2, set-point experiment, rigid configuration: LQR (blue), Reyes-Báez et al. (orange) and Dirksz and Scherpen (yellow).

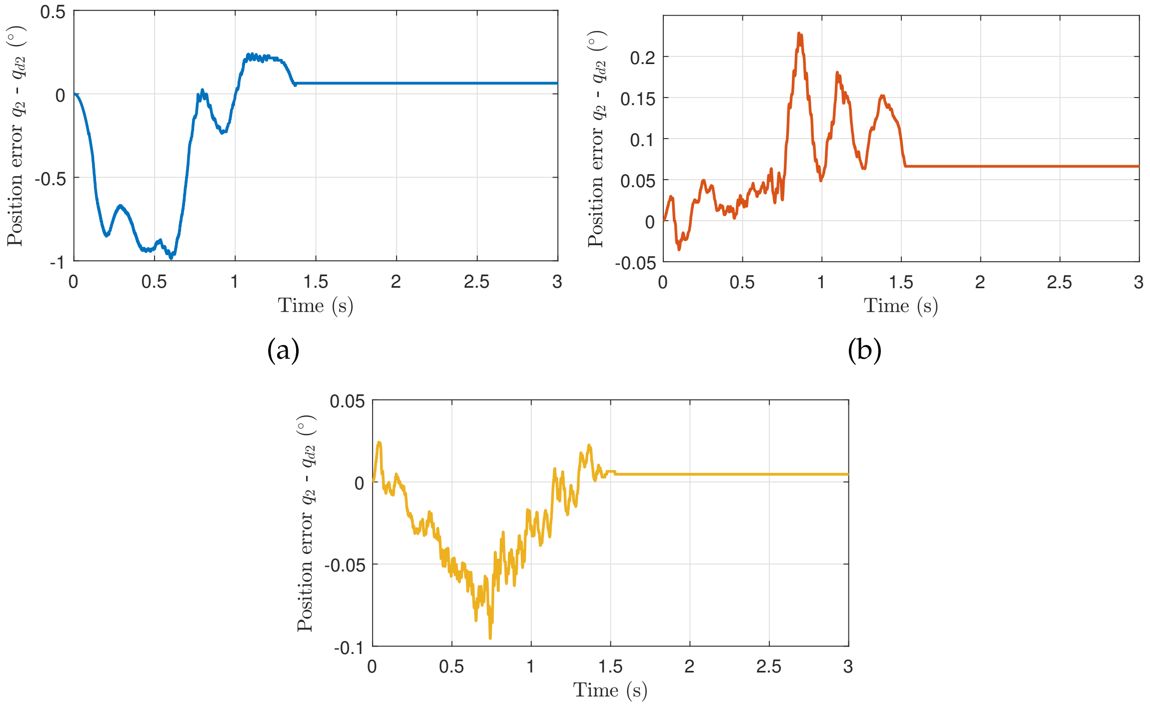

(a)

(b)

(c)

Figure 5.5 Position error for J_2, set-point experiment, rigid configuration: (a) LQR. (b) Reyes-Báez et al.. (c) Dirksz and Scherpen.

Figures 5.4 and 5.5 shows the position error for J_2. Like the results for J_1, both port-Hamiltonian controllers prove to have a better performance in the position error than the LQR controller proposed by Quanser. Once again, the position error for the Reyes-Báez et al. controller has a lower accuracy in comparison with Jardón-Kojakhmetov et al. controller. However, unlike the results for J_1 the transient behavior is slightly better for the Dirksz and Scherpen controller.

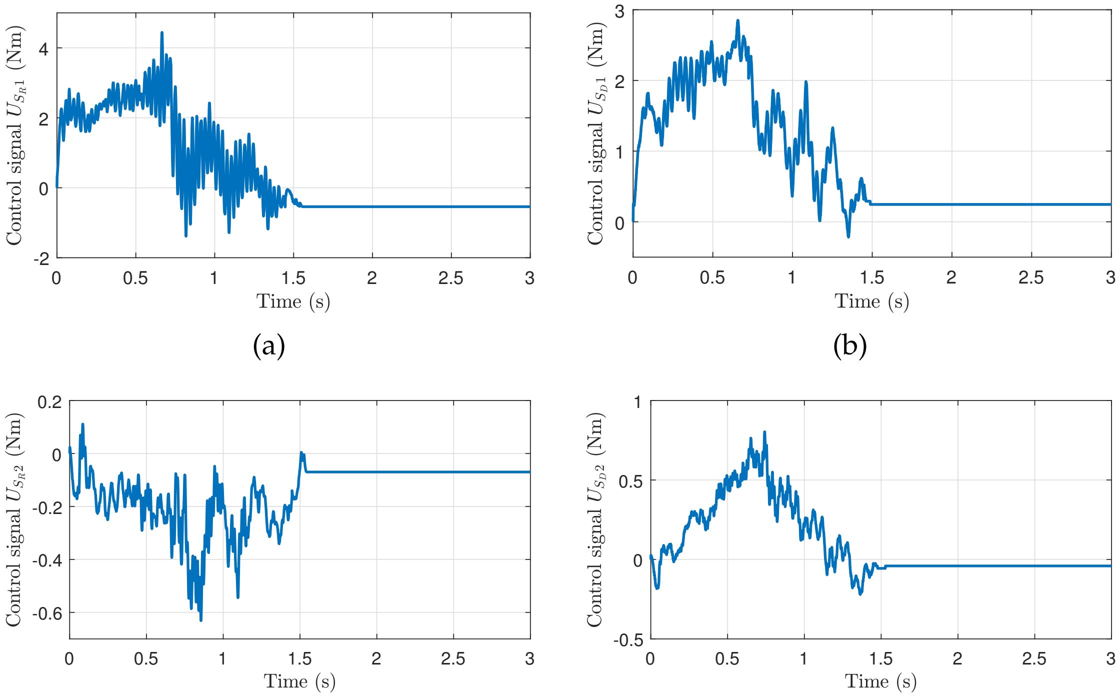

(a) (b)

(c) (d)

Figure 5.6 Control signal, set-point experiment, rigid configuration: (a) Reyes-Báez et al. controller for J_1. (b) Dirksz and Scherpen controller for J_1. (c) Reyes-Báez et al. controller for J_2. (d) Dirksz and Scherpen controller for J_2

Finally, Figure 5.6 shows the control signal created by the controller for J_1 and J_2, which converges at zero after the control action has stabilized the position error. As can be seen, the energy necessary to control the position for the manipulator is similar for both port-Hamiltonian controllers for J_1 and J_2.

5.1.2 Trajectory tracking experiment.

For this test, both joints were set to follow a sinusoidal trajectory described by the equations $c_1 sin(w_1 t)$ and $c_2 sin(w_2 t)$ respectively. Then, for J_2, the frequency of the movement were set to be twice as fast as the frequency for J_1. The amplitude of the movements was set to 30°. For the Reyes-Báez et al. (2016) controller the parameters used have been set as $K_d = diag(-20, -2.8)$ and $\lambda = diag(35,3.1)$, while for the Dirksz and Scherpen controller the parameters used have been set as $K_d = diag(3,3)$, $K_c = diag(300,40)$ and $K_p = diag(500,60)$. The trajectory measured by the sensors can be seen in Figure 5.7.

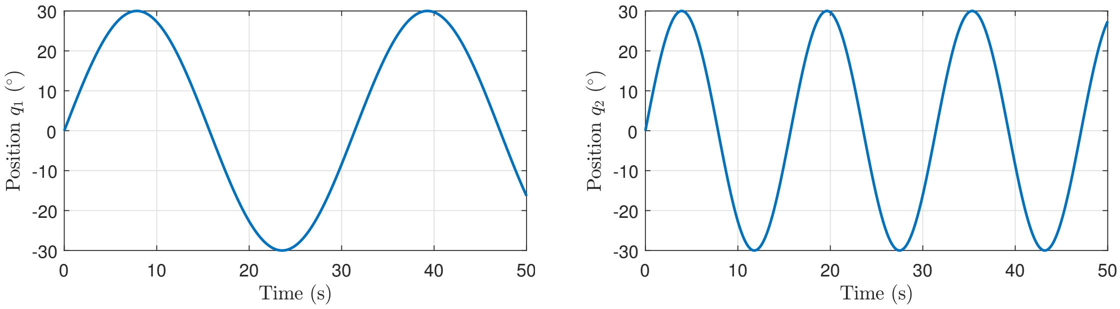

(a) (b)

Figure 5.7 Trajectory tracking experiment, rigid configuration: (a) Position trajectory for J_1. (b) Position trajectory for J_2

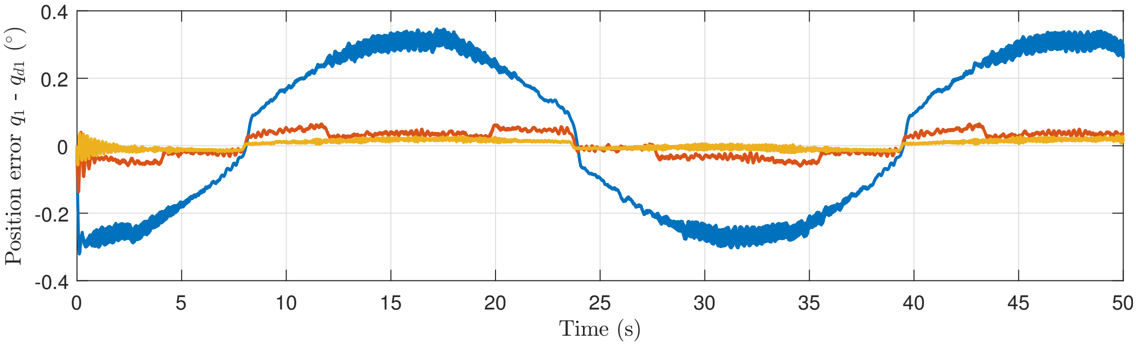

Figure 5.8 Position error comparison for J_1, trajectory tracking experiment, rigid configuration: LQR (blue), Reyes-Báez et al. (orange) and Dirksz and Scherpen (yellow).

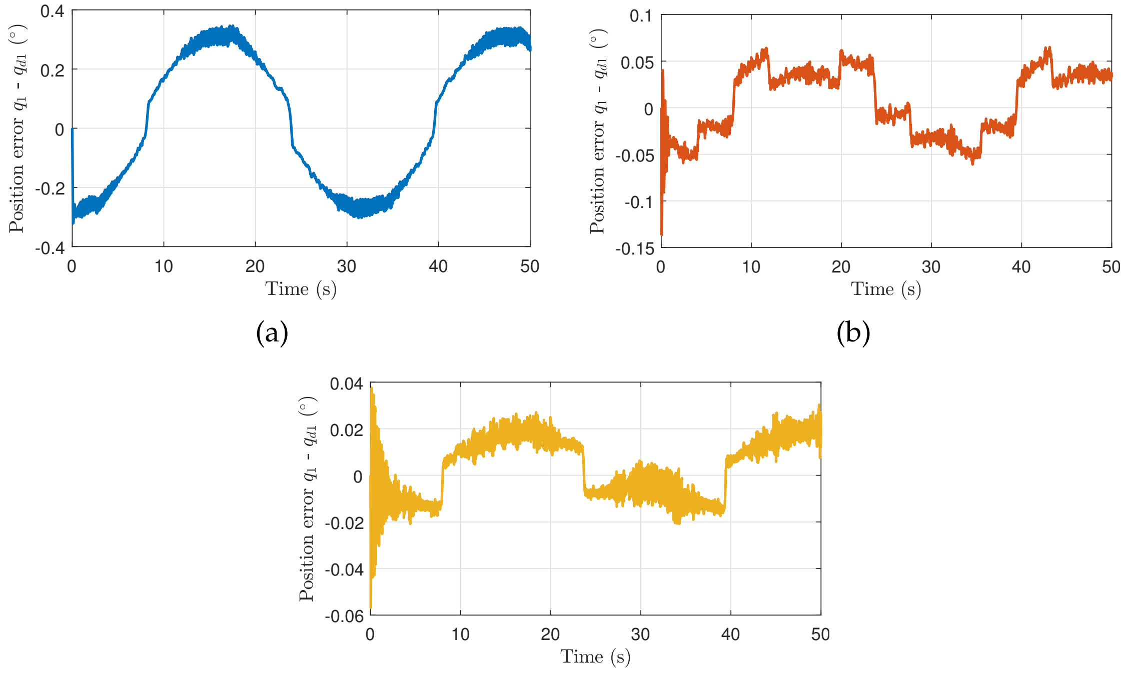

(a)

(b)

(c)

Figure 5.9 Position error for J_1, trajectory tracking experiment, rigid configuration: (a) LQR. (b) Reyes-Báez et al.. (c) Dirksz and Scherpen.

Figures 5.8 and 5.9 show the position error for J_1. The graphics shows that for a trajectory tracking the Dirksz and Scherpen controller also has a better performance than the Reyes-Báez et al. controller. The LQR proposed by the manufacturer shows to be very inaccurate in comparison with both Hamiltonian controllers. The maximum error for the Dirksz and Scherpen controller is 0.03° which is almost ten times lower than the error for the LQR controller.

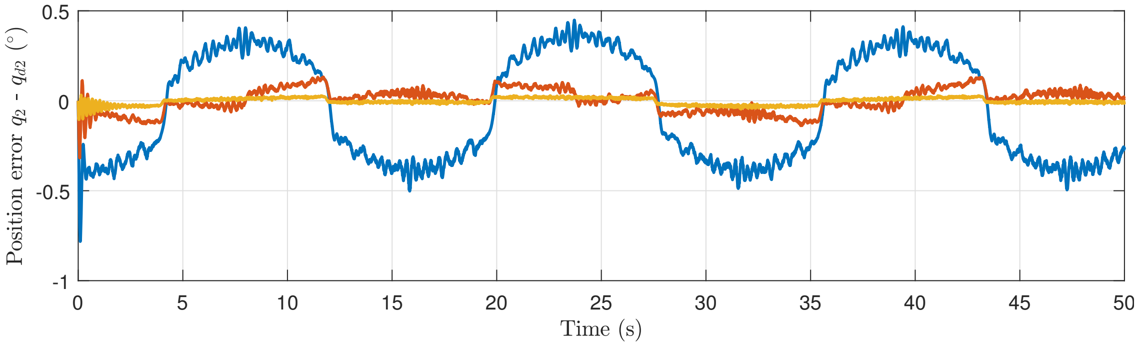

Figure 5.10 Position error comparison for J_2, trajectory tracking experiment, rigid configuration: LQR (blue), Reyes-Báez et al. (orange) and Dirksz and Scherpen (yellow).

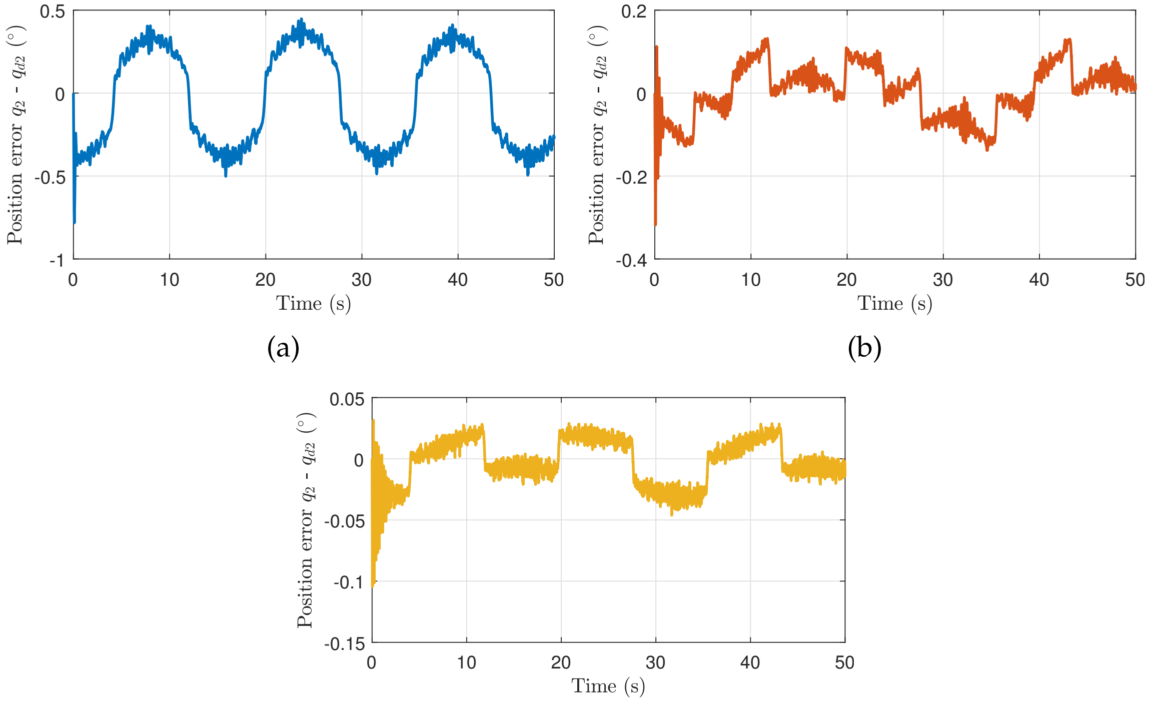

(a)

(b)

(c)

Figure 5.11 Position error for J_2, trajectory tracking experiment, rigid configuration: (a) LQR. (b) Reyes-Báez et al.. (c) Dirksz and Scherpen.

Figures 5.10 and 5.11 show the position error for J_2. As expected, the same behavior that showed Figure 5.8 for J_1 applies for J_2. The Dirksz and Scherpen controller has a better performance than the other two controllers. For J_2 the difference between the two port-Hamiltonian controllers increases, as the error in Reyes-Báez et al. controller is more important than in the articulation J_1.

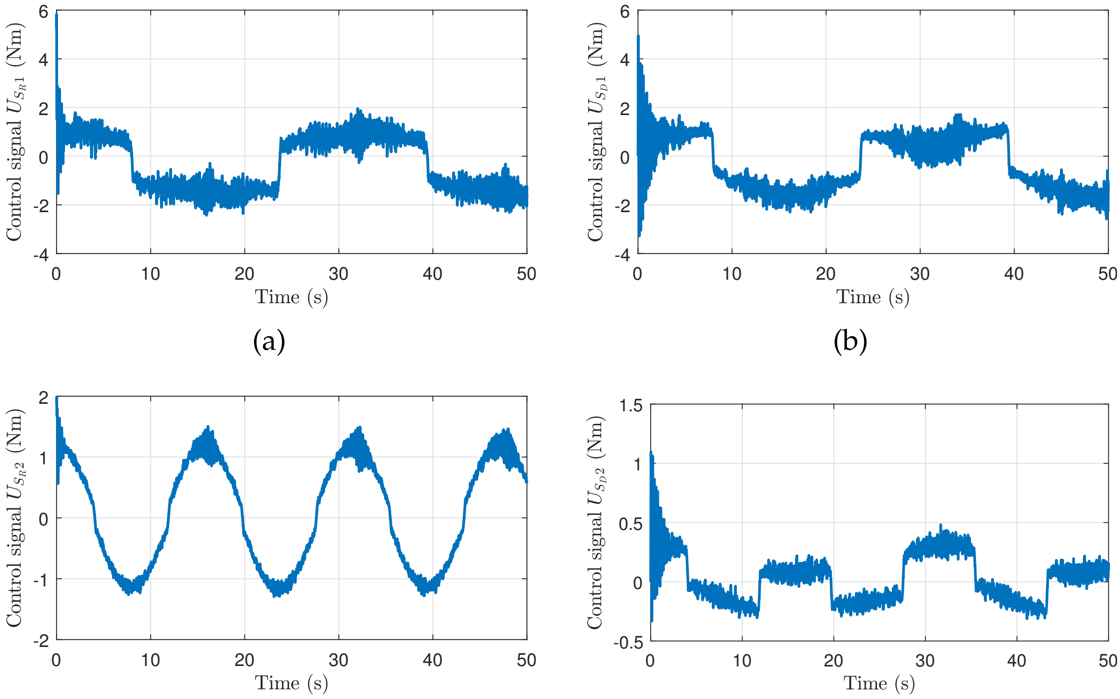

(a) (b)

(c) (d)

Figure 5.12 Control signal, trajectory tracking experiment, rigid configuration: (a) Reyes-Báez et al. controller for J_1. (b) Dirksz and Scherpen controller for J_1. (c) Reyes-Báez et al. controller for J_2. (d) Dirksz and Scherpen controller for J_2

Finally, Figure 5.12 shows the control signal created by the controller for both, J_1 and J_2, which converges at zero after the control action has stabilized the position error. Like the previous experiment, it is interesting to remark that even tough the Dirksz and Scherpen controller was able to achieve a better performance, it does not require more energy to accomplish the stabilization of the joints.

5.2 Flexible model.

In this section, the trajectory tracking controller for the 2R planar manipulator is tested in order to prove the performance of the proposed Hamiltonian control law as a multi-scale system. Two different experiments have been carried out in order to test the performance of the controllers: the movement of the joints to a fixed position and the movement following a time-variant trajectory.

Recalling Chapter 3 for the flexible configuration the system has a PH structure described in (3.16) with the explicit equations for the derivatives of the Hamiltonian in (4.11), (4.12), (4.13), (4.15), (4.16), (4.17) and (4.18). Moreover, for the Reyes-Báez et al. multi-scale system described in (3.37), (3.38), (3.39) and 3.54, the explicit equations can be found in (4.21), (4.23) and (4.24) alongside the explicit inertia matrix in (4.8). Furthermore, for the Jardón-Kojakhmetov et al. multi-scale system described in (3.52) and 3.53, the explicit equations can be found in (4.25), (4.26), (4.27), (4.28), (4.29) and (4.31) alongside the explicit inertia matrix given by (4.9).

5.2.1 Set-point experiment.

For this test, both joints were set to a fixed position of 30°. For the Reyes-Báez et al. (2016) multi-scale controller the parameters used have been set as $K_d = diag(-5,-1)$, $\lambda = diag(50,5)$, $K_v = diag(-14,-16)$ and $\epsilon = 0.3$, while for the Jardón-Kojakhmetov et al. multi-scale controller the parameters used have been set as $K_d = diag(3,3)$, $K_c = diag(100,100)$, $K_p = diag(300,200)$, $L_d = diag(3,3)$, $L_c = diag(300,300)$ and $L_p = diag(200,100)$ and $\epsilon = 0.03$. The trajectory measured by the sensors in each articulations can be seen in Figure 5.13.

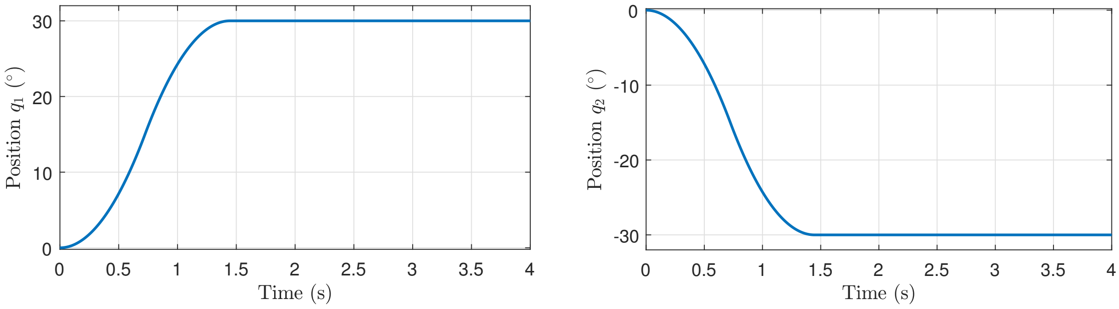

(a) (b)

Figure 5.13 Set-point experiment, flexible configuration: (a) Position trajectory for J_1. (b) Position trajectory for J_2

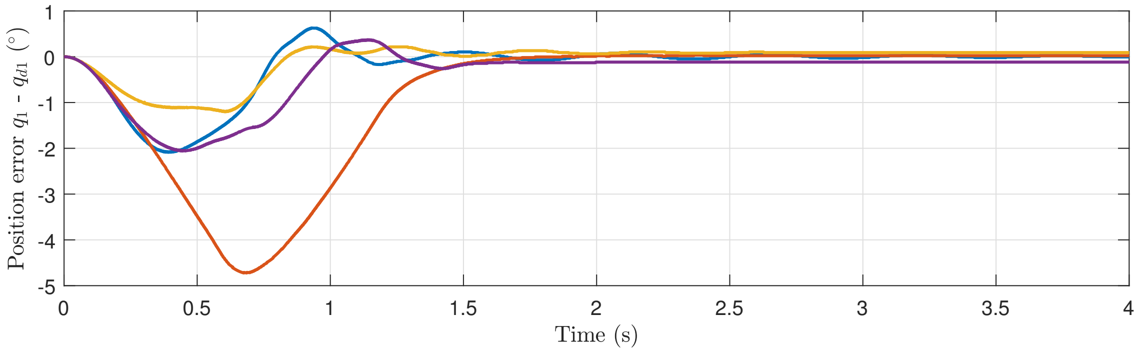

Figure 5.14 Position error comparison for J_1, set-point experiment, flexible configuration: Partial-state feedback LQR (blue), Full state feedback LQR (orange) Reyes-Báez et al. slow controller (yellow) and Jardón-Kojakhmetov et al. slow controller (purple).

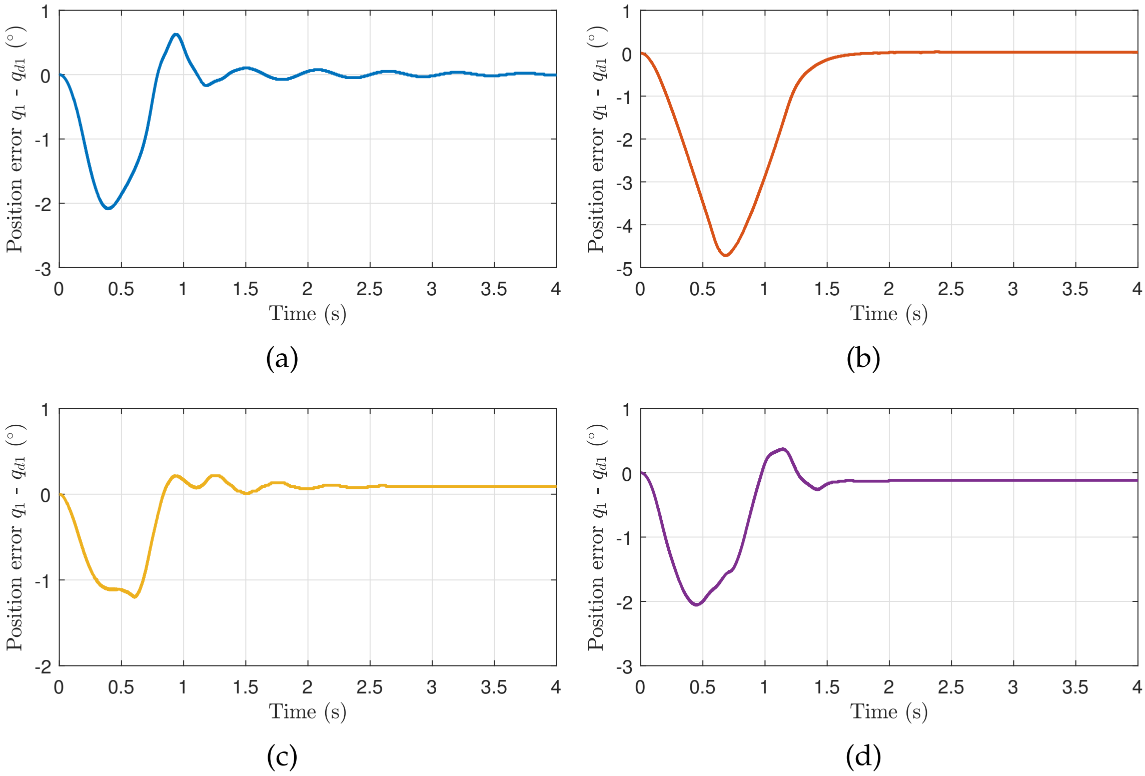

(a) (b) (c) (d)

Figure 5.15 Position error for J_1, set-point experiment, flexible configuration: (a) Partial-state feedback LQR. (b) Full-state feedback LQR. (c) Reyes-Báez et al. slow controller. (d) Jardón-Kojakhmetov et al. slow controller

Figures 5.14 and 5.15 show the position error for J_1. The smoother transient behavior is generated by the LQR Full-State Feedback controller, however the Jardón-Kojakhmetov et al. controller experiences a lower error and a similar settling time.

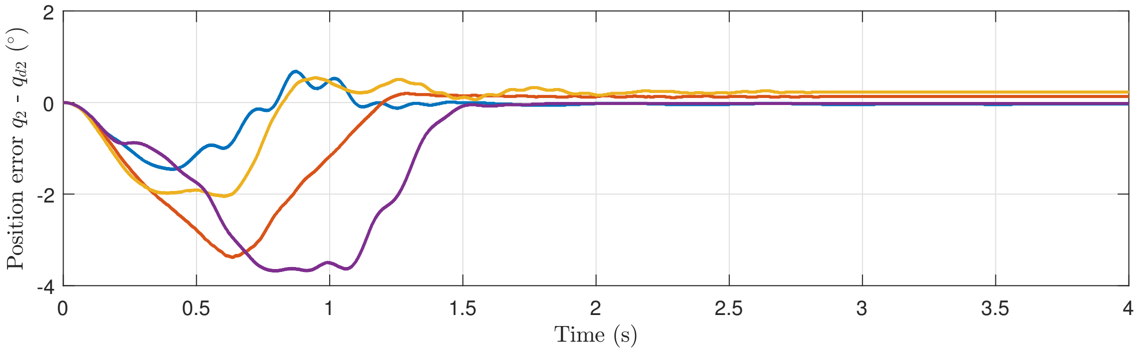

Figure 5.16 Position error comparison for J_2, set-point experiment, flexible configuration: Partial-state feedback LQR (blue), Full-state feedback LQR (orange) Reyes-Báez et al. slow controller (yellow) and Jardón-Kojakhmetov et al. slow controller (purple).

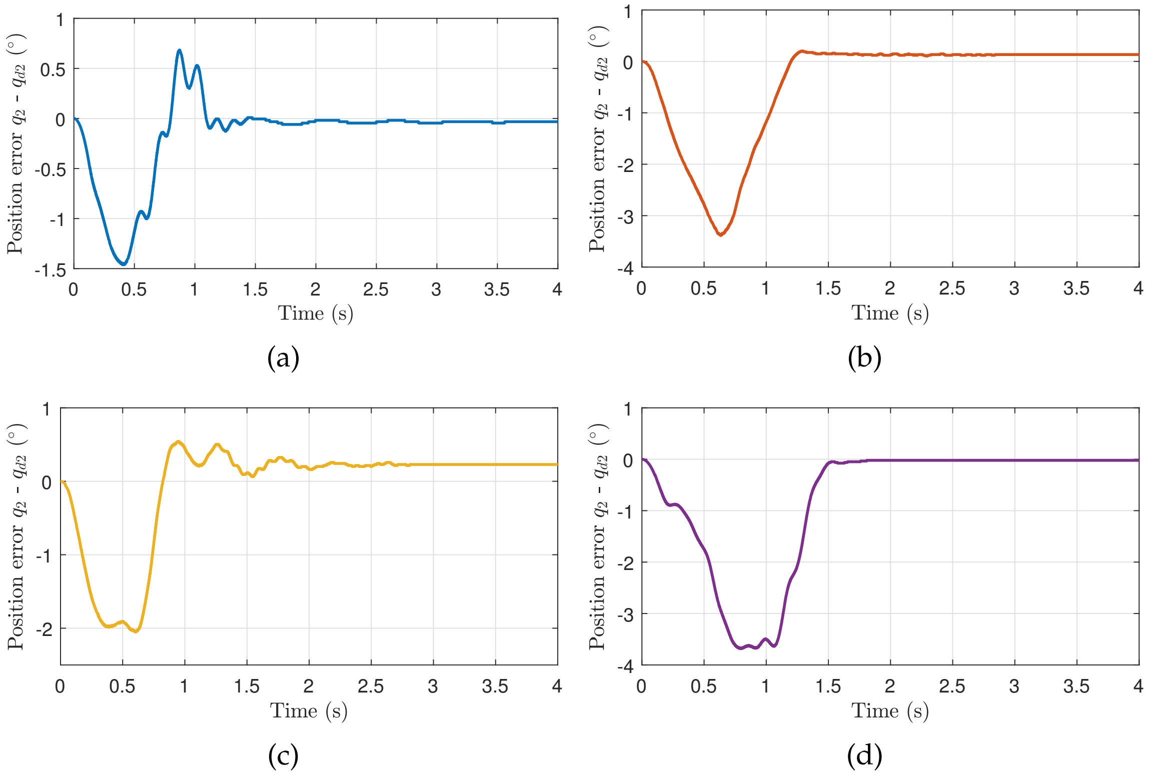

(a) (b)

(c) (d)

Figure 5.17 Position error for J_2, set-point experiment, flexible configuration: (a) Partial-state feedback LQR. (b) Full-state feedback LQR. (c) Reyes-Báez et al. slow controller. (d) Jardón-Kojakhmetov et al. slow controller.

Figures 5.16 and 5.17 shows the position error for J_2. Jardón-Kojakhmetov et al. controller has the best behavior with a lower settling time, only comparable with the settling time for the Full-state feedback LQR controller.

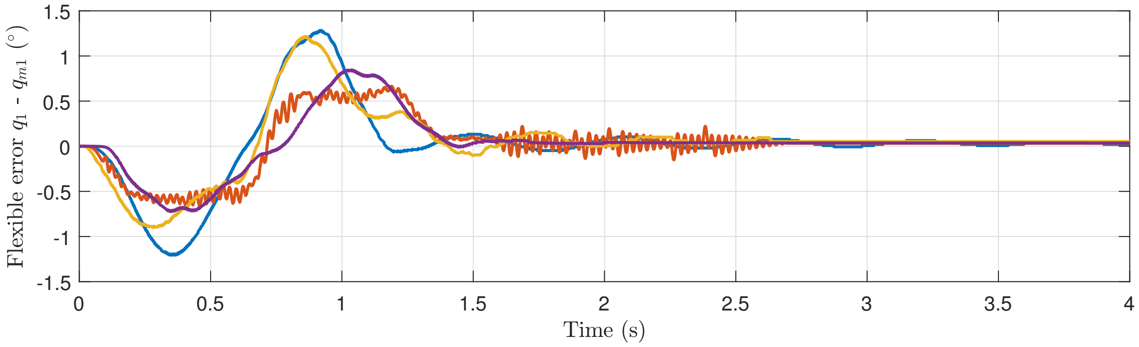

Figure 5.18 Flexible error comparison for J_1, set-point experiment, flexible configuration: Partial-state feedback LQR (blue), Full-state feedback LQR (orange) Spong fast controller (yellow) and Jardón-Kojakhmetov et al. fast controller (purple).

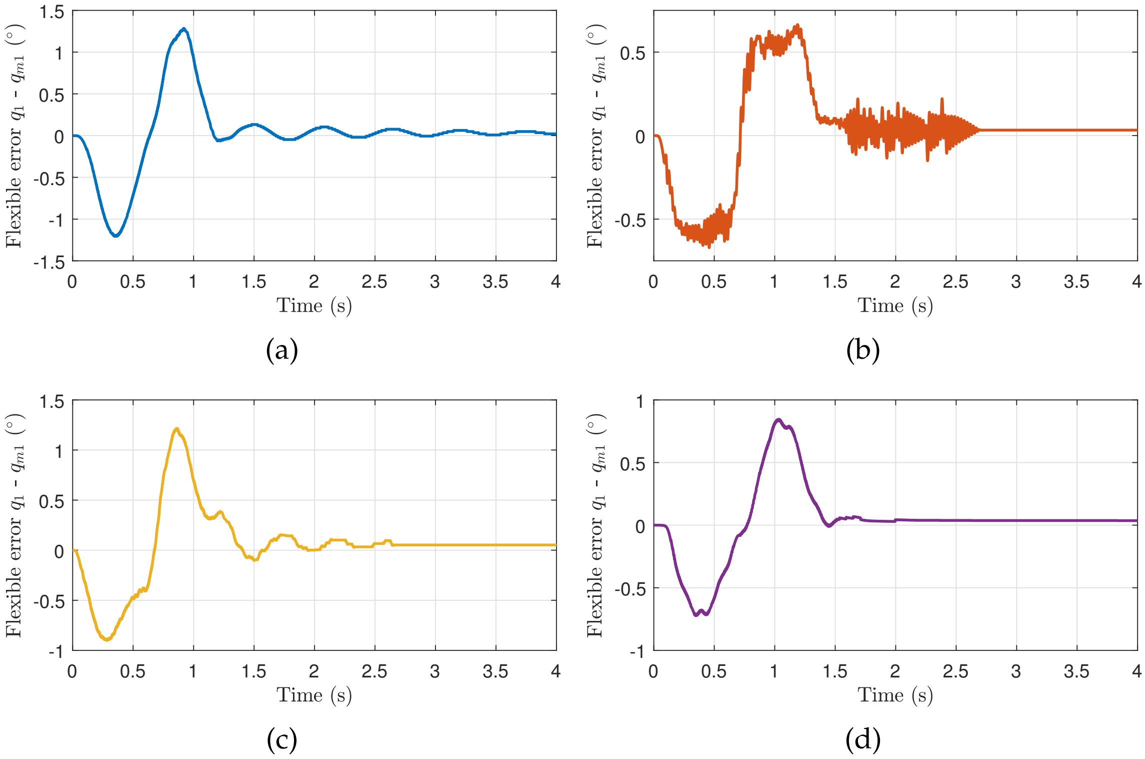

Figure 5.19 Flexible error for J_1, set-point experiment, flexible configuration: (a) Partial-state feedback LQR. (b) Full-state feedback LQR. (c) Spong fast controller. (d) Jardón-Kojakhmetov et al. fast controller

Figures 5.18 and 5.19 shows the flexible error for J_1. As expected, the worst behavior is produced by the LQR Partial-State Feedback controller, as it does not take into account the displacement between motor position and link position. On the other hand, the Jardón-Kojakhmetov et al. fast controller proves to be able to damp the oscillations faster than any other controller.

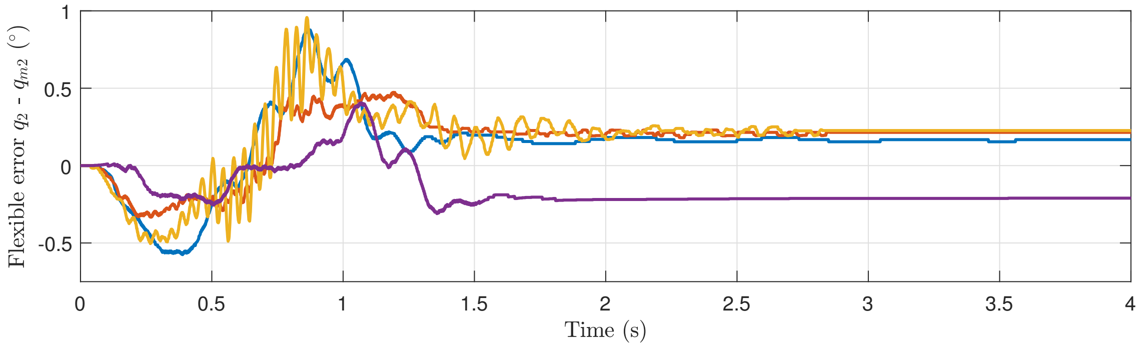

Figure 5.20 Flexible error comparison for J_2, set-point experiment, flexible configuration: Partial-state feedback LQR (blue), Full-state feedback LQR (orange) Spong fast controller (yellow) and Jardón-Kojakhmetov et al. fast controller (purple).

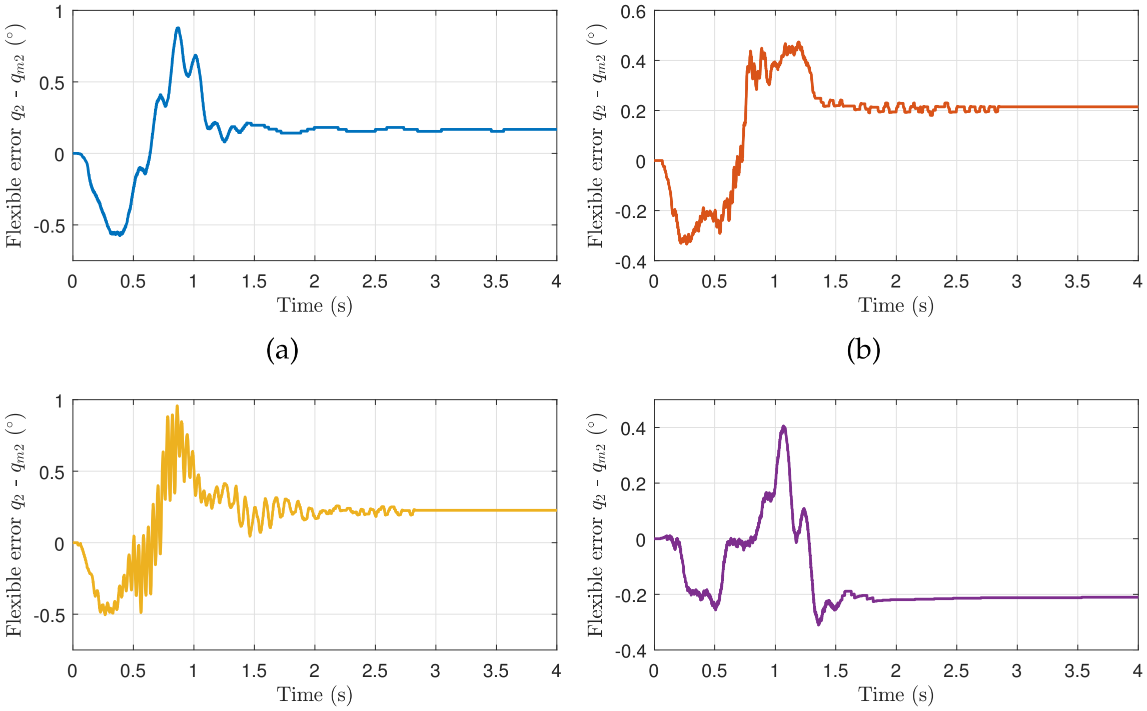

Figure 5.21 Flexible error for J_2, set-point experiment, flexible configuration: (a) Partial-state feedback LQR. (b) Full-state feedback LQR. (c) Spong fast controller. (d) Jardón-Kojakhmetov et al. fast controller

Figures 5.20 and 5.21 show the flexible error for J_2. The Jardón-Kojakhmetov et al. (2017) fast controller proves to be able to damp the oscillations faster than any other controller at 2s while the response of both the LQR controllers are not able to properly stabilize the difference in the position of the link.

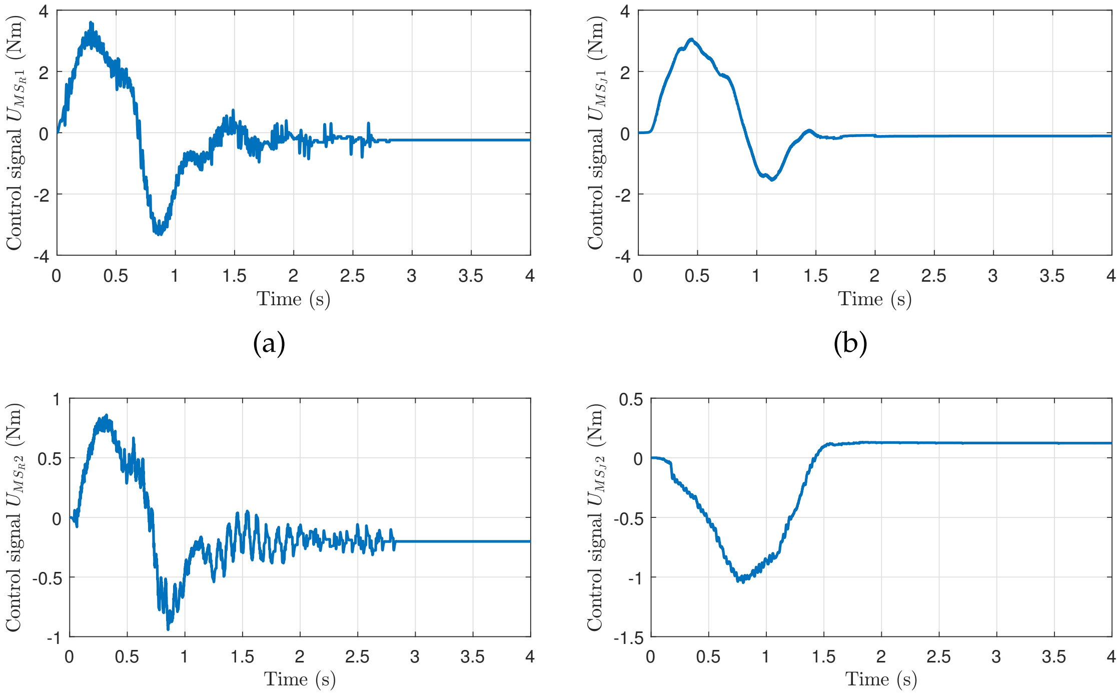

(c) (d)

Figure 5.22 Control signal, set-point experiment, flexible configuration: (a) Reyes-Báez et al. multi-scale controller for J_1. (b) Jardón-Kojakhmetov et al. multi-scale controller for J_1. (c) Reyes-Báez et al. multi-scale controller for J_2. (d) Jardón-Kojakhmetov et al. multi-scale controller for J_2

Figure 5.22 shows the control signal created by the controller for both, J_1 and J_2, which converges at zero after the control action has stabilized the position error.

5.2.2 Trajectory tracking experiment.

For this test, both joints were set to follow a sinusoidal trajectory described by the equations $c_1 sin(w_1 t)$ and $c_2 sin(w_2 t)$ respectively. For J_2, the frequency of the movement were set to be twice as fast as the frequency for J_1. The amplitude of the movements was set to 30°. For the Reyes-Báez et al. (2016) multi-scale controller the parameters used have been set as $K_d = diag(-5,-1)$, $\lambda = diag(50,5)$, $K_v = diag(-14,-16)$ and $\epsilon = 0.3$, while for the Jardón-Kojakhmetov et al. multi-scale controller the parameters used have been set as $K_d = diag(3,3)$, $K_c = diag(100,100)$, $K_p = diag(300,200)$, $L_d = diag(3,3)$, $L_c = diag(300,300)$ and $L_p = diag(200,100)$ and $\epsilon = 0.03$. The trajectory followed can be seen in Figure 5.23.

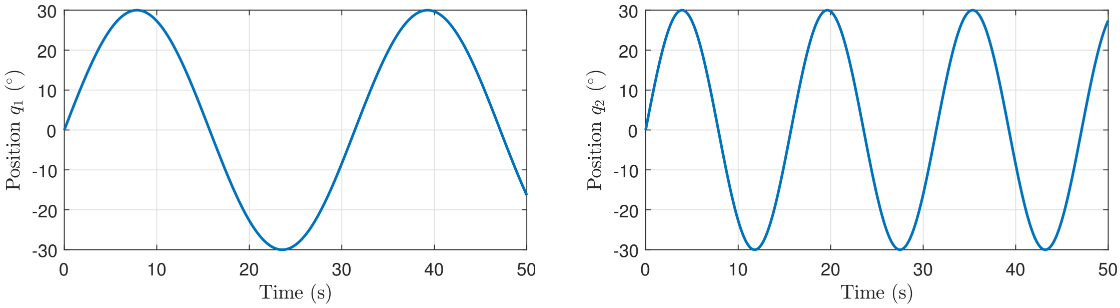

(a) (b)

Figure 5.23 trajectory tracking experiment experiment, flexible configuration: (a) Position trajectory for J_1. (b) Position trajectory for J_2

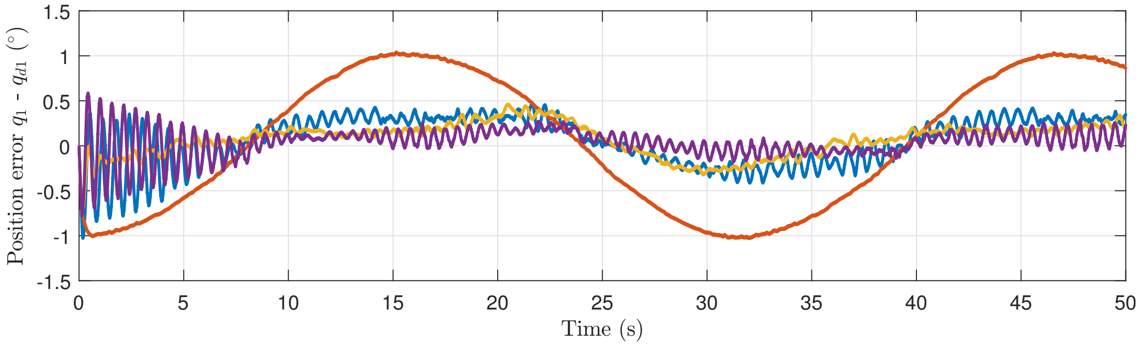

Figure 5.24 Position error comparison for J_1, trajectory tracking experiment, flexible configuration: Partial-state feedback LQR (blue), Full-state feedback LQR (orange) Reyes-Báez et al. slow controller (yellow) and Jardón-Kojakhmetov et al. slow controller (purple).

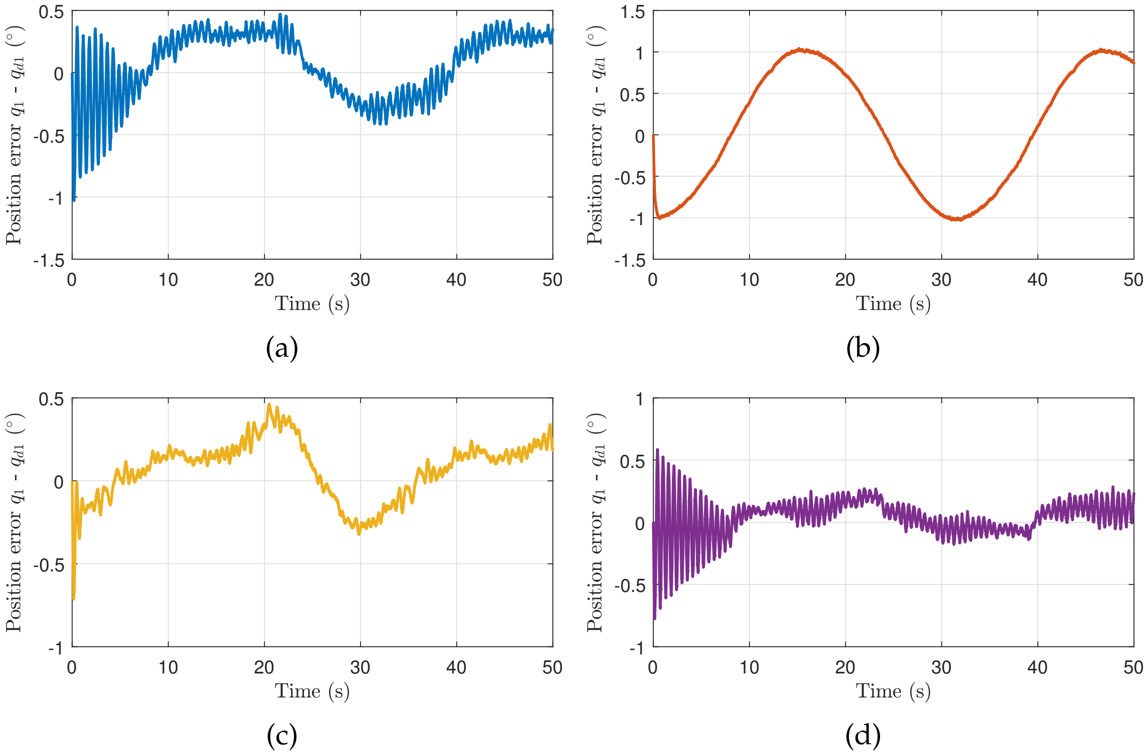

Figure 5.25 Position error for J_1, trajectory tracking experiment, flexible configuration: (a) Partial-state feedback LQR. (b) Full-state feedback LQR. (c) Reyes-Báez et al. slow controller. (d) Jardón-Kojakhmetov et al. slow controller

Figures 5.24 and 5.25 show the position error for the Joint 1, where the full-state feedback prove to be inefficient for trajectory tracking movement. On the other hand both the Reyes-Báez et al. and the Jardón-Kojakhmetov et al. controller prove to have a better stability for trajectory tracking.

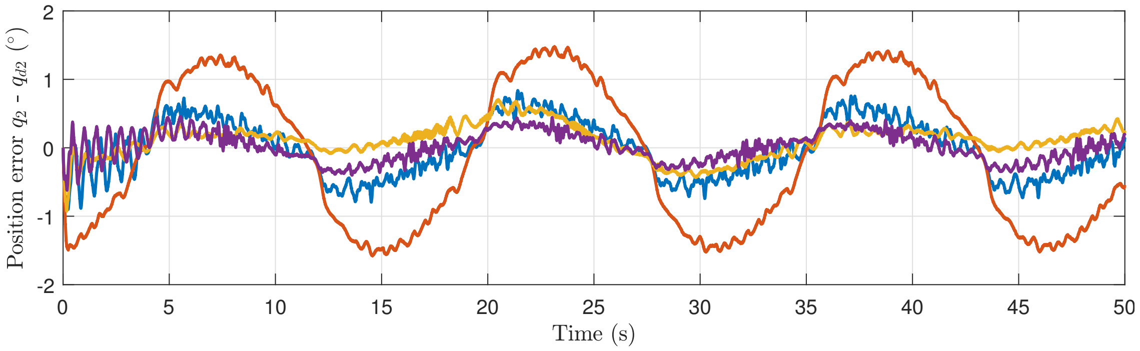

Figure 5.26 Position error comparison for J_2, trajectory tracking experiment, flexible configuration: Partial-state feedback LQR (blue), Full-state feedback LQR (orange) Reyes-Báez et al. slow controller (yellow) and Jardón-Kojakhmetov et al. slow controller (purple).

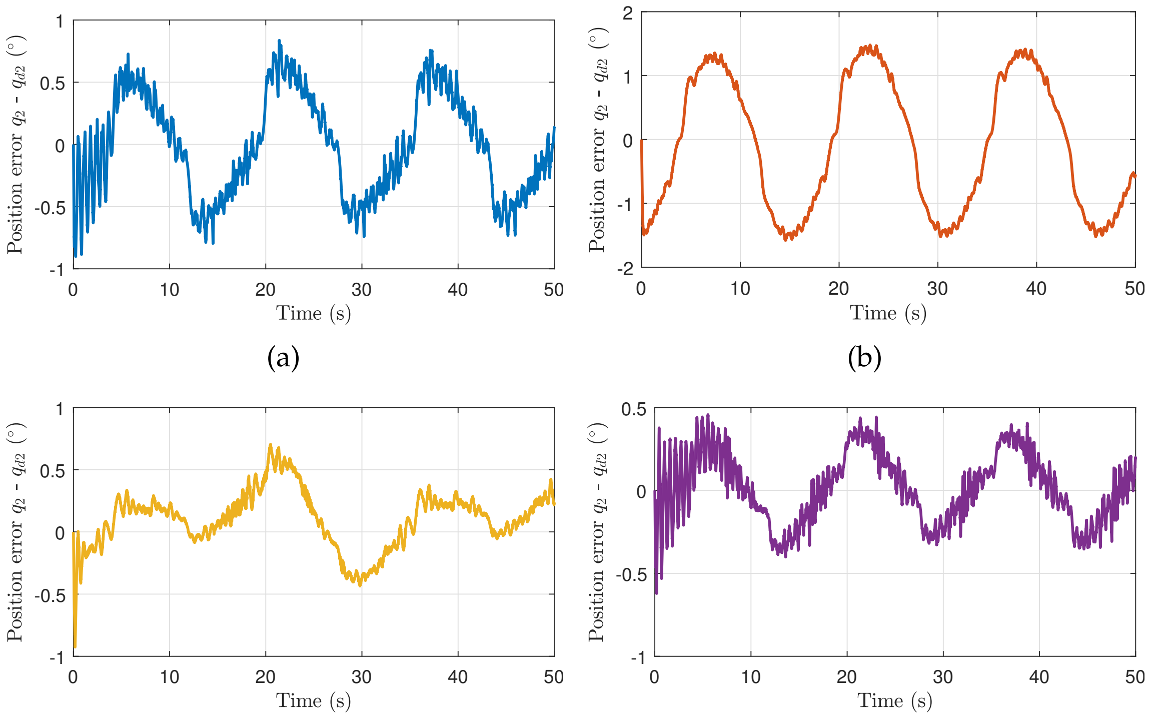

(a) (b)

(c) (d)

Figure 5.27 Position error for J_2, trajectory tracking experiment, flexible configuration: (a) Partial-state feedback LQR. (b) Full-state feedback LQR. (c) Reyes-Báez et al. slow controller. (d) Jardón-Kojakhmetov et al. slow controller

Figures 5.26 and 5.27 show the position error for the Joint 2, where The Full-State feedback controller has a higher position error in comparison to the rest of the controllers, while both PH systems have similar performance..

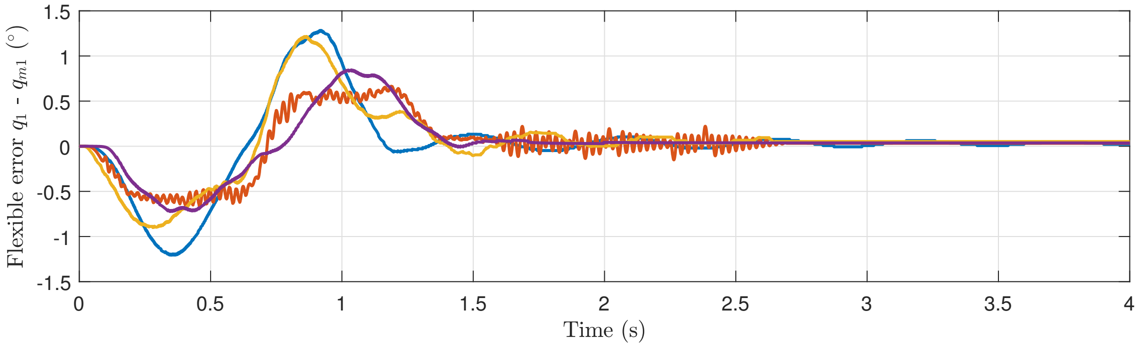

Figure 5.28 Flexible error comparison for J_1, trajectory tracking experiment, flexible configuration: Partial-state feedback LQR (blue), Full-state feedback LQR (orange) Spong fast controller (yellow) and Jardón-Kojakhmetov et al. fast controller (purple).

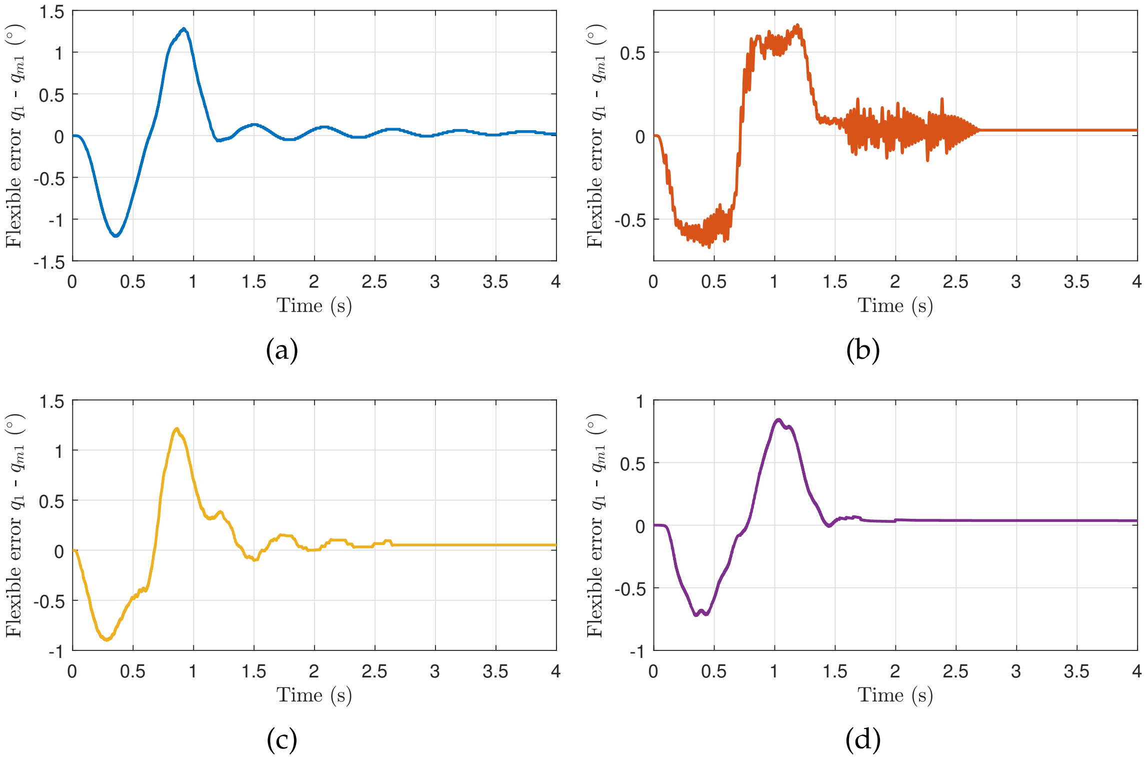

Figure 5.29 Flexible error for J_1, trajectory tracking experiment, flexible configuration: (a) Partial-state feedback LQR. (b) Full-state feedback LQR. (c) Spong fast controller. (d) Jardón-Kojakhmetov et al. fast controller

Figures 5.28 and 5.29 show the flexible error for the Joint 1. As can be seen, the flexible error for the Jardón-Kojakhmetov et al. fast controller struggles to stabilize at first but has a lower error later on in comparison with the other controllers.

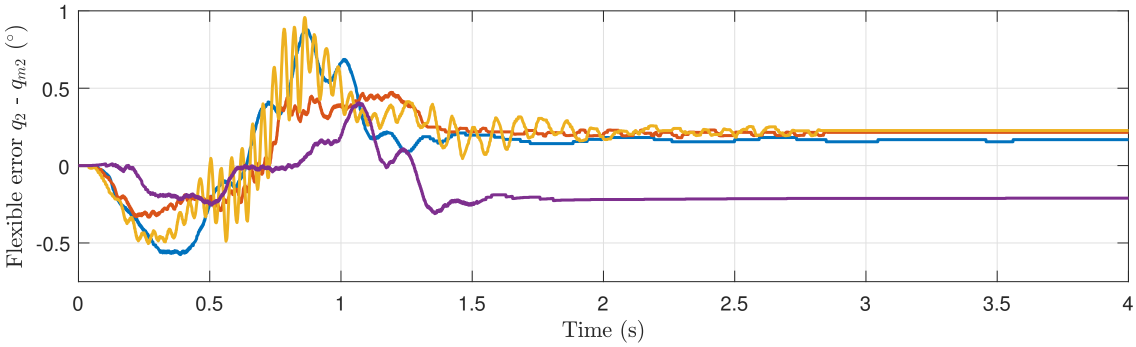

Figure 5.30 Flexible error comparison for J_2, trajectory tracking experiment, flexible configuration: Partial-state feedback LQR (blue), Full-state feedback LQR (orange) Spong fast controller (yellow) and Jardón-Kojakhmetov et al. fast controller (purple).

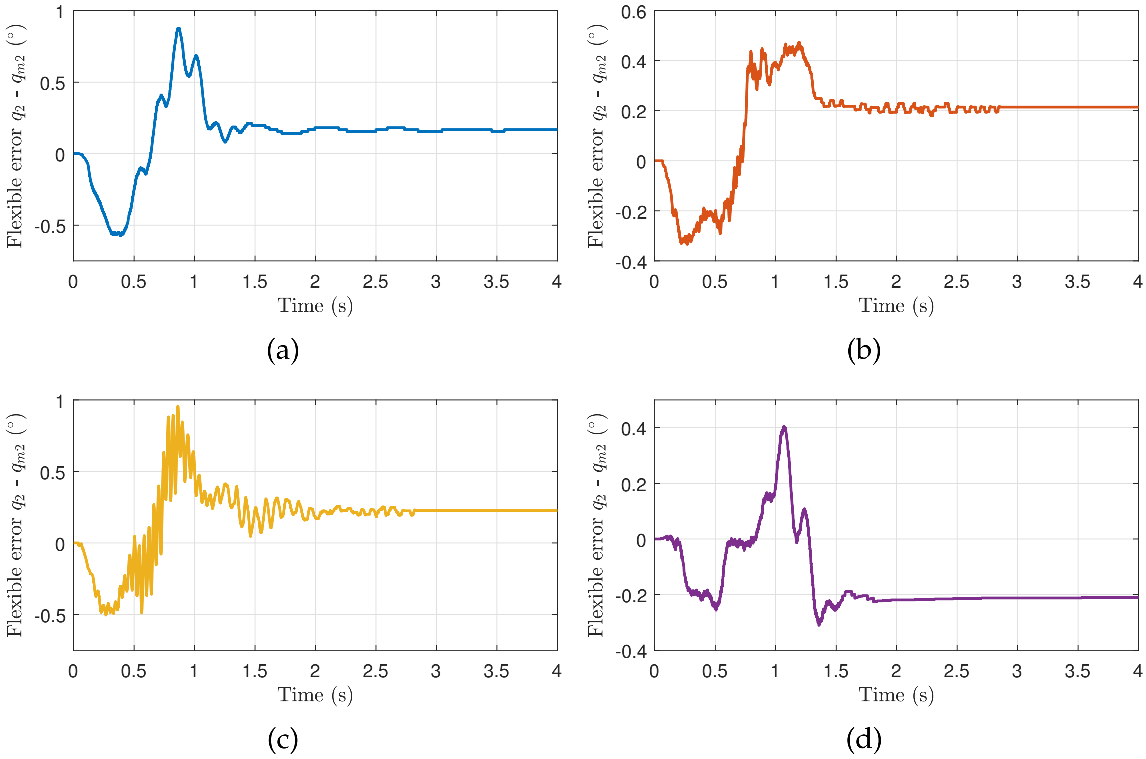

Figure 5.31 Flexible error for J_2, trajectory tracking experiment, flexible configuration: (a) Partial-state feedback LQR. (b) Full-state feedback LQR. (c) Spong fast controller. (d) Jardón-Kojakhmetov et al. fast controller.

Figures 5.30 and 5.31 show the flexible error for the Joint 2. As can be seen, the Spong fast controller experiences chaotic oscillations in two different occasions, but the controller managed to stabilize them. The best performance with respect to the error is experienced by the Jardón-Kojakhmetov et al. fast controller.

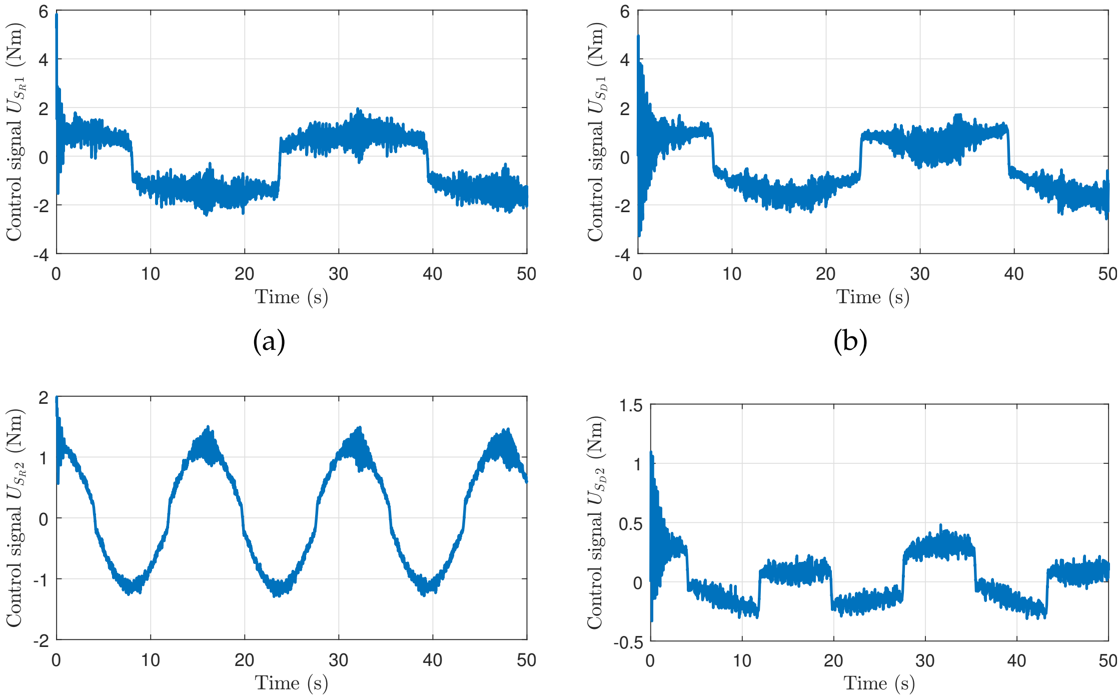

(a) (b) (c) (d)

Figure 5.32 Control signal, trajectory tracking experiment, flexible configuration: (a) Reyes-Báez et al. multi-scale controller for J_1. (b) Jardón-Kojakhmetov et al. multi-scale controller for J_1. (c) Reyes-Báez et al. multi-scale controller for J_2. (d) Jardón-Kojakhmetov et al. multi-scale controller for J_2.

Figure 5.32 shows the control signal for J_1 and J_2. As can be seen, both controllers demand roughly the same energy for the control action with a similar response. Under these circumstances the the energy used is not a determining factor when choosing between the two controllers.

5.3 Chapter 5 concluding remarks.

This chapter presented the graphics for the experimental results for the rigid and the flexible configuration. For the set-point experiment with the rigid configuration, the comparison between the graphics of the position error can be seen in Figures 5.2 and 5.4. Furthermore, for the trajectory-tracking experiment with the rigid configuration, the comparison between the results for the position error can be seen in Figures 5.8 and 5.10.

Now, for the set-point experiment with the flexible configuration, the comparison between the graphics of the position error can be seen in Figures 5.14 and 5.16, while the comparison between the graphics of the flexible error can be seen in Figures 5.18 and 5.20. Likewise, for the trajectory-tracking experiment with the flexible configuration, the comparison between the graphics of the position error can be seen in Figures 5.24 and 5.26, while the comparison between the graphics of the flexible error can be seen in Figures 5.28 and 5.30.

Next, the discussion of the experimental results and the simulations regarding the performance of the controllers is presented in order to verify compliance with the objectives.

Chapter 6

Discussion.

In this section the results achieved by the simulations in Chapter 4 and the experimental implementation of the controllers in Chapter 5 is analyzed with the aim of thoroughly understand their behavior. As has been the custom throughout the document, the analysis has taken place separately for the rigid configuration as well as for the flexible configuration.

6.1 Rigid configuration analysis.

While for the Reyes-Báez et al. controller the simulations gave rise to graphics with the same behavior as former experiments carried out with the controller as in Reyes-Báez et al. (2016), the simulations for Dirksz and Scherpen yielded graphics with a different response as the previous work in Dirksz (2011). This is due to the parameters used for the controller in both simulations: while the parameters used in Dirksz (2011) have been able to stabilize the system with lower transient oscillations, once implemented in the physical system the controller was not able to follow the desired trajectory. On the other hand, the parameters used in this document succeeded in the control task, as proven by the results shown in Figures 5.3 and 5.5.

Comparing the results of the simulation for Reyes-Báez et al. controller and Dirksz and Scherpen (2013) controller, as well as the results obtained by other experiments (see Reyes-Báez et al. (2016) and Dirksz (2011)), the first controller is able to stabilize faster than the second, as well as having lower oscillations in the transient state. The later can be explained by the way both controllers have been designed: while the Reyes-Báez et al. controller uses both position and velocities to accomplish the control action, the Dirksz and Scherpen controller limits itself to the use of only position measurements.

As for the experimental results, the first test performed for the rigid configuration was the set-point experiment, which has been performed to analyze the accuracy in the steady state and the speed with which the system error converges to zero. As expected, Figures 5.2 and 5.3 show that the response obtained by the LQR controller has a higher error than both the PH-controllers. Even tough the results for the PH controllers are similar, the Dirksz and Scherpen (2013) controller appears to have a better performance than the Reyes-Báez et al. (2016) controller.

For the trajectory tracking experiment, the results obtained follow the same behavior as the set-point experiment. The LQR controller is not able to minimize the position error, while both PH controllers have been able to reduce it at least ten times. One of the most important observations regarding the trajectory tracking experiment is that even tough in the simulations exposed in Figures 4.2 and 4.5 the position error converges to zero, none of the controllers implemented is able to achieve the same results experimentally. This can be caused by several reasons like:

- Parameters uncertainties in M(q) which causes the system to have a different behavior in the simulations.
- Internal friction could provoke a damping effect which increases the response time. Also, ignoring the internal damping effect forces the controller to exceed the energy truly necessary to stabilize the system.
- Hysteresis in the motor could cause a lag in the response, and a range of position error in which the energy supplied is not enough to start the movement.
- The simulations ignore the parameters necessary to transform the desired torque into the input current, such as the gear ratio, the maximum current input and the torque constants of the motor.

Another side effect of the difference in the position error in comparison to the simulations is the energy needed to stabilize the system. While for the simulations the energy values was in the order of 10^-3, the experimental results are considerably higher. Comparing the experimental results, the energy used by each controller is roughly the same for similar results, which means that the energy necessary to achieve the control task is not a factor to determine which controller to use.

Using statistics methods to compare the results for the trajectory tracking of the rigid robot, an algorithm to calculate the l_2 norm (the square root of the sum of the

Table 6.1 l_2 norm for the position error, trajectory tracking for the rigid model

Controller	l_2 norm	
	J_1	J_2
Quanser LQR	51.1230	67.4221
Reyes-Báez et al.	8.1541	14.1194
Dirksz and Scherpen	2.9949	4.2283

absolute values squared) was used to compare the position error for each controllers, the results are exposed in Table 6.1. Unlike in the simulations, the results for the position error for the Dirksz and Scherpen controller have better performance than the results for Reyes-Báez et al.. As has been stated, the second controller uses both the position and the velocity of the system, which is a problem with the 2DoF Quanser manipulator robot as it only has position sensors. The velocity of the system is calculated with a derivative filter which is not an ideal measurement method, causing a lot of undesired oscillations and uncertainties. That's why a controller with only position measurements as the proposed by Dirksz and Scherpen is far better suited to the task.

The same results regarding the performance of the controllers have been achieved with the analysis of the RMS value of each signal, as can be seen in Table 6.2. In this table, the RMS values calculated for each controller are shown, as well as the rate error obtained after the comparison of the RMS value of the position error with the RMS value of the desired trajectory (experimentally, with a sinusoidal wave with an amplitude of 30° should be around the theoretical value of 21.21°). As can be seen, the error rate for the LQR controller is considerably bigger in comparison with the error rate achieved by the proposed PH controllers.

Table 6.2 RMS analysis for the position error, trajectory tracking for the rigid model

Controller	RMS (°)		Error rate (%)	
	J_1	J_2	J_1	J_2
Quanser LQR	0.2286	0.3015	1.1032	1.4348
Reyes-Báez et al.	0.0172	0.0438	0.0832	0.2085
Dirksz and Scherpen	0.0134	0.0189	0.0646	0.0900

6.2 Flexible configuration analysis.

Unlike for the rigid configuration experiments which have been developed in van Logtestijn (2010) (at least for the Dirksz and Scherpen controller), there is not a single study for the experimental implementation of PH controllers in a flexible robot. Thus the analysis of the results obtained for the flexible configuration can not be compared with some previous work.

However, for the simulations of the flexible configuration and the expanded mechanical system there exist previous work as in Jardón-Kojakhmetov et al. (2017) and the Reyes-Báez et al. (2017) for the respective multi-scale controllers. Once again, the same behavior as for the rigid configuration appeared: The Reyes-Báez et al. yielded similar results as those obtained by the author, while for the Jardón-Kojakhmetov et al. resulted in different graphics as those obtained in the previous work of van Logtestijn (2010) and Jardón-Kojakhmetov et al. (2017) due to the difference in the parameters, as has already been explained in the previous section.

Now, comparing the results of the simulations between the Reyes-Báez et al. multi-scale controller and the Jardón-Kojakhmetov et al. multi-scale controller, we can observe the same general behavior as for the rigid configuration. The Reyes-Báez et al. multi-scale controller is able to stabilize the error faster than the Jardón-Kojakhmetov et al. multi-scale controller, having lower oscillations in the transient state. Besides, the flexible error for both cases is minimum and can be despised in comparison with the position error.

As for the experimental results, and like for the rigid configuration, the first test performed was the set-point experiment to analyze the accuracy in the steady state and the speed with which the position error and the flexible error converge to zero. Figures 5.15 and 5.17 show that the response obtained by the Partial state feedback LQR controller is highly inaccurate because of the oscillations due to the flexible joint, while the full-state feedback LQR controller solves the oscillations but increases the overshoot of the error. Now for the PH controllers, the Reyes-Báez et al. multi-scale controller is not able to damp the oscillations, unlike the Jardón-Kojakhmetov et al. multi-scale controller which seems to have the best response. This improvement in the convergence of the error because of the better control of the flexible error for the Jardón-Kojakhmetov et al. controller, as can be seen in Figures 5.19 and 5.21. The fast controller has an structure designed following the same model as the slow controller, unlike the Spong fast controller which has just a proportional gain.

Now for the trajectory tracking experiment, Figures 5.25 and 5.27 show that the partial-state feedback is not able to minimize the flexible error due to the springs in the joints, while the full-state feedback LQR controller shows an improvement in the response of the system in comparison with the set-point experiment. Moreover, the proposed PH controllers are able to minimize the error even more than the full-state LQR controller. For the flexible error in Figures 5.29 and 5.31, the same behavior as for the set-point experiment was observed: the Jardón-Kojakhmetov et al. fast controller was able to damp completely the oscillations after 2 seconds, unlike the Spong fast controller and the full-state feedback LQR controller which had both a slower response. It is important to notice that like for the rigid model configuration the trajectory tracking graphics are different in comparison with the simulations for the flexible configuration in Figures 4.8 and 4.13 The position error is not able to converge completely to zero as in the simulations and the flexible error is not little enough to be despised. In the last section several reasons for the difference between the simulations and the experimental results have been given, however for the flexible configuration there exist more reasons like:

- The increase in the number of variables of the system multiplies the uncertainties related to the parameters of the system. Besides, new parameters like the spring coefficient are needed for the flexible configuration.
- The sensor for the position of the links does not have enough precision as it would be desired. The change in the position of the link is measured with the change of resistance of a potentiometer, unlike the position of the motor which is read with an encoder.
- The shaft of the potentiometer used to measure the link position is coupled to the motor by means of friction, however the friction coefficient of the materials is not enough as to ensure the absence of some sliding effects.

Regarding the energy used by the system, the amount of energy necessary to stabilize the system for the experimental implementation is higher in comparison with the simulations, due to the fact that the position error and the flexible error are considerably bigger. Comparing the experimental results, the energy used by each controller is roughly the same for similar results, which means that the energy is not a factor to determine which controller to use.

Using statistics methods to compare the results for the trajectory tracking of the flexible configuration, and like it has already been performed for the rigid model, Table 6.3 l_2 norm for the position error, trajectory tracking for the rigid model

Controller	l_2 norm	
	J_1	J_2
Partial-state feedback LQR	164.7326	232.8625
Full-state feedback LQR	61.9786	90.8298
Reyes-Báez et al.	42.6991	56.4968
Dirksz and Scherpen	35.8799	46.9208

an algorithm to calculate the l_2 norm of the position and the flexible error was used and the results are exposed in Table 6.3. As was observed in the graphics, the Jardón-Kojakhmetov et al. multi-scale controller have a better performance than the Reyes-Báez et al. multi-scale controller.

The same results regarding the performance of the controllers have been achieved with the analysis of the RMS value of each error signal, as can be seen in Table 6.4. In this table, the RMS values calculated for each controller as shown as well as the rate error obtained after the comparison of the RMS value of the position error with the RMS value of the desired trajectory.

6.3 Chapter 6 concluding remarks.

The validity of the proposed PH control law's is validated by the simulation shown in Chapter 4. Even tough in previous work as Dirksz and Scherpen (2013) and Reyes-Báez et al. (2016) the graphics are quite different to the ones achieved during this work, the parameters used have proven to be far more efficient for the experimental tests.

According to the set-point experiment, the proposed PH controllers are far better suited for the task of stabilization of the position error than the benchmark LQR

Table 6.4 RMS analysis for the position error, trajectory tracking for the rigid model

Controller	RMS (°)		Error rate (%)	
	J_1	J_2	J_1	J_2
Partial-state feedback LQR	0.7367	1.0414	3.4734	4.9099
Full-state feedback LQR	0.2772	0.4062	1.3068	1.9151
Reyes-Báez et al.	0.1910	0.2527	0.9003	1.1912
Jardón-Kojakhmetov et al.	0.1605	0.2098	0.7565	0.9893

controller proposed by Quanser, which was evident because of the absence of an overshoot in the graphics. Moreover, for the trajectory tracking experiment on the rigid configuration, both PH controllers have been able to stabilize the system with an error lower than 0.1° as was established by the objectives of the research, with the Dirksz and Scherpen as the best controller for the task, followed closely by the Reyes-Báez et al. controller. The last statement can be attributed to the structure in the design of the last, regarding the unavailability of velocity measures on the physical plant. The performance of the controller has been analyzed using l_2 norm of the signals as well as the analysis of the RMS values of the position error.

Now, for the set-pint experiment on the flexible configuration, the need for better controllers to damp the oscillations caused by the spring was evident, as only the Jardón-Kojakhmetov et al. fast controller has been able to stabilize the system with a low settling time. Furthermore, for the trajectory tracking experiment on the flexible configuration both PH controllers have been able to stabilize the system with an error lower than 0.5° as was established by the objectives of the research. The best performance in the control of the position error and the flexible error of the expanded system has been achieved by the Jardón-Kojakhmetov et al. multi-scale controller. Once again, the performance of the controller has been analyzed using l_2 norm of the signals as well as the analysis of the RMS values of the position error.

Next, and according to the discussion carried out on this chapter, the conclusions drawn for this work are presented, as well as the recommendations for the future work on the study of nonlinear flexible robots.

Chapter 7

Conclusion and recommendations.

In this chapter the conclusions for the research are presented, according to the results achieved in Chapters 4 and 5 and the discussion in Chapter 6. Furthermore, the recommendations for the research in nonlinear controllers for flexible robots is proposed in order to guide the future work.

7.1 Conclusions.

The mathematical theory for PH controllers in Jardón-Kojakhmetov et al. (2017), Dirksz and Scherpen (2013) and Reyes-Báez et al. (2016) has been adapted to the 2DoF Quanser Model for the rigid configuration and expanded for the flexible configuration. Besides, the mathematical description of the Quanser manipulator have been summarized in order to ease the future work with the physical plant.

Moreover, the mathematical model for the 2DoF Quanser manipulator robot and the proposed PH controllers have been simulated in order to test the performance of the proposed controllers for both the rigid and the flexible configuration. Even tough in both cases the desired settling time has been satisfied, the Dirksz and Scherpen controller presented the best performance due to the robot characteristics as has been discussed in the previous chapter.

Furthermore and considerably the main contribution of this research consists in the experimental tests performed after the physical implementation of the proposed PH controllers in the 2DoF Quanser manipulator robot. Until the date of publication of this research, there is not a single similar experiment performed with PH controllers for a flexible robot. For the Reyes-Báez et al. rigid controller it is the first time that results are achieved after the experimental implementation of the controller and the graphics showed in this document will be presented in several conferences in European universities. For the Dirksz and Scherpen (2013) rigid controller, the experimental results achieved by this research are far superior to the previous work carried out in van Logtestijn (2010) in terms of position error. For the flexible configuration, both PH controllers have been physically implemented for the first time and the parameters established in the objectives have been fulfilled, with the Jardón-Kojakhmetov et al. multi-scale controller showing the best system response, as has been discussed in the previous section.

7.2 Recommendations.

The job realized and summarized in this document is just one more step within a bigger project for the research group of the Discrete Technology and Production Automation department.

For the Reyes-Báez et al. multi-scale controller, the fast system have been taken from Spong (1990) and for that reason the control of the flexible error is not as optimal as in the Jardón-Kojakhmetov et al. multi-scale controller. A new publication regarding the control of flexible robots using the contraction methods theory is currently being developed in order to achieve a more detailed expanded control law. For future work, the Spong fast controller could be substituted by the new fast controller proposed by Reyes-Báez et al. (2017).

Furthermore, even when the proposed PH controllers have been able to achieve better results than the LQR controller proposed by Quanser, the mathematical model used by the second is more accurate because it considers several values which the mathematical model described in this document ignores, such as the internal friction of the motors. A new mathematical model for the physical plant could help to improve the response of the system.

Moreover, the parameters used by the proposed PH controllers have been achieved by a systematic trial-and-error procedure, while the LQR controller applies a tunning software to achieve the best possible results. The development of a tunning algorithm for the PH controllers could help to improve the performance of the controllers.

Finally, following the schedule of the Discrete Technology and Production Automation department, after a few more experiments and new controllers are tested in the 2DoF Quanser manipulator robot, the next step is to develop nonlinear PH controllers for a robotic arm with rigid joints and flexible articulations.

Bibliography

Andrieu, V., Jayawardhana, B., and Praly, L. (2016). Transverse exponential stability and applications. *IEEE Transactions on Automatic Control*.

Arnold, V. (1989). *Mathematical methods of classical mechanics*. Springer-Verlag, 2 edition.

Canudas de Vit, C., Siciliano, B., and Bastin, G. (1996). *Theory of robot control*. Springer.

de Luca, A. (2014). Flexible Robots. . *Encyclopedia of Systems and Control*.

Dirksz, D. A. (2011). *Robust energy-and power-based control design Port-Hamiltonian and Brayton-Moser systems*.

Dirksz, D. A. and Scherpen, J. M. A. (2013). On tracking control of rigid-joint robots with only position measurements. *IEEE Transactions on Control Systems Technology*.

F. Beer, E. Russel, J. D. and Mazurek, D. (2013). *Mechanic of materials*. McGraw Hill Education.

Feliu, V. (2006). Robots flexibles: hacia una generación de robots con nuevas prestaciones. . *Revista Iberoamericana de Automática e Informática Industrial*, 3(3):24–41.

Ghorbel, F. and Spong, M. (2016). Integral manifolds of singularly perturbed systems with application to rigid-link flexible-joint multibody systems . *International Journal of Nonlinear Mechanics*.

Jardón-Kojakhmetov, H., Muñoz-Arias, M., and Scherpen, J. M. A. (2017). Model reduction of a flexible-joint robot: a port-Hamiltonian approach.

Kokotovic, P. (1984). Applications of Singular Perturbation techniques to Control problems. 26(4):501–550.

Kokotovic, P., Khalil, H., and O'Reilly, J. (1986). *Singular Perturbation methods in Control: Analysis and Design*.

Kokotovic, P., O'Malley, R., and Sannuti, P. (1976). Singular perturbation and order reduction in control theory An overview. 12(2):123–132.

Landau, L. and Lifshitz, E. (1969). *Mechanics*, volume 1. Pergamon Press, 2 edition.

Ortega, R., Loría, A., Nicklasson, J., and Sira-Ram, H. (1998). *Passivity-based Control of Euler-Lagrange Systems: Mechanical, Electrical and Electromechanical Applications*. Springer.

Quanser (2006). *2DOF Serial Flexible Joint Robot. Reference Manual*.

Reyes-Báez, R., van der Schaft, A., and Jayawardhana, B. (2016). Tracking Control of Fully-actuated Mechanical port-Hamiltonian Systems using Sliding Manifolds and Contraction.

Reyes-Báez, R., Jardón-Kojakhmetov, H., van der Schaft, A., Jayawardhana, B., and Scherpen, J. (2017). Trajectory tracking control of robots with flexible-joints in the port-hamiltonian framework via contraction techniques. In *proceedings*.

Shapiro, J. (2003). *Classical Mechanics*.

Slotine, J.-J. and Li, W. (1991). *Applied nonlinear control*. Prentice Hall.

Spong, M. W. (1990). Control of flexible joint robots: a survey. technical, University of Illinois at Urbana-Champaign.

Spong, M. W. (2014). Modeling and Control of Elastic Joint Robots. . *Journal of Dynamic Systems, Measurement, and Control*.

Van Der Schaft, A. (2000). Port-controlled Hamiltonian systems: towards a theory for control and design of nonlinear physical systems. *Journal of the Society of Instrument and Control Engineers of Japan (SICE)*, 39(2):91–98.

Van Der Schaft, A. and Maschke, B. (2003). *Port-Hamiltonian systems: a theory for modeling, simulation and control of complex physical systems.*

van Logtestijn, M. (2010). Stabilization and tracking control of a planar robot with only position measurements. bachelor thesis, University of Groningen.

Appendix A

Robot Specifications.

Table A.1 2DoF Quanser robot parameters

Symbol	Description	Value	Units
J_1	Moment of inertia of link 1	0.23041858	Kgm^2
J_2	Moment of inertia of link 2	0.010724	Kgm^2
l_1	Length to center of mass of link 1	0.343	m
l_2	Length to center of mass of link 2	0.267	m
m_1	Mass at the end of link 1	1.9585	Kg
m_2	Mass at the end of link 2	0.1504	Kg
	Torque constant motor 1	0.119	Nm/A
	Torque constant motor 2	0.0234	Nm/A
	Maximum continuous current motor 1	0.944	A
	Maximum continuous current motor 2	1.21	A
	Gear ratio harmonic drive 1	100	
	Gear ratio harmonic drive 2	50	
	2DoF Flexible link total length	0.610	m
	Lenghth link 1	0.343	m
	Lenghth link 2	0.267	m
	lines per revolution	1024	

Appendix B

Simulink diagrams.

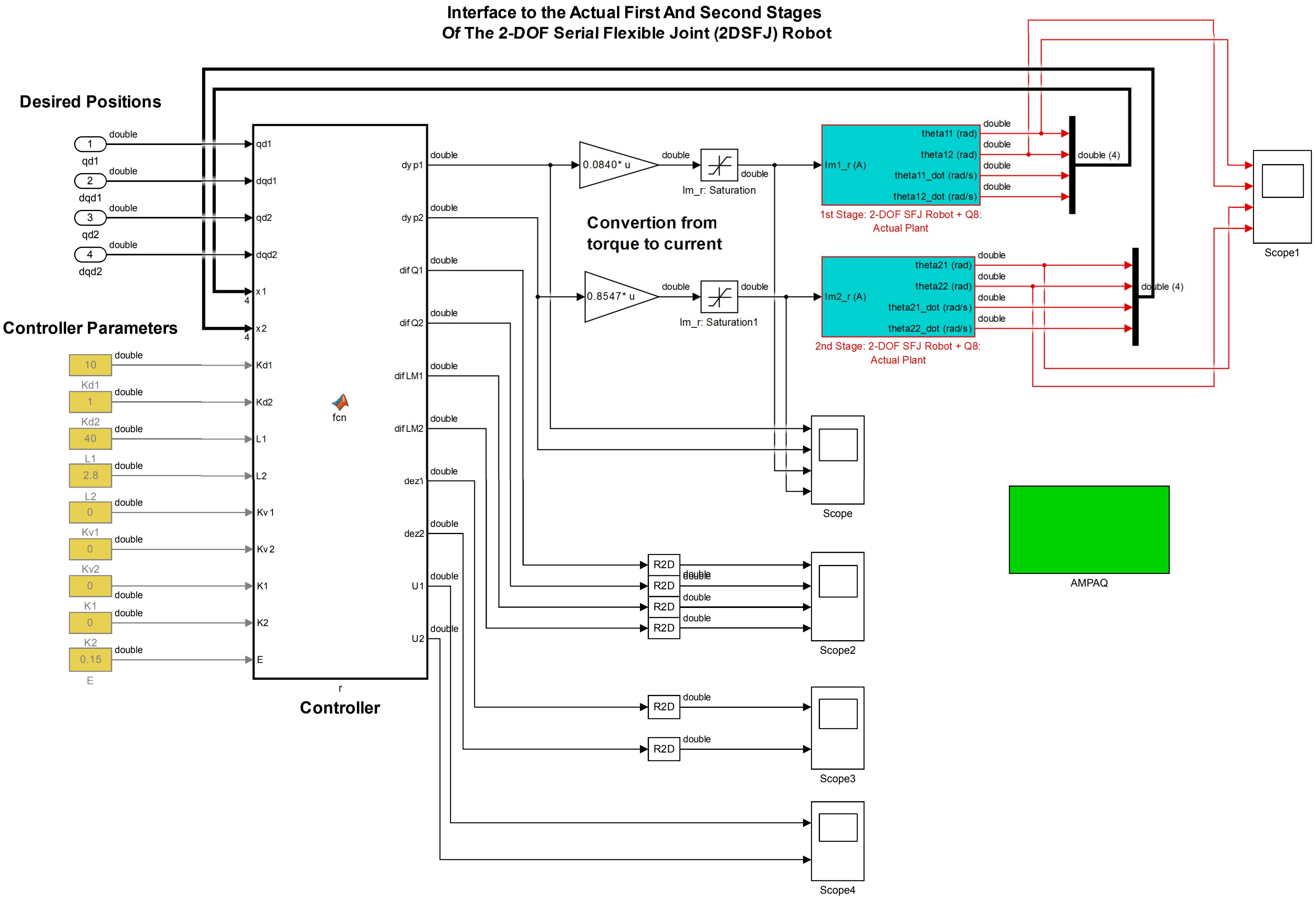
Interface to the Actual First And Second Stages
Of The 2-DOF Serial Flexible Joint (2DSFJ) Robot
Desired Positions
1
qd1
2
dqd1
3
qd2
4
dqd2
double
Controller Parameters
10
Kd1
1
Kd2
40
L1
2.8
L2
0
Kv1
0
Kv2
0
K1
0
K2
0.15
E
qd1
dqd1
qd2
dqd2
x1
x2
4
Kd1
Kd2
L1
L2
Kv1
Kv2
K1
K2
E
fcn
r
Controller
dy p1
dy p2
dif Q1
dif Q2
dif LM1
dif LM2
dez1
dez2
U1
U2
0.0840* u
0.8547* u
Im_r: Saturation
Im_r: Saturation1
Convertion from
torque to current
Im1_r (A)
theta11 (rad)
theta12 (rad)
theta11_dot (rad/s)
theta12_dot (rad/s)
1st Stage: 2-DOF SFJ Robot + Q8:
Actual Plant
Im2_r (A)
theta21 (rad)
theta22 (rad)
theta21_dot (rad/s)
theta22_dot (rad/s)
2nd Stage: 2-DOF SFJ Robot + Q8:
Actual Plant
double (4)
R2D
Scope
Scope1
Scope2
Scope3
Scope4
AMPAQ

Figure B.1 System diagram Reyes-Báez et al. controller

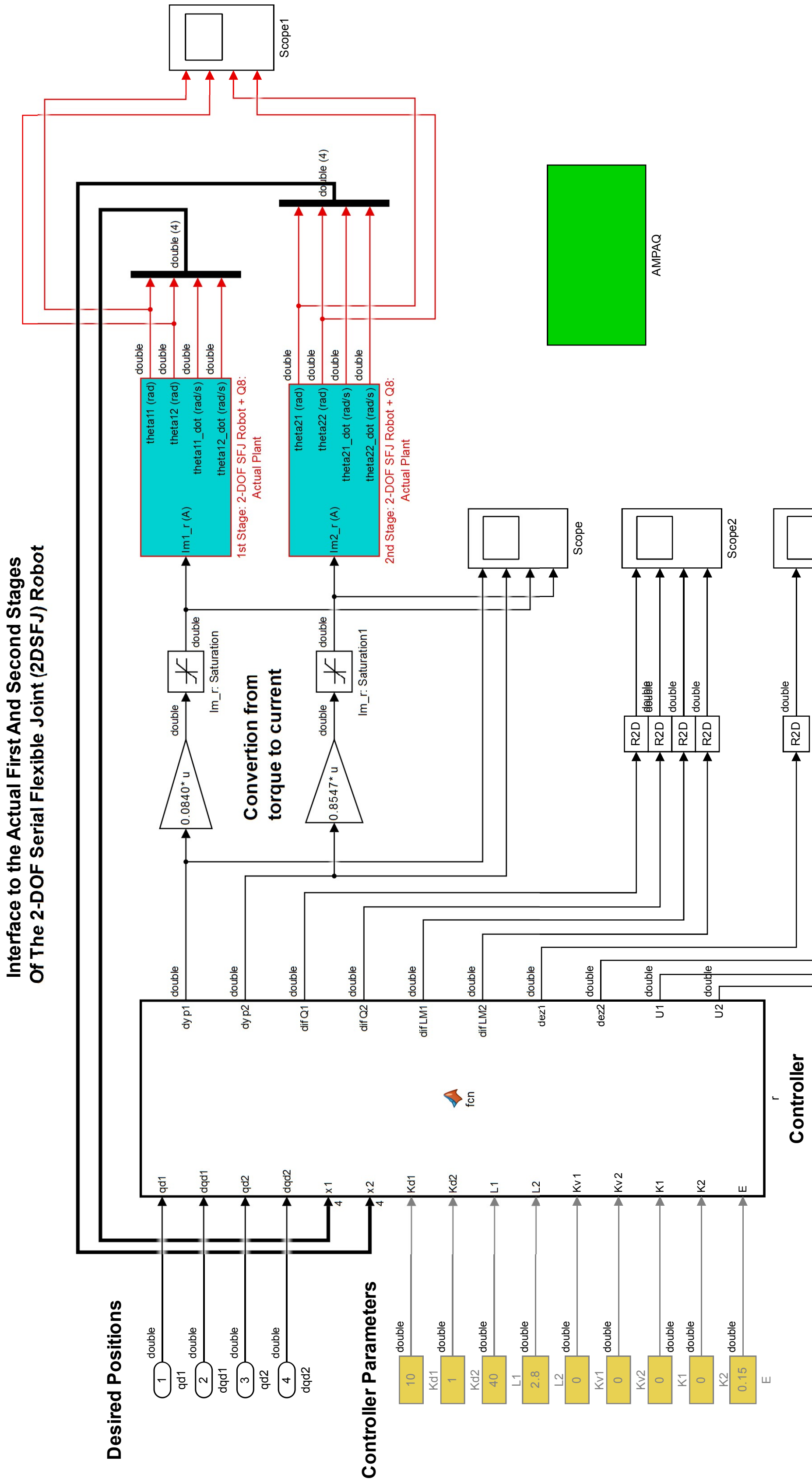
Interface to the Actual First And Second Stages
Of The 2-DOF Serial Flexible Joint (2DSFJ) Robot
Desired Positions
1 qd1
2 dqd1
3 qd2
4 dqd2
Controller Parameters
10 Kd1
1 Kd2
40 L1
2.8 L2
0 Kv1
0 Kv2
0 K1
0 K2
0.15 E
qd1
dqd1
qd2
dqd2
x1
x2
Kd1
Kd2
L1
L2
Kv1
Kv2
K1
K2
E
fcn
dyp1
dyp2
difQ1
difQ2
difLM1
difLM2
dez1
dez2
U1
U2
r
Controller
double
double (4)
0.0840* u
0.8547* u
Im_r: Saturation
Im_r: Saturation1
Convertion from
torque to current
Im1_r (A)
theta11 (rad)
theta12 (rad)
theta11_dot (rad/s)
theta12_dot (rad/s)
1st Stage: 2-DOF SFJ Robot + Q8:
Actual Plant
Im2_r (A)
theta21 (rad)
theta22 (rad)
theta21_dot (rad/s)
theta22_dot (rad/s)
2nd Stage: 2-DOF SFJ Robot + Q8:
Actual Plant
R2D
Scope
Scope1
Scope2
Scope3
Scope4
AMPAQ

Figure B.2 System diagram Jardón-Kojakhmetov et al. controller

Appendix C

Matlab code.

C.1 Reyes-Báez et al. controller for the rigid model.

```matlab
% Rigid model simulation, Reyes-Baez et al. controller
clear;close all;clc;

% Define the variables
syms q1 q2 p1 p2 dq1 dq2 real
syms d1 d2 u1 u2 real
syms t real
syms qc1 qc2 real
syms Q1 Q2 real

% Define the constants
m1 = 1.9585;
m2 = 0.1504;
I1 = 0.23041858;
I2 = 0.010724;
r1 = 0.2;
r2 = 0.25;
l1 = 0.343;
l2 = 0.267;
c1 = 30*(pi/180);
c2 = 30*(pi/180);
w1 = 0.2;
w2 = 0.4;
d1 = 0.5;
d2 = 0.1;
```

Figure C.1 Matlab code for Reyes-Báez et al. controller, rigid configuration, part 1.

```
Im1 = 0.1;
Im2 = 0.1;

% Defining variable vectors
p = [p1 ; p2];
q = [q1 ; q2];

% Defining Mass-Inertia Matrix
a1 = m1*r1^2 + m2*l1^2 + I1;
a2 = m2*r2^2 + I2;
b = m2*l1*r2;

M = [a1+a2+2*b*cos(q2) a2+b*cos(q2);a2+b*cos(q2) a2];

% Define the Hamiltonian
H=simplify(0.5*[p1 p2]*(M^(-1))*[p1;p2]);

% Matrices
B = [1 0; 0 1];
D = [d1 0; 0 d2];
U=[u1; u2];
I = eye(2);
O = zeros(2);

% Full system in Hamiltonian
Eq=simplify([O I; -I ...
    -D]*[diff(H,q1);diff(H,q2);diff(H,p1);diff(H,p2)]+[O;B]*U);

% *********************  Controller approach  ****************/
% Define desired trajectory
q1d = c1*sin(w1*t);
q2d = c2*sin(w2*t);
qd = [q1d; q2d];

dq1d = diff(q1d,t);
dq2d = diff(q2d,t);
dqd = [dq1d; dq2d];

Ddq1d = diff(dq1d,t);
Ddq2d = diff(dq2d,t);
Ddqd = [Ddq1d; Ddq2d];

% Change of variables
M2 = subs(M,q2,q2d);
P = simplify(M2*dqd);

% Defining Matrix
Kd = [-20 0; 0 -2.6];
```

Figure C.2 Matlab code for Reyes-Báez et al. controller, rigid configuration, part 2.

```
% System error
Q = q - qd;

pdo = simplify(M*dqd);
Lambda = [35 0 ; 0 3.1];
pr = simplify(pdo - Lambda*Q);
S = p - pr;

% Controller dynamics
dpr = (diff(M,q1)*dq1+diff(M,q2)*dq2)*dqd + M*Ddqd - Lambda*([dq1; ...
    dq2]-dqd);
Hpr = subs(H, p1, p1-S(1,1));
Hpr = subs(Hpr, p2, p2-S(2,1));
HS = subs(H, p1, p1-pr(1,1));
HS = subs(HS, p2, p2-pr(2,1));

U1 = dpr + [diff(Hpr,q1);diff(Hpr,q2)] + D*[diff(Hpr, ...
    p1);diff(Hpr,p2)];
U2 = simplify(-Kd*[diff(HS,p1);diff(HS,p2)] - (M^(-1))*Lambda*Q + ...
    [diff(pr'*(M^(-1))*S,q1) ; diff(pr'*(M^(-1))*S,q2)]);

U = U1 + U2;
QN = M^(-1)*p;
U = subs(U,dq1,QN(1,1));
U = subs(U,dq2,QN(2,1));


% Final System Equations
CEQ = simplify([O I; -I ...
    -D]*[diff(H,q1);diff(H,q2);diff(H,p1);diff(H,p2)]+[O;B]*U);
```

Figure C.3 Matlab code for Reyes-Báez et al. controller, rigid configuration, part 3.

C.2 Dirksz and Scherpen controller for the rigid model.

```
% Rigid model simulation, Dirksz and Scherpen controller
% Programmed by Juan Jose Padilla-Mora

clear;close all;clc;

% Define the variables
syms q1 q2 p1 p2 real
syms m1 m2 r1 r2 l1 l2 I1 I2 real
syms d1 d2 u1 u2 real
syms t c1 c2 w1 w2 real
syms qc1 qc2 real
syms kp1 kp2 kd1 kd2 kc1 kc2 real

Define the constants Constants
m1 = 1.9585;
m2 = 0.1504;
I1 = 0.23041858;
I2 = 0.010724;
r1 = 0.2;
r2 = 0.25;
l1 = 0.343;
l2 = 0.267;
c1 = 30*(pi/180);
c2 = 30*(pi/180);
w1 = 0.2;
w2 = 0.4;
d1 = 0.5;
d2 = 0.1;
Im1 = 0.1;
Im2 = 0.1;

% Defining vector variables
p = [p1 ; p2];
q = [q1 ; q2];

%Define Inertia-matrix
m11 = m1*l1^2+m2*((l1^2) +(l2^2) +2*l1*l2*cos(q2));
m21 = m2*((l2^2) +2*l1*l2*cos(q2));
m22 = m2*(l2^2);

M = [m11 m21; m21 m22];
```

Figure C.4 Matlab code Dirksz and Scherpen controller, rigid configuration, part 1.

```
% Defining the Hamiltonian
H=simplify(0.5*[p1 p2]*(M^(-1))*[p1;p2]);

% Constant matrices
B = [1 0; 0 1];
D = [d1 0; 0 d2];
U=[u1; u2];
I = eye(2);
O = zeros(2);

% ***************************  controller  **********************/
% Defining Matrix
Kp = [5000 0; 0 600];
Kc = [3000 0; 0 400];
Kd = [3 0; 0 3];

% Desired trajectory
q1d = c1*sin(w1*t);
q2d = c2*sin(w2*t);
qd = [q1d; q2d];

dq1d = diff(q1d,t);
dq2d = diff(q2d,t);
dqd = [dq1d; dq2d];

Ddq1d = diff(dq1d,t);
Ddq2d = diff(dq2d,t);
Ddqd = [Ddq1d; Ddq2d];
```

Figure C.5 Matlab code Dirksz and Scherpen controller, rigid configuration, part 2.

```
% Change of variables
Q = [q1; q2] - [q1d; q2d];
P = [p1; p2] - M*[dq1d; dq2d];
NH = 0.5*P'*(M^(-1))*P+0.5*Q'*Kp*Q;

% Controller dynamics
qc = [qc1;qc2];
v = Q - qc;
dcq = (Kd^(-1))*Kc*(Q - qc)

% Creating the input U
F1 = M*Ddqd;

VF1 = M*dqd;
DiffMatrix1 = [(diff(VF1(1,1), q1)) (diff(VF1(1,1), q2)); ...
    (diff(VF1(2,1), q1)) (diff(VF1(2,1), q2))];
F2 = DiffMatrix1*dqd;

EF1 = dqd'*M*dqd;
F3 = 0.5*[(diff(EF1, q1)); (diff(EF1, q2))];

F4 = Kp*Q;
F5 = Kc*v;

U = F1+F2-F3-F4-F5;

% Final System Equations
EqF = [O I; -I ...
    -D]*[diff(NH,q1);diff(NH,q2);diff(NH,p1);diff(NH,p2)]+[O;B]*U
```

Figure C.6 Matlab code Dirksz and Scherpen controller, rigid configuration, part 3.

C.3 Reyes-Báez et al. multi-scale controller for the flexible model.

```
% Flexible model simulation, Reyes-Baez et al. multi-scale controller
% Programmed by Juan Jose Padilla-Mora
clear;close all;clc;

% Define the variables
syms q1 q2 p1 p2 dq1 dq2 real
syms qm1 qm2 pm1 pm2 dqm1 dqm2 real
syms z1 z2 pz1 pz2 dz1 dz2 real
syms t E
aux1 = sym('aux1(t)');
aux2 = sym('aux2(t)');

% Define the constants
m1 = 1.9585;
m2 = 0.1504;
I1 = 0.23041858;
I2 = 0.010724;
r1 = 0.2;
r2 = 0.25;
l1 = 0.343;
l2 = 0.267;
c1 = 30*(pi/180);
c2 = 30*(pi/180);
w1 = 0.2;
w2 = 0.4;
d1 = 0.5;
d2 = 0.1;
Im1 = 0.1;
Im2 = 0.1;
K1 = 78.6765;
K2 = 30.4639;
```

Figure C.7 Matlab code for Reyes-Báez et al. multi-scale controller, flexible configuration, part 1.

```
% Defining vector variables
p = [p1 ; p2];
pm = [pm1 ; pm2];
q = [q1 ; q2];
qm = [qm1 ; qm2];
z = [z1; z2];
pz = [pz1; pz2];
dq = [dq1; dq2];
dqm = [dqm1; dqm2];

qE_z = [q;z];
qE_q = [q;(q-qm)/E];

% Change of variables
pE_z = [p;pz];
pE_p = [p;(p-pm)/E];

QM = q-z*E;
PM = p-pz*E;

% Constant Matrix
I = eye(2);
O = zeros(2);
K = [K1 0; 0 K2];
IN = [Im1 0; 0 Im2];

% Define expanded Mass-Inertia matrix
a1 = m1*r1^2 + m2*l1^2 + I1;
a2 = m2*r2^2 + I2;
b = m2*l1*r2;

M = [a1+a2+2*b*cos(q2) a2+b*cos(q2);a2+b*cos(q2) a2];
ME = simplify([M O; O IN]);

% Defining the Hamiltonian
HE= simplify(0.5*pE_z'*(ME^(-1))*pE_z)+0.5*(E*z)'*K*(E*z);
HE2 = subs(HE, [z1 z2 pz1 pz2], [qE_q(3), qE_q(4), pE_p(3), pE_p(4)]);

% Constant matrix
D = [0 0 0 0; 0 0 0 0; 0 0 0 0; 0 0 0 0];
I = eye(4);
O = zeros(4);
```

Figure C.8 Matlab code for Reyes-Báez et al. multi-scale controller, flexible configuration, part 2.

```
% Derivatives of the Hamiltonian
dif1 = simplify(diff(HE2,q1));
dif2 = simplify(diff(HE2,q2));
dif3 = simplify(diff(HE,z1));
dif4 = simplify(diff(HE,z2));
dif5 = simplify(diff(HE2,p1));
dif6 = simplify(diff(HE2,p2));
dif7 = simplify(diff(HE,pz1));
dif8 = simplify(diff(HE,pz2));
HM = [dif1; dif2; dif3; dif4; dif5; dif6; dif7; dif8];

% Full system in Hamiltonian without controller
Eq=simplify([O I; -I -D]*HM);

% *********************  Multi-scale controller  ****************/
% Defining desired trajectory
q1d = c1*sin(w1*t);
q2d = c2*sin(w2*t);
qd = [q1d; q2d];

dq1d = diff(q1d,t);
dq2d = diff(q2d,t);
dqd = [dq1d; dq2d];

Ddq1d = diff(dq1d,t);
Ddq2d = diff(dq2d,t);
Ddqd = [Ddq1d; Ddq2d];

% Change of variables
M2 = subs(M,q2,q2d);
P = simplify(M2*dqd);

%Controller parameters
Kd = [-5.5 0; 0 -1];
Lambda = [50 0 ; 0 5];
```

Figure C.9 Matlab code for Reyes-Báez et al. multi-scale controller, flexible configuration, part 3.

```matlab
% System error
Q = q - qd;

pdo = simplify(M*dqd);
pr = simplify(pdo - Lambda*Q);
S = p - pr;

% Slow controller dynamics
dpr = (diff(M,q1)*dq1+diff(M,q2)*dq2)*dqd + M*Ddqd - Lambda*([dq1; ...
    dq2]-dqd);

Hpr = subs(HE2, p1, p1-S(1,1));
Hpr = subs(Hpr, p2, p2-S(2,1));
HS = subs(HE2, p1, p1-pr(1,1));
HS = subs(HS, p2, p2-pr(2,1));

U1 = simplify((dpr + [diff(Hpr,q1);diff(Hpr,q2)]));
U2 = simplify((-Kd*[diff(HS,p1);diff(HS,p2)] - (M^(-1))*Lambda*Q + ...
    [diff(pr'*(M^(-1))*S,q1) ; diff(pr'*(M^(-1))*S,q2)]));
Us = U1 + U2;

QN = M^(-1)*p;
Us = subs(Us,dq1,QN(1,1));
Us = subs(Us,dq2,QN(2,1));

% Fast controller
kv = [-14 0; 0 -16];
dEz = (dq-dqm);
Uf = kv*dEz;

% Final System Dynamics
U = Us+Uf;
ErrorQ = (M^(-1))*p - (M2^(-1))*(pr+Lambda*(q-qd));
ErrorZ = (M^(-1))*(p-pm);

EqF = [Eq(1); Eq(2); Eq(3); Eq(4); Eq(5); Eq(6); Eq(7)+U(1); ...
    Eq(8)+U(2)];
qF = (M^(-1))*p;
qFm = (M^(-1))*pm;
EqF = subs(EqF, [dq1 dq2 dqm1 dqm2], [qF(1) qF(2) qFm(1) qFm(2)]);
EqF = subs(EqF, [qm1 qm2 pm1 pm2], [QM(1) QM(2) PM(1) PM(2)]);
```

Figure C.10 Matlab code for Reyes-Báez et al. multi-scale controller, flexible configuration, part 4.

C.4 Jardón-Kojakhmetov et al. multi-scale controller for the flexible model.

```
% Flexible model simulation, Jardon-Kojakhmetov et al. multi-scale ...
    controller
% Programmed by Juan Jose Padilla-Mora

% Define variables
syms q1 q2 p1 p2 real
syms qm1 qm2 pm1 pm2 real
syms z1 z2 pz1 pz2 real
t = sym('t','positive');
E = sym('E','positive');
syms qc1 qc2 Zc1 Zc2 real

% Define the constants
m1 = 1.9585;
m2 = 0.1504;
I1 = 0.23041858;
I2 = 0.010724;
r1 = 0.2;
r2 = 0.25;
l1 = 0.343;
l2 = 0.267;
c1 = 30*(pi/180);
c2 = 30*(pi/180);
w1 = 0.2;
w2 = 0.4;
d1 = 0.5;
d2 = 0.1;
Im1 = 0.1;
Im2 = 0.1;
K1 = 78.6765;
K2 = 30.4639;
```

Figure C.11 Matlab code for Jardón-Kojakhmetov et al. multi-scale controller, flexible configuration, part 1.

```
% Defining vector variables variables
p = [p1; p2];
pm = [pm1; pm2];
q = [q1 ; q2];
qm = [qm1 ; qm2];
z = [z1; z2];
pz = [pz1; pz2];

% Change of variables
qE_z = [q;z];
qE_q = [q;(q-qm)/E];
pE_z = [p;pz];
pE_p = [p;(p-pm)/E];
QM = q-z*E;
PM = p-pz*E;

% Constant Matrix
I = eye(2);
O = zeros(2);
K = [K1 0; 0 K2];
IN = [Im1 0; 0 Im2];

% Expanded Mass-Inertia matrix
m11 = m1*l1^2+m2*((l1^2) +(l2^2) +2*l1*l2*cos(q2));
m21 = m2*((l2^2) +2*l1*l2*cos(q2));
m22 = m2*(l2^2);

M = [m11 m21; m21 m22];
ME = simplify([M+IN -E*IN; -E*IN E*E*IN]);

% TE Matrix
TE = simplify(chol(ME,'lower', 'nocheck'));
t1 = simplify([TE(1,1) TE(1,2); TE(2,1) TE(2,2)]);
T = t1*t1';
t2 = simplify([TE(3,1) TE(3,2); TE(4,1) TE(4,2)]);
t3 = simplify([TE(3,3) TE(3,4); TE(4,3) TE(4,4)]);
t4 = simplify(chol(IN-IN*(T^-1)*IN,'lower', 'nocheck'));
```

Figure C.12 Matlab code for Jardón-Kojakhmetov et al. multi-scale controller, flexible configuration, part 2.

```matlab
% Constants
alpha = simplify((t4^-1)*I*(T^-1));
eq1 = (t1^-1)*p;
beta = simplify([diff(eq1, q1) diff(eq1, q2)]);
eq2 = alpha*p;
gama = simplify([diff(eq2, q1) diff(eq2, q2)]);

% TE inversa
TEin = [(t1^-1) O; alpha (t4^-1)/E];

% JE Matrix
j1 = simplify(beta*(t1^-1)'-(t1^-1)*beta');

j21 = simplify(-beta*alpha'-(t1^-1)*gama');
eq3 = (t4^-1)*pz;
eq3 = subs(eq3, [pz1 pz2], [pE_p(3) pE_p(4)]);
j22 = simplify((t1^-1)*[diff(eq3,q1) diff(eq3,q2)]);
j2 = simplify(j21-(1/E)*j22);

j31 = simplify(-gama*alpha'+alpha*gama');
eq4 = (t4^-1)*pz;
eq4 = subs(eq4, [pz1 pz2], [pE_p(3) pE_p(4)]);
j32 = simplify([diff(eq4,q1) ...
    diff(eq4,q2)]*alpha'-alpha*[diff(eq4,q1) diff(eq4,q2)]');
j3 = simplify(j31-(1/E)*j32);

% Final Matrix
FM = [O O (t1^-1) alpha'; O O O (t4^-1)'/E; -(t1^-1) O j1 ...
    j21-j22/E; -alpha' -(t4^-1)/E -j21+j22/E -j32/E];

% Hamiltonian Matrix
HE = simplify(0.5*pE_z'*pE_z+0.5*(E*z)'*K*(E*z));
HE2 = subs(HE, [z1 z2 pz1 pz2], [qE_q(3), qE_q(4), pE_p(3), pE_p(4)]);

% derivatives of the Hamiltonian
dif1 = simplify(diff(HE2,q1));
dif2 = simplify(diff(HE2,q2));
dif3 = simplify(diff(HE,z1));
dif4 = simplify(diff(HE,z2));
dif5 = simplify(diff(HE2,p1));
dif6 = simplify(diff(HE2,p2));
dif7 = simplify(diff(HE,pz1));
dif8 = simplify(diff(HE,pz2));
HM = [dif1; dif2; dif3; dif4; dif5; dif6; dif7; dif8];
```

Figure C.13 Matlab code for Jardón-Kojakhmetov et al. multi-scale controller, flexible configuration, part 3.

```
% System Dynamics
Maux1 = FM*HM;
Maux2 = [Maux1(5); Maux1(6); Maux1(7); Maux1(8)];

% desired trajectory
q1d = c1*sin(w1*t);
q2d = c2*sin(w2*t);
qd = [q1d; q2d];

dq1d = diff(q1d,t);
dq2d = diff(q2d,t);
dqd = [dq1d; dq2d];

Ddq1d = diff(dq1d,t);
Ddq2d = diff(dq2d,t);
Ddqd = [Ddq1d; Ddq2d];

% Slow Controller
Kp = [300 0; 0 200];
Kc = [100 0; 0 100];
Kd = [3 0; 0 3];

% Slow controller dynamics
QC = [qc1;qc2];
dqc = (Kd^-1)*Kc*(q-qd-QC);

% Slow controller components
Us1 = M*Ddqd;

eq5 = M*dqd;
Us2 = [diff(eq5,q1) diff(eq5,q2)]*dqd;
```

Figure C.14 Matlab code for Jardón-Kojakhmetov et al. multi-scale controller, flexible configuration, part 4.

```
eq6 = dqd'*M*dqd;
Us3 = -0.5*[diff(eq6,q1); diff(eq6,q2)];

Us4 = -Kp*(q-qd);
Us5 = -Kc*(q-qd-QC);

Us = simplify(Us1+Us2+Us3+Us4+Us5);

% Fast Controller
Lp = [200 0; 0 100];
Lc = [300 0; 0 300];
Ld = [3 0; 0 3];

% Fast controller dynamics
Zc = [Zc1;Zc2];
dzc = (Ld^-1)*Lc*(z-Zc);
Uf = simplify(-Lp*z-Lc*(z-Zc));

% Final System Dynamics
U = [Us;Uf];
Maux3 = Maux2+U;
SD = [Maux1(1); Maux1(2); Maux1(3); Maux1(4); Maux3(1); Maux3(2); ...
    Maux3(3); Maux3(4)];

Md = subs(M, q2, q2d);
pd = Md*dqd;

SD = subs(SD, [qm1 qm2 pm1 pm2], [QM(1) QM(2) PM(1) PM(2)]);
```

Figure C.15 Matlab code for Jardón-Kojakhmetov et al. multi-scale controller, flexible configuration, part 5.

Appendix D

Spring coupling mechanical design.

This appendix is focused in the design of a mechanical extension for the springs of the 2DoF Quanser manipulator robot. The joints are originally adapted to be used with a pair of springs which will simulate the elastic behavior of a mechanical joint. Several improvements have been sketched, presenting here the simplest, cheapest and with the less impact in the system functioning.

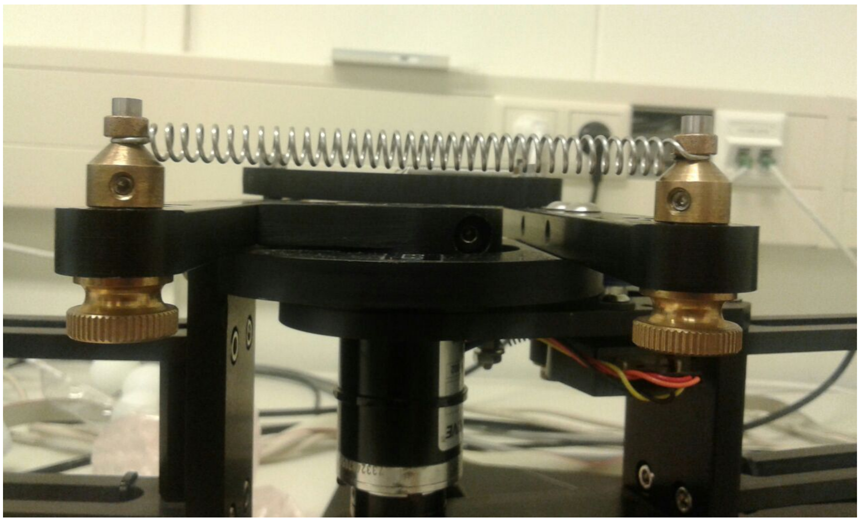

Figure D.1 Original spring attachments

Figure D.1 shows the simple mechanical connection of the springs. It consists of an assembly of two bronze components with a screwed coupling which fixes the spring to the robot joint; a stainless steel pin in which the ring of the spring is secured; and a mechanical spacer. The individual components of the assembly can be seen in Figure D.2.

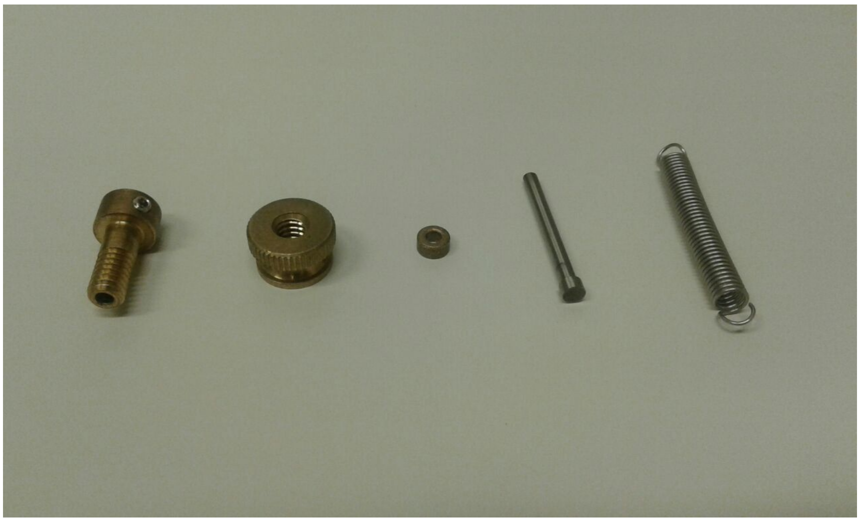

Figure D.2 Spring attachment components: (from left to right) upper bronze coupling, lower bronze coupling, mechanical spacer, stainless steel pin, spring.

As can be seen in Figure D.1, each coupling is designed to support only one spring. If needed, the spring constant for the joint can only be increased by changing the spring. A new mechanical attachment with the possibility to attach several springs in parallel to increase the value of such constant is justified.

D.1 Proposal 1.

The proposed change for the spring coupling in the joint is shown in the Figure D.3. It consists of an enlargement of the stainless steel pin supporting the springs, as well as a mechanical spacers concentric to the pin in order to physically separate the springs.

The spacers will not be subjected to any kind of forces, so they can be manufactured with a material similar to PLA in a 3D printer machine. On the other hand, the pin will be experiencing shear forces due to the action of the springs. For this reason, an analysis of the mechanical stresses handled by the pin is necessary.

The pin has been studied as in F. Beer and Mazurek (2013) as a cantilevered beam subjected to a force P at its end. If a cut in the beam is made at a distance x from the support, the internal forces are a force P' equal and opposite to P, and a moment M with a magnitude $M = Px$.

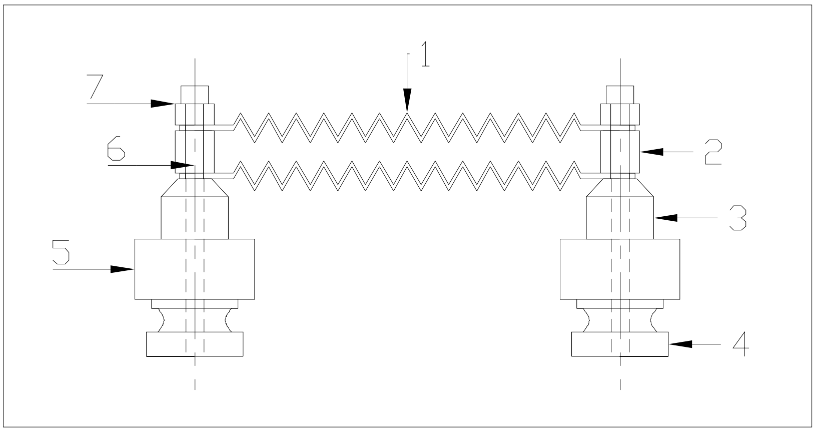

Figure D.3 Schematic of spring attachments: 1. springs, 2. designed mechanical spacers, 3. upper bronze coupling, 4. lower bronze coupling, 5. support bar, 6. stainless steel pin and 7. original mechanical spacer

This moment causes a sheer stress in the beam. Having I as the moment of inertia of the beam of the cross-section with respect to it's centroidal axis to the plane of M, the stress is defined as

$$\sigma_m = \frac{Mc}{I} = \frac{Pxc}{I}, \tag{D.1}$$

where P is defined as the force experienced by the pin because of the potential energy stored in the springs, $P = -kx$. Assuming the worst scenario, in which 2 springs of 3,5 lbs/in are attached to the joint coupling, a single spring of 7 lb/in can be modeled for the control system. Besides, the analysis has been carried out at a distance of 8.5mm, which is the distance where the last spring will be secured. The springs have a maximum elongation of 5mm. Then, the force applied by each spring is

$$\begin{aligned} P &= -kx \\ &= 3.5 lb/in \cdot 5cm \cdot 0{,}393701 \\ &\approx 6.89 lb \\ &\approx 30.65 N, \end{aligned} \tag{D.2}$$

Finally, According to F. Beer and Mazurek (2013), the yield stress for the stainless steel AISI 302 is $150MPa$. The maximum sheer stress experienced by the pin if manufactured with those materials is:

$$\begin{aligned}
\sigma_{steel} &= \frac{Pxc}{I}, \\
&= \frac{(P_1x_1 + P_2x_2)c}{I}, \\
&= \frac{P(x_1 + x_2 + x_3)c}{I}, \\
&= \frac{30.65N \cdot (0.5mm + 8.5mm) \cdot 1.55mm}{0.25 \cdot \pi \cdot 1.55mm^4}, \\
&\approx 94.3MPa.
\end{aligned} \tag{D.3}$$

D.2 Proposal 2.

The proposed change for the spring coupling in the joint is shown in the Figure D.4. In this proposal, the component of interest is the upper bronze coupling, which has been modified eliminating the through hole and creating an extension in the form of a cantilevered beam. At its end, the beam ends with a screw thread to secure the springs

Once again, there is a cantilevered beam subjected to a force P at its end, as studied in F. Beer and Mazurek (2013). If a cut in the beam is made at a distance x from the support, the internal forces are a force P' equal and opposite to P, and a moment M with a magnitude $M = Px$. This moment causes a sheer stress in the beam. Having I as the moment of inertia of the beam Of the cross-section with respect to it's centroidal axis to the plane of M, the stress is calculated as

$$\sigma_m = \frac{Mc}{I} = \frac{Pxc}{I}, \tag{D.4}$$

where P is defined as the force experienced by the pin because of the potential energy stored in the springs, $P = -kx$. Assuming the worst scenario, in which 3 springs of 3,5 lbs/in are attached to the joint coupling, a single spring of 10.5 lb/in can be modeled for the control system. Besides, the analysis has been carried out at a distance of 16.5mm, which is the distance where the last spring will be secured. The springs have a maximum elongation of 5mm. The force applied by each spring is the same as in D.2:

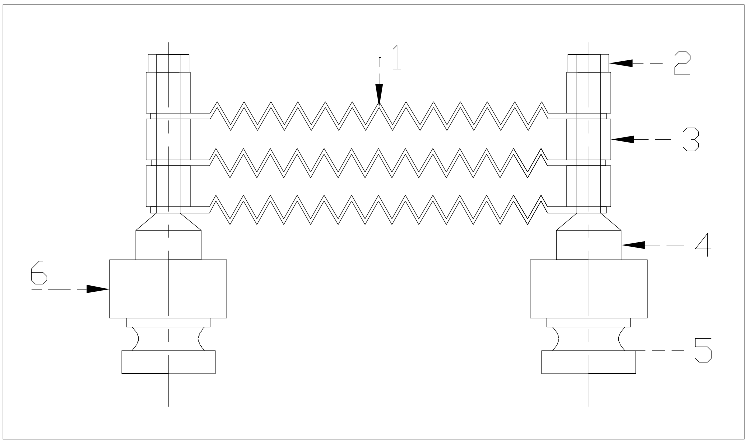

Figure D.4 Schematic of spring attachments: 1. springs, 2. nut, 3. mechanical spacer, 4. upper bronze coupling, 5. lower bronze coupling and 6. support bar.

According to F. Beer and Mazurek (2013), the yield stress for the aluminum 6061 is $140MPa$. The maximum sheer stress experienced by the pin if manufactured with aluminum 6061 is:

$$\begin{aligned}\sigma_{aluminum} &= \frac{Pxc}{I},\\ &= \frac{(P_1x_1 + P_2x_2 + P_3x_3)c}{I},\\ &= \frac{P(x_1 + x_2 + x_3 + P_3x_3)c}{I},\\ &= \frac{30.65N \cdot (0.5mm + 8.5mm + 16.5mm) \cdot 2mm}{0.25 \cdot \pi \cdot 2^4},\\ &\approx 124.4MPa.\end{aligned} \tag{D.5}$$

D.3 Discussion.

The first design has the advantage of being easy to manufacture. The changes to the original design are minimum, and the new parts are easy to machine by a lathe. However, the dimensions of the original beam reduce the amount of springs that can actually be set in that configurations (only two), because of the high sheer stress that would experience due to the force of the springs. Even changing the material of the pin probably would not be enough to safely be able to attach another spring.

The second design has the advantage of being relatively easy to manufacture (tough more complex than the proposal 1) and has the possibility to couple three springs instead of two, because the area of the cantilevered beam is higher. The material proposed is an aluminum 6061, but there are several other aluminum allows that can be used, assuming a yield stress higher than 125MPa. Other materials as stainless steel can be used to ensure the safety of the piece, however the price of the work would rise.

The proposed designs presented in this document have been analyzed with theoretical values and materials. The analysis shall be repeated once the design has been approved and a clearest context of the local mechanical workshops (materials, availability...) and the customer interest (time, budget...) to make a decision.